

Time-dependent deformation of flysch rock mass

Grošić, Mirko

Doctoral thesis / Disertacija

2014

Degree Grantor / Ustanova koja je dodijelila akademski / stručni stupanj: **University of Rijeka, Faculty of Civil Engineering / Sveučilište u Rijeci, Građevinski fakultet**

Permanent link / Trajna poveznica: <https://um.nsk.hr/um:nbn:hr:188:815488>

Rights / Prava: [Attribution-NonCommercial-NoDerivatives 4.0 International](#)/[Imenovanje-Nekomercijalno-Bez prerada 4.0 međunarodna](#)

Download date / Datum preuzimanja: **2024-05-13**



Repository / Repozitorij:

[Repository of the University of Rijeka Library - SVKRI Repository](#)



UNIVERSITY OF RIJEKA
FACULTY OF CIVIL ENGINEERING

Mirko Grošić

**TIME-DEPENDENT DEFORMATION OF
FLYSCH ROCK MASS**

DOCTORAL THESIS

Supervisor: Professor Željko Arbanas

Rijeka, 2014.

Mentor rada: izv.prof.dr.sc. Željko Arbanas

Doktorski rad obranjen je dana _____ u/na

_____, pred povjerenstvom u sastavu:

1. prof. dr. sc. Čedomir Benac, Građevinski fakultet Sveučilišta u Rijeci,
predsjednik
2. prof. dr. sc. Leo Matešić, Građevinski fakultet Sveučilišta u Rijeci, član
3. prof. dr. sc. Jakob Likar, Univerza v Ljubljani, Naravoslovnotehniška
fakulteta, vanjski član
4. prof. dr. sc. Meho Saša Kovačević, Građevinski fakultet Sveučilišta u
Zagrebu, vanjski član
5. izv. prof. dr. sc. Željko Arbanas, Građevinski fakultet Sveučilišta u Rijeci,
član mentor

ACKNOWLEDGEMENTS

I want to thank my supervisor prof.dr.sc. Željko Arbanas. It has been an honour to have the opportunity to work and research with him. Thanks for contributions of time, ideas, discussions and advice during the creation of this thesis.

Also, I would like to thanks to my colleagues from Geotech, Faculty of Civil Engineering University of Rijeka and Zagreb, Civil engineering Institute of Croatia and all other that have helped me with advice, ideas, reports, measurement data and other.

Special thanks to my whole family and friends that have helped me and supported me during work on this research: my wife Daria, kids Ena and Filip, parents Neda and Boris. I feel sorry for every moment that I have not been with you.

It was very hard work to finish this thesis, but also an interesting journey with a lot of happiness, excitement and inspiration through every step of research. I hope this is only the beginning of the next step of research in science that would bring me a lot of new challenges, colleagues, friends and experiences.

ABSTRACT

Rock mass deformations and their influences on construction are observed during construction and even during service period. Observations of reinforced cuts along the Adriatic motorway near the City of Rijeka, Croatia, were conducted over a time period of three to seven years during construction phase and service period. Measured displacements reached significant magnitudes during the service period (up to 50% of displacements of construction phase) as a consequence of the time dependent behaviour of the rock mass.

This thesis presents findings related to flysch rock mass weathering profile and its characteristics based on detailed geotechnical investigations and monitoring results coupled with numerical back analysis. It was found possible to detect the thickness of the flysch rock mass weathering profile by performing detailed geotechnical field investigations. According to the seismic refraction method that utilized the refraction of seismic waves on geologic layers and rock/soil units, the numerical model was divided into geotechnical units with similar geotechnical properties.

To obtain deformability and creep properties of geotechnical units the direct approach to back analysis was used in numerical modelling. Numerical modelling was divided into two phases: modelling of construction phase using the linear elastoplastic Mohr-Coulomb model and modelling of service period using the visco-plastic Burger-Mohr-Coulomb model. Verification of the numerical model and parameters was based on comparison of simulation data and measured data of horizontal displacements at vertical inclinometer.

Recommendations for the strength, deformability and creep properties of the geotechnical units of the weathering profile of a flysch rock mass are given together with guidelines for future investigations and research.

SAŽETAK

Deformacije stijenske mase i njihov utjecaj na konstrukciju prisutne su u fazi izvođenja same konstrukcije, ali i tijekom eksploatacije građevine. Opservacija ojačanih padina duž Jadranske autoceste u okolici grada Rijeke, u Hrvatskoj, provedena je u vremenskom period od tri do sedam godina te je obuhvaćala fazu izgradnje, ali i fazu eksploatacije građevine. Izmjereni pomaci u fazi eksploatacije su značajni (reda veličine 50% od pomaka izmjerenih u fazi izgradnje), a rezultat su vremenski ovisnog ponašanja stijenske mase.

Ovaj rad predstavlja rezultate istraživanja flišne stijenske mase i pripadajućeg profila trošenja temeljem provedenih detaljnih geotehničkih istražnih radova i rezultata monitoringa povezanih sa povratnim numeričkim analizama. Utvrđeno je da je moguće ustanoviti debljinu profila trošenja flišne stijenske mase provedbom detaljnih geotehničkih istražnih radova. Primjenom metode plitke seizmičke refrakcije koja koristi refrakciju seizmičkih valova u geološkim jedinicama stijenske mase/tla, numerički model podijeljen je na nekoliko geotehničkih jedinica sa sličnim značajkama.

Kako bi se dobili parametri deformabilnosti i puzanja pojedinih geotehničkih jedinica korišten je direktni pristup u numeričkom povratnom modeliranju. Numeričke povratne analize podijeljene su u dvije faze: modeliranje faze izgradnje primjenom linearnog elastoplastičnog Mohr-Coulombovog modela i modeliranje faze eksploatacije primjenom Burger-Mohr-Coulombovog modela. Verifikacija modela i dobivenih parametara temeljena je na usporedbi rezultata dobivenih simulacijom i izmjerenih horizontalnih pomaka na vertikalnom inklinometru.

Dane su preporuke za parametre čvrstoće, deformabilnosti i puzanja za geotehničke jedinice profila trošnosti flišne stijenske te smjernice za daljnja istraživanja.

KEYWORDS

Keywords: time dependent behaviour, weak rock mass, flysch, back analysis, reinforced cut

Ključne riječi: vremenski ovisno ponašanje, meka stijenska masa, fliš, povratne analize, ojačani zasjek

TABLE OF CONTENTS

ACKNOWLEDGEMENTS	I
ABSTRACT	II
SAŽETAK	IV
KEYWORDS	VI
TABLE OF CONTENTS	VII
1. INTRODUCTION	1
1.1. Purpose of the study	1
1.2. Scope of the study	2
1.3. Methodology of the research	3
1.4. Structure of the thesis	4
2. ROCK AND ROCK MASS PROPERTIES	7
2.1. About weak rocks	7
2.2. Weathering of rock mass	10
2.3. Rock mass classification.....	15
2.4. Strength criteria	22
2.5. Deformability	27
2.6. In-situ stress condition.....	31
3. CREEP AND TIME DEPENDENT BEHAVIOUR OF ROCK MASS.....	33
3.1. About rheology and creep mechanics.....	33
3.2. Laboratory tests of creep of intact rock	37
3.3. Creep of intact rock	41
3.4. In-situ creep test of rock mass	53
3.5. Monitoring of rock-mass behaviour	58
3.6. Time dependent behaviour of rock mass	60
3.7. Time dependent behaviour of reinforced cuts	71
4. MODELING OF TIME DEPENDENT BEHAVIOUR OF ENGINEERED SLOPES.....	73

4.1.	Numerical modelling and finite difference method.....	73
4.2.	FLAC software	73
4.3.	Modelling of material response and reinforcing system.....	75
4.4.	Mohr-Coulomb model	78
4.5.	Buger elasto-plastic model	82
4.6.	Reinforcing system.....	84
4.7.	Observational method and back analysis.....	86
4.8.	Methodology.....	89
5.	APPLICATION – THE ADRIATIC MOTORWAY CASE STUDY	94
5.1.	Outline of the project.....	94
5.2.	Geological overview.....	97
5.3.	Weathering profile of flysch rock mass in Draga Valley	98
5.4.	Geotechnical conditions	100
5.5.	Monitoring data and interpretation.....	109
5.6.	Numerical back analysis of construction phase – cross section at km 2+380	116
5.7.	Numerical back analysis of service period – cross section at km 2+380	121
5.8.	Numerical back analysis of construction phase – cross section at km 2+440	123
5.9.	Numerical back analysis of service period – cross section at km 2+440	128
6.	RESULTS OF THE NUMERICAL BACK ANALYSIS AND INTERPRETATION	131
6.1.	Results of construction phase analysis – cross section at km 2+380.....	131
6.2.	Results of service period analysis – cross section at km 2+380	136
6.3.	Results of construction phase analysis – cross section at km 2+440.....	140
6.4.	Results of service period analysis – cross section at km 2+440	144
6.5.	Verification of the numerical model and parameters	148
6.6.	Influence of time dependent behaviour of slope on the reinforcing system	150
7.	PREDICTING THE TIME DEPENDENT BEHAVIOUR OF REINFORCED CUTS	155
7.1.	Predicting the time dependent behaviour – cross section at km 2+380.....	155

7.2. Predicting the time dependent behaviour – cross section at km 2+440	157
8. DISCUSSION AND CONCLUSIONS.....	159
8.1. Overview of the thesis	159
8.2. Conclusions	160
8.3. Future researches	164
REFERENCES	166
LIST OF FIGURES.....	178
LIST OF TABLES.....	182
APPENDIX 1 – NUMERICAL CODE KM 2+380.....	183
APPENDIX 2 – NUMERICAL CODE KM 2+440.....	187
BIOGRAPHY	191

1. INTRODUCTION

1.1. Purpose of the study

Changes in the local stress state due to excavation or mining perturb the stability of the rock mass surrounding excavations. The subsequent readjustment of the rock mass towards a new equilibrium does not occur instantaneously; it is a gradual process over time (Malan, 1999).

The problem is how to evaluate the corresponding creep parameters of the model in simulation of geotechnical structures. It is suggested that they should be back analysed from the in-situ monitoring data if these data are available (Guan et al, 2008).

In time dependent behaviour of rock mass at a certain moment of construction phase a rock mass cut surface becomes stress free due to excavation. One of the major parameters involved in the rock support interaction time dependent analysis is the time of application of the support system after the excavation. If this time is short, then the support may fail due to overloading; if this time is too long, then a failure of the rock mass cuts is possible due to excessive deformation (Cristescu et al, 1987).

In practice, service life of the geotechnical construction such as reinforced cuts exceeds the period of monitoring time of the same structure. Monitoring phase is often limited to construction period or sometimes to several years after finishing the construction, but it almost never reaches the whole service life that ranges from 50 to 100 years for most of the infrastructure projects.

Therefore it is necessary to predict time dependent behaviour of geotechnical constructions in the long time period of service period.

1.2. Scope of the study

Measured data from installed monitoring equipment at the construction phase and in the time period of 3 years of service period were analysed at Adriatic Motorway, section Orehovica – Draga - Sv. Kuzam at D8 road near the City of Rijeka. Analysing the data from installed monitoring equipment at reinforced flysch cuts it is observed that significant displacements are realized during the service period of construction after the reinforcing works on the slopes were completed. Existence of these displacements indicates that the time dependent behaviour of reinforced cuts in flysch rock mass should be investigated in more detail.

The scope of this research is focused on selecting a numerical model and obtaining its deformability and creep parameters to model and to predict the time dependent behaviour of reinforced cuts in flysch rock mass. Knowing the values of the deformability and creep parameters it is possible to predict the time dependent behaviour of the reinforced cuts in weak rock mass such as flysch. It will be possible to predict the time dependent behaviour during the construction phase and also during the long time service period.

Based on this research the deformability and creep parameters and their relationships could be estimated for similar materials for future projects. Guidelines for designing reinforced cuts in similar materials would enable prediction of the time dependent behaviour of reinforcing system.

1.3. Methodology of the research

Numerical analysis and the results of the analysis in this paper will be presented for the models established at cuts of the Adriatic Motorway near the City of Rijeka. The geological fabric of the Draga Valley steep slopes is composed of limestone rock masses, and at the bottom of the valley there are deposits of Palaeogene flysch rock, which mainly consist of siltstone with rare layers of sand, marl, and breccia.

For numerical modelling of time dependent behaviour of engineered slopes the FLAC software v7.0 will be used. FLAC uses the finite difference method and an explicit time-marching method to solve algebraic equations and perform a Lagrangian analysis. Numerical analysis will be performed in two phases: a construction phase and a service period phase.

According to performed geotechnical field investigations results, the representative models will be divided into several geotechnical units with same or similar geotechnical properties. Disposition and thickness of these geotechnical units will be determined on the basis of geophysical measurement results and will be confirmed by geotechnical drilling logs. According to the seismic refraction geophysical method that utilized the refraction of seismic waves on geologic layers and rock/soil units, the numerical model will be divided into several geotechnical units with similar geotechnical properties. In the upper layer, where the difference between parameters is pronounced with depth, grouping will be defined with smaller longitudinal seismic wave velocities. On the other hand, where the difference between parameters is not significantly pronounced with depth, grouping of the geotechnical units at lower half of model will be defined with higher longitudinal seismic wave velocities.

To obtain deformability and creep properties of these units the direct approach to back analysis will be used in numerical modelling. Back analysis of the behaviour of engineered slopes in the flysch rock mass will be performed using a trial and error method to obtain the deformability and creep parameters of geotechnical units in the numerical model.

Verification of numerical modelling will be based on comparison of simulation data (obtained from numerical analysis) and measured data (obtained from measurement results). Comparison will be directed on horizontal displacements at vertical inclinometer since these are the most significant indicator of displacements of engineered cuts in the construction phase and in the service period. The weathering profile of flysch rock mass is clearly visible from the diagram of horizontal displacements per depth of vertical inclinometers. Verification and calibration of numerical model will be carried out on several points through the upper part of the cut where most of the displacements occur; in every 1.0 to 3.0 m.

1.4. Structure of the thesis

This doctoral thesis consists of eight chapters. Chapter *1. Introduction* gives the purpose of the study, scope of the study, methodology of the study and structure of the thesis.

Chapter *2. Rock and rock mass properties* describes properties of the weak rock, weathering of rock mass, presents the classifications of rock mass, strength criteria, deformability properties and in-situ stress condition. This chapter is the introduction into basic properties and features of the intact rock and rock mass. The content of this chapter is focused on the weak rock mass and flysch.

Chapter 3. *Creep and time dependent behaviour of rock mass* is a more detailed introduction to the thesis theme and it presents the state of the art of the domain of the time dependent behaviour in connection with reinforced cut and creep and time dependent behaviour of the weak rocks such as flysch. The chapter is divided into seven subchapters: *About rheology and creep mechanics*, *Laboratory tests of creep of intact rock*, *Creep of intact rock*, *In-situ creep test of rock mass*, *Monitoring of rock mass behaviour*, *Time dependent behaviour of rock mass* and *Time dependent behaviour of reinforced cuts*.

Chapter 4. *Modelling of time dependent behaviour of engineered slopes* presents the methodology of the research and gives detailed description of numerical modelling and software, describes modelling of material response and reinforcing system, presents models that will be used for simulations, presents the observational method and analysis procedure and at the end gives detailed methodology of the research.

Chapter 5. *Application – The Adriatic motorway case study* presents in detail geological and geotechnical properties and conditions of the Draga location near the City of Rijeka through which the motorway was build. In the second part of the chapter models of the numerical back analysis for cross sections in km 2+380 and km 2+440 are described.

Chapter 6. *Results of the numerical back analysis and interpretation* presents the results obtained from the numerical back analysis (construction phase and service period) and verification of the models and results using comparison with the data obtained from installed monitoring equipment.

Chapter 7. *Predicting the time dependent behaviour of reinforced cuts* gives the prediction of a long period of 25 years of reinforced cuts' service period behaviour,

based on the models and deformability and creep parameters obtained from the back analysis.

Chapter 8. *Discussion and conclusions* gives the overview of the thesis, conclusions and gives the recommendations and guidelines for future researches.

2. ROCK AND ROCK MASS PROPERTIES

2.1. About weak rocks

Some types of rocks are inherently weak while other rocks become weak during time due to weathering processes. Weathering is a process that defines and describes a state of rock or rock mass. Low values of mechanical properties (strength or deformability) of rock or rock mass are often presented by term weak.

Due to their geotechnical behaviour, weak rocks constitute an intermediate stage between (cohesive) soils on the one hand and hard rocks on the other hand. These three groups are linked by geological processes (cementation and weathering), so the borders between them are variable (Nickmann et al., 2006) - Figure 2.1.

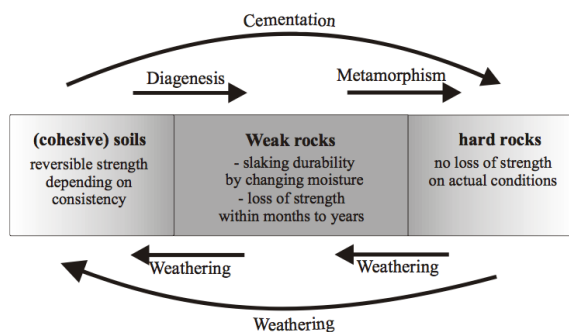


Figure 2.1 Position of weak rock between cohesive soils and hard rocks (Nickmann et al., 2006)

The definition of rock quality is very well formulated by the classification system, but the definition of weak rock mass is not so well described, explained or classified. Weak rocks can be defined as all rocks having poor mechanical characteristics ranging from soft or weathered rocks, which are intensely fractured or altered rock masses, to faults and rocks having characteristics that somehow make them comparable to soil (Foo et al., 2011).

Klein (2001) and Clerici (1992) defined weak rock based on their uniaxial compressive strength (UCS). The classification for weak rock is based on International Society for Rock Mechanics rating (ISRM, 1981), where 0.25–25 MPa UCS is considered as “extremely weak to weak” for tunnelling projects (Klein, 2001). According to Clerici (1992), weak rock might be defined as rock when uniaxial compressive strength of rock material is less than 20.0 MPa, or else when the static modulus of elasticity of the rock mass is from 150 to 2,000 MPa. Hoek (1999) considers rock mass as weak rock when in-situ UCS is less than approximately one third of the in-situ stress acting on the rock mass being excavated. Other criteria used to determinate weak rock are presented in

Table 2.1.

Table 2.1 Summary of engineering properties of weak rock from the literature (Santi, 2006)

Test or Property	Value or Range for Weak Rock	Reference
Compressive strength	1 – 20 MPa	Afrouz, 1992
Standard penetration test	50 – 300 blows per ft (15 – 90 blows per m')	White and Richardson, 1987 Sowers, 1973
Rock quality designation	< 25 – 75 %	Santi and Doyle, 1997
Hammer rebound	≥ Category 4	Santi, 1995
Seismic wave velocity	< 7,000 ft per second* (2,100 m/s)	Caterpillar, 1996 White and Richardson, 1987
Ratio of weathered matrix to unweathered blocks	> 75 % matrix	Geological Society, 1995
Jar slake	≤ 4	Santi, 1995
Slake durability, I _d (2), ASTM D4644-87	< 90 %	Santi and Doyle, 1997 Lee and de Freitas, 1989
Free swell	> 3 – 4 %	Welsh and others, 1991 Underwood, 1967
Natural moisture content	> 1 % for igneous and metamorphic rocks > 5 – 15 % for clayey rocks	Santi and Doyle, 1997
Dearman weathering classification	≥ Category 4	Santi, 1995
CSIR rock mass rating (Bieniawski, 1976)	< 35 - 60	Santi, 1995
Norwegian Geotechnical Institute “Q” rating	< 2	Santi, 1995

* Lower velocities may be appropriate, depending on equipment used and degree of rock fracturing

In some national standards (DIN 4022 T1, DIN EN 14689-1, ASTM D 4644) weak rocks are part of the group of rocks, in opposition to soils. The difference from hard rocks is their nature to disintegrate within a short time period (days to several years)

when being exposed to water and climatic changes. This loss of strength is not reversible under normal conditions, whereas in cohesive soils it is possible due to changes in water content (Nickmann et al., 2006).

There are many definitions and values or ranges that describe the term “weak rock”. For all of them it is common that the term describes a rock or a rock mass with low values of strength or deformability parameters. On weak rock or rock mass, the criteria from rock mechanics should be applied.

2.2. Weathering of rock mass

Weathering of rocks is a result of the destructive processes from atmospheric agents at or near the Earth's surface, while alteration is typically brought about by the action of hydrothermal processes. Both processes produce changes of the mineralogical composition of a rock, affecting colour, texture, composition, firmness or form; features that result in reduction of the mechanical properties of a rock. Deterioration from weathering and alteration generally affects the walls of the discontinuities more than the interior of the rock (Piteau, 1970). During these processes fresh rock mass gradually transforms into residual soil.

The need to describe the weathering profile in an objective and precise way, as well as classifying of the rock materials in relation to the state of weathering has been the basis of a great deal of classification that has been proposed during the last 50 years. This was due to the recognition of the effect which weathering has on the geotechnical behaviour of those materials in engineering work (Pinho et al., 2006).

Weathering could be studied as weathering of rock and weathering of rock mass. At the dimension of rock, weathering was studied in detail by Moye (1955), Melton

(1965), Little (1969), Newbery (1970), Wakeling (1970), Geotechnical Control Office Hong Kong (1979) and Hencher and Martin (1982). The description and classification of the state of weathering of rock mass for engineering purposes has been studied in detail by Vargas (1953), Ruxton and Berry (1957), Knill and Jones (1957), Ward et al. (1968), Barata (1969), Chandler (1969), Saunders and Fookes (1970), Fookes and Horswill (1970), Neilson (1970), Deere and Patton (1971), Lama and Vutukuri (1978), Sancio and Brown (1980), Geological Society Engineering Group (1995), Fookes (1997) and Eberhardt et al. (2005).

Most of these classifications were established for a specific case, but the standard classification systems that have been recommended by several international bodies have a wide utilization and are most common in use:

- International Society for Rock Mechanics (ISRM, 1978),
- British Standard Institution (BSI, 1981),
- International Association of Engineering Geology (IAEG, 1981).

Some agreements between these classification systems exist, concerning the fact that that degree of weathering of intact rock should be classified into five to six grades. The most used classification system of weathering grades of rock mass is one presented in

Table 2.2. Rock mass is divided into six different weathering grades going from residual soil to fresh rock mass.

Table 2.2 Scale of weathering grades of rock mass (Dearman, 1976.)

Term	Symbol	Description	Grade
Fresh	F	No visible sign of rock material weathering; perhaps a slight discoloration on major discontinuity surfaces.	I
Slightly weathered	SW	Discoloration indicates weathering of rock material and discontinuity surfaces. All the rock material may be discoloured by weathering.	II
Moderately weathered	MW	Less than half of the rock material is decomposed or disintegrated to a soil. Fresh or discoloured rock is present either as continuous framework or as corestones.	III
Highly weathered	HW	More than half of the rock material is decomposed or disintegrated to a soil. Fresh or discoloured rock is present either as discontinuous framework or as corestones.	IV
Completely weathered	CW	All rock material is decomposed and or disintegrated to soil. The original mass structure is still largely intact.	V
Residual soil	RS	All rock material is converted to soil. The mass structure and material fabric are destroyed. There is a large change in volume, but the soil has not been significantly transported.	VI

In site investigation for engineering purposes of the grade of weathering of rock mass is provided mostly by visual inspection of the geologist, and significant differences can occur because the description of a rock material is always somewhat subjective. The discussion of the reliability of assessing the state of weathering of rocks by visual inspection was studied in detail and compared by Pinho et al. (2006). The results of that study showed many divergent opinions among the assessors. This points out the qualitative character of the visual evaluation and its subjectivity. In spite of the consensus that exists among the majority of the assessors, significant evaluation errors happened for 72% of the samples and very significant errors occurred for 12% of the samples. It was verified that the subjectivity of this assessment depends to a considerable degree on the lithology, the state of weathering and the heterogeneity of

the samples. With respect to the state of weathering, the distinction between the moderately, highly and completely weathered degrees is not difficult in certain rock types, but it is almost impossible in the case of siltstones such as the shales of flysch group from this case study. In the case under study, it was found that opinions diverged more about the moderately to highly weathered than about the slightly weathered samples.

Geological Society Engineering Group (1995) has thoroughly investigated and described disadvantages and advantages of using the classifications proposed for weathered rock.

Weak rock masses like flysch have prominent weathering profile below the surface that vary from residual soil (RS) and completely weathered (CW) near surface, over highly weathered (HW) and moderately weathered (MW) to slightly weathered (SW) and fresh rock mass (F). Consequence of these different grades is variation of deformation and strength parameters with depth.

The deformation modulus for rock mass weakened by weathering processes varies from low values for residual soils at the surface to very high values for fresh rock mass by several dozen times in only few meters of thickness of weathering profile. Strength reduction through the marl slope layers due to weathering, which has a similar geological profile as the case study used in this research, was investigated and numerically modelled by Eberhardt et al. (2005) during the investigation of the Ruffi Landslide in Switzerland.

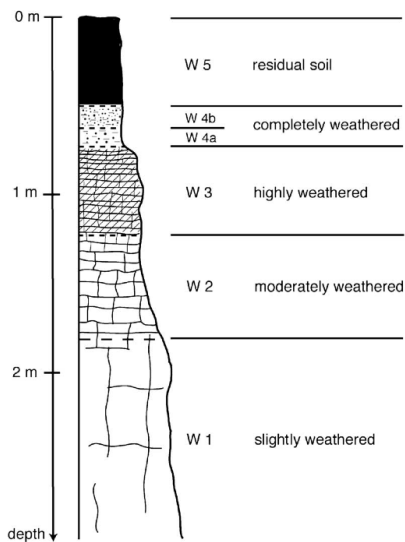


Figure 2.2 Schematic diagram of the weathering profile mapped in the Ruffi slide area (Eberhardt et al., 2005)

Flysch rock mass and flysch deposits are materials prone to the chemical weathering. The most prominent is the leaching of the CaCO_3 component and the oxidation processes of swelling, which is significant for the change of physical-mechanical characteristics of the flysch complex. Chemical decomposition is especially expressed in fine-grained members, especially in the various silts. Due to the mentioned processes flysch rock mass increases in volume in time, melts and turns into silt and clay. Gradual degradation turns it into the clayey-silty zone of weathering, whose physical-mechanical characteristics are more like engineering soil. The consequence of such geomorphological on goings is the sporadic accumulation of eroded deposits that can potentially be prone to sliding (Arbanas et al., 1999).

All classification systems of weathering of rock mass are mostly provided by visual inspection and because of that the results are subjective. Therefore, results of these classification systems should be treated only as description of rock mass and not as engineering input parameters for strength or deformability criteria or estimations. Further researches should be conducted to find correlation between weathering grades

and one of the measured in-situ methods such as geophysical measurements for each type of rock.

2.3. Rock mass classification

Two terms are used for “describing” the properties of the rock mass; classify and characterize. Rock mass characterisation is describing the rock with emphasis on colour, shape, weight, properties etc. while the rock mass classification is when one arranges and combines different features of a rock mass into different groups or classes following a specific system or principle (Palmström, 1995). In further text the term of rock mass classification shall be used.

Rock mass classifications form the core of the empirical design approach and are widely used in rock engineering. Classification is a powerful tool and is widely used during design phase, but also during construction phase, as one of the monitoring method. According to Singh and Goel (2011) rock mass classification systems have been widely used with great success for the following reasons:

- They provide better communication between planners, geologists, designers, contractors and engineers,
- An engineer’s observations, experience and judgment are correlated and consolidated more effectively by an engineering (quantitative) classification system,
- Engineers prefer numbers in place of descriptions; hence, an engineering classification system has considerable application in an overall assessment of the rock mass quality,
- The classification approach helps in the organization of knowledge and is amazingly successful,

- An ideal application of engineering rock mass classification occurs in the planning of hydroelectric projects, tunnels, caverns, bridges, silos, building complexes, hill roads, rail tunnels and so forth.

There are numerous rock mass classification systems developed up today by different authors: Rock load theory by Terzaghi (1946), Stand up time by Lauffer (1958), Rock Quality Designation (RQD) by Deere et al. (1966), Rock Mass Rating (RMR) system by Bieniawski (1989), Q system by Barton et al. (1974), Slope mass rating (SMR) by Romana (1985), Geological Strength Index (GSI) by Hoek and Brown (1997), Rock Mass index (RMI) by Palmström (1995) and many others. Most of these classification systems were updated and modified during time. A detailed review of custom classification systems and their application was elaborated in detail by Edlbro (2003), Aksoy (2008) and Singh and Goel (2011).



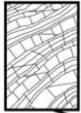
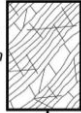

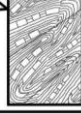
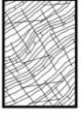
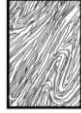
Classification systems are developed for general purposes but also in local rock mass conditions for specific application such as tunnels, slopes, mines and foundations, and input parameters included in these classifications systems significantly vary. Since different classification systems pay attention to different parameters, it is often recommended that at least two methods should be used when classifying a rock mass (Hoek, 2000).

A single classification system cannot describe the rock mass anisotropy and time dependent behaviour. Nor do these systems consider failure mechanisms, deformation or rock reinforcement interaction since they are oversimplified approaches based on too many classifications input parameters to make reliable conclusion (Riedmüller et al., 1999).

Widely used classification, also applied in this research, is Geological Strength Index rock mass classification introduced by Hoek and Brown (1997) for both hard and weak rock mass as complement for their strength criteria. GSI classification provides a system for estimating the reduction in rock mass strength criteria for different geological conditions as identified by field observations (lithology, structure and discontinuities surface conditions). The value of GSI is estimated based in terms of blockness and discontinuity conditions of rock mass. Structure can vary from intact or massive to laminated or sheared rock mass while discontinuity conditions can vary from very good to very poor surface condition. GSI classification is simple, fast, reliable and based on the visual inspection of geological condition.

To estimate geotechnical properties of heterogeneous rock mass such as flysch, a methodology for estimating the GSI and the rock mass properties for these geological formations are presented by Marinos and Hoek (2001). A chart for estimating the GSI value for heterogeneous rock masses such as flysch is presented in Table 2.3.

Table 2.3 GSI estimate for heterogeneous rock masses such as flysch (Marinos and Hoek, 2001)

GSI FOR HETEROGENEOUS ROCK MASSES SUCH AS FLYSCH (Marinos,P and Hoek. E, 2000)		SURFACE CONDITIONS OF DISCONTINUITIES (Predominantly bedding planes)		COMPOSITION AND STRUCTURE							
From a description of the lithology, structure and surface conditions (particularly of the bedding planes), choose a box in the chart. Locate the position in the box that corresponds to the condition of the discontinuities and estimate the average value of GSI from the contours. Do not attempt to be too precise. Quoting a range from 33 to 37 is more realistic than giving GSI = 35. Note that the Hoek-Brown criterion does not apply to structurally controlled failures. Where unfavourably oriented continuous weak planar discontinuities are present, these will dominate the behaviour of the rock mass. The strength of some rock masses is reduced by the presence of groundwater and this can be allowed for by a slight shift to the right in the columns for fair, poor and very poor conditions. Water pressure does not change the value of GSI and it is dealt with by using effective stress analysis.		VERY GOOD - Very rough, fresh unweathered surfaces		GOOD - Rough, slightly weathered surfaces		FAIR - Smooth, moderately weathered and altered surfaces		POOR - Very smooth, occasionally slickensided surfaces with compact coatings or fillings with angular fragments		VERY POOR - Very smooth slickensided or highly weathered surfaces with soft clay coatings or fillings	
 <p>A. Thick bedded, very blocky sandstone The effect of pelitic coatings on the bedding planes is minimized by the confinement of the rock mass. In shallow tunnels or slopes these bedding planes may cause structurally controlled instability.</p>		70 60		A							
 <p>B. Sandstone with thin inter-layers of siltstone</p>				50 40		B		C		D	
 <p>C. Sandstone and siltstone in similar amounts</p>											
 <p>D. Siltstone or silty shale with sandstone layers</p>											
 <p>E. Weak siltstone or clayey shale with sandstone layers</p>											
C,D, E and G - may be more or less folded than illustrated but this does not change the strength. Tectonic deformation, faulting and loss of continuity moves these categories to F and H.						30					
 <p>F. Tectonically deformed, intensively folded/faulted, sheared clayey shale or siltstone with broken and deformed sandstone layers forming an almost chaotic structure</p>								20		F	
 <p>G. Undisturbed silty or clayey shale with or without a few very thin sandstone layers</p>										G	
 <p>H. Tectonically deformed silty or clayey shale forming a chaotic structure with pockets of clay. Thin layers of sandstone are transformed into small rock pieces.</p>										H 10	

→ : Means deformation after tectonic disturbance

To apply Hoek and Brown strength criterion to rock masses such as flysch two other parameters apart from GSI value are required:

- The uniaxial compressive strength (UCS) σ_{ci} ,
- The constant m_i .

Uniaxial compressive strength (UCS) of the intact rock is in most cases obtained by laboratory testing, but in heterogeneous and weathered rock masses such as flysch it is very difficult to obtain intact specimen from geotechnical boring to provide these tests in laboratory (Hoek and Marinos, 2001). These specimens are especially hard to sample in disintegrated rock mass such as highly to moderately weathered siltstones.

Almost every sample obtained from rock masses in these conditions will contain discontinuities in the form of bedding and schistosity planes or joints. Consequently,

any laboratory tests carried out on core samples will result in a strength value that is lower than the uniaxial compressive strength σ_{ci} required for input into the Hoek-Brown criterion. Using the results of such tests will impose a double penalty on the strength (in addition to that imposed by GSI) and will give unrealistically low values for the rock mass strength (Hoek and Marinos, 2001).

To obtain uniaxial compressive strength in such conditions it is possible to carry out tests in large-scale triaxial test facilities on rock mass (instead of rock specimens) but only in cases where rock mass is very closely jointed and where there is possibility to obtain undisturbed samples (Jaeger, 1971).

The other possibility is to use Point Load Test (PLT) in which load can be applied normally to the bedding (Hoek and Marinos, 2001). It is recommended to use PLT in the field on samples immediately after boring and sampling to avoid further weathering and strength reduction. A disadvantage of PLTs is the large dispersion of test results, which occurs especially in weak rock masses such as flysch. This dispersion of results is caused by rock mass layers, layer orientation during sampling and sample size, and the weathering of flysch rock mass. However, regardless of its disadvantages, the use of the point load test method is recommended when there is a lack of more reliable testing, a lack of appropriate representative samples, and in combination with detailed descriptions of tested samples from the flysch rock mass. The acceptable values of uniaxial strength from PLTs must be based on the statistical mean from numerous tests excluding extreme values (Arbanas et al., 2008b).

Where it is not possible to obtain samples for PLT, the only remaining alternative is to turn to a qualitative description of the rock material in order to estimate the uniaxial

compressive strength of the intact rock. A table listing such a qualitative description is given in Table 2.4 based on Hoek and Brown (1997).

Table 2.4 Field estimates of uniaxial compressive strength of intact rock (Hoek and Marinos, 2001)

Grade*	Term	Uniaxial Comp. Strength (MPa)	Point Load Index (MPa)	Field estimate of strength	Examples
R6	Extremely Strong	> 250	>10	Specimen can only be chipped with a geological hammer	Fresh basalt, chert, diabase, gneiss, granite, quartzite
R5	Very strong	100 - 250	4 - 10	Specimen requires many blows of a geological hammer to fracture it	Amphibolite, sandstone, basalt, gabbro, gneiss, granodiorite, peridotite , rhyolite, tuff
R4	Strong	50 - 100	2 - 4	Specimen requires more than one blow of a geological hammer to fracture it	Limestone, marble, sandstone, schist
R3	Medium strong	25 - 50	1 - 2	Cannot be scraped or peeled with a pocket knife, specimen can be fractured with a single blow from a geological hammer	Concete, phyllite, schist, siltstone
R2	Weak	5 - 25	**	Can be peeled with a pocket knife with difficulty, shallow indentation made by firm blow with point of a geological hammer	Chalk, claystone, potash, marl, siltstone, shale, rocksalt,
R1	Very weak	1 - 5	**	Crumbles under firm blows with point of a geological hammer, can be peeled by a pocket knife	Highly weathered or altered rock, shale
R0	Extremely weak	0.25 - 1	**	Indented by thumbnail	Stiff fault gouge

* Grade according to Brown (1981).

** Point load tests on rocks with a uniaxial compressive strength below 25 MPa are likely to yield highly ambiguous results.

The second parameter, constant m_i , defines the frictional characteristics of the component minerals in the rock mass. This constant can only be determined by triaxial testing on core samples, or estimated from a qualitative description of the rock material as described by Hoek and Brown (1997). This parameter depends upon the frictional characteristics of the component minerals in the intact rock sample and it has a significant influence on the strength characteristics of rock (Hoek and Marinos, 2001). In case that triaxial testing is not possible an estimate of constant m_i can be obtained from Table 2.5.

Table 2.5 Values of the constant m_i (Hoek and Marinos, 2001)

Rock type	Class	Group	Texture			
			Coarse	Medium	Fine	Very fine
SEDIMENTARY	Clastic		Conglomerates (21 ± 3) Breccias (19 ± 5)	Sandstones 17 ± 4	Siltstones 7 ± 2 Greywackes (18 ± 3)	Claystones 4 ± 2 Shales (6 ± 2) Marls (7 ± 2)
		Non-Clastic	Carbonates	Crystalline Limestone (12 ± 3)	Sparitic Limestones (10 ± 2)	Micritic Limestones (9 ± 2)
	Evaporites			Gypsum 8 ± 2	Anhydrite 12 ± 2	
	Organic					Chalk 7 ± 2
METAMORPHIC	Non Foliated		Marble 9 ± 3	Hornfels (19 ± 4) Metasandstone (19 ± 3)	Quartzites 20 ± 3	
	Slightly foliated		Migmatite (29 ± 3)	Amphibolites 26 ± 6	Gneiss 28 ± 5	
	Foliated*			Schists 12 ± 3	Phyllites (7 ± 3)	Slates 7 ± 4
IGNEOUS	Plutonic	Light	Granite 32 ± 3 Granodiorite (29 ± 3)	Diorite 25 ± 5		
		Dark	Gabbro 27 ± 3 Norite 20 ± 5	Dolerite (16 ± 5)		
	Hypabyssal		Porphyries (20 ± 5)		Diabase (15 ± 5)	Peridotite (25 ± 5)
	Volcanic	Lava	Rhyolite (25 ± 5) Andesite 25 ± 5		Dacite (25 ± 3) Basalt (25 ± 5)	
		Pyroclastic	Agglomerate (19 ± 3)	Volcanic breccia (19 ± 5)	Tuff (13 ± 5)	

* These values are for intact rock specimens tested normal to bedding or foliation. The value of m_i will be significantly different if failure occurs along a weakness plane.

Engineering geological classification of weak rock mass was studied in detail by Nickmann et al. (2006) where a practicable method for testing and a new classification system for weak rock mass was introduced. Over 40 types of rocks from 7 different locations were tested. The test program from this study contains testing methods from rock mechanics as well as from soil mechanics domains (determining the slake durability, mineralogical and petrographical testing, determining petrophysical properties, determining the strength). Based on a 3-cyclic wetting-

drying-test, crystallization test and pore volume, a new classification system of weak rock was developed and 7 categories of durability (VK) were introduced - Table 2.6.

Table 2.6 Classification of weak rocks based on the behaviour in the 3-cyclic wetting-drying-test and the crystallization test (Nickmann et al., 2006)

VK	I _v	class	Description
VK 0	285-300	Hard rock	No change up to the 3 rd wetting-drying-cycle, maybe small losses because of loosened aggregates during sample preparation (< 5 %), no reaction in the crystallisation test (loss < 10 %)
VK 1	195-285	Low slake durability	No change up to the 3 rd wetting-drying-cycle, maybe small losses because of loosened aggregates during sample preparation (< 5 %), losses in the crystallisation test > 10%
VK 2	145-195	Slow slake durability	No reaction during 1 st wetting, up to the 3 rd cycle cracking and /or beginning of decay up to 50 % of the original mass
VK 3	92,5-145	Medium slake durability	During 1 st wetting cracking or loss of smaller aggregates (max. 10 % of mass), but the sample remains preserved. Up to the 3 rd cycle decay into aggregates > 2,5 % of the original mass
VK 4	27,5-92,5	Rapid and high slake durability	During 1 st wetting disintegration up to 75 %, up to the 3 rd cycle decay into aggregates < 2,5 % of the original mass
VK 5	< 27,5	Immediate and very high slake durability	Spontaneous decay into aggregates < 25 % during 1 st wetting, up to the 3 rd cycle into flakes < 0,1 %

Detailed classification and description should be conducted on weak rocks and on weathering grade to ensure enough input information for further estimation of strength and deformability parameters.

2.4. Strength criteria

Knowledge of failure criteria of materials is one of the crucial steps in performing geotechnical stability design. The strength of the rock mass is conducted by the combined strength of the intact rock and the various discontinuities in the rock mass, while the strength criteria in soil mechanics depends on cohesion and internal friction angle.

Failure in the materials can generally be divided into two main groups based on its characteristics; the ductile and the brittle behaviour. Weathered and weak rocks and rock masses are classified as ductile manner of failure.

Tensile failure occurs in the rock mass when the absolute value of the minor principal stress σ_3 is less than the absolute value of the tensile strength of the rock mass σ_{tm} .

The tensile strength of discontinuities and rock masses is normally assumed to be zero (Edelbro, 2003).

The Mohr-Coulomb failure criterion is generally used in soil mechanics but is also applied in rock mechanics for shear failure in rock, rock joints and rock masses. One of the reasons that Mohr-Coulomb criterion is often used in rock mechanics is that it is described by simple mathematical expression, is easily understood and simple to use (Edelbro, 2003).

Charles-Augustin de Coulomb (1773) introduced a strength criterion based on research on shear failure of glass and around the end of the 19th century Christian Otto Mohr developed a generalised form of the theory often referred to as the Mohr-Coulomb criterion. Mohr-Coulomb equation is written in the form:

$$\tau_f = c + \sigma_n \cdot \tan\varphi \quad (3.1)$$

where

- τ_f is the shear stress along the shear plane at failure,
- c is the cohesion,
- σ_n is the normal stress acting on the shear plane,
- φ is the friction angle of the shear plane.

The criterion assumes that failure occurs along a plane without any dilatation.

During the 20th century a number of empirical strength criteria of intact rock have been published based on empirical studies. These empirical failure criteria have been proposed based on laboratory tests of rock specimens. One of the widely used criteria

that have great practical experience is the Hoek-Brown criterion (Hoek and Brown, 1980) and has been updated and re-developed during years (Hoek et al., 1992).

Rock mass failure criteria are based on large-scale and laboratory testing, experience and back analysis. Most widely used rock mass criteria are those established by Hoek and Brown (1980), Yudhbir et al. (1983), Sheorey et al. (1989) and Rammamurthy (1995).

The most well known and widely used is the Hoek-Brown criterion that has been updated in 1983, 1988, 1992, 1995, 1997, 2001 and 2002. Although the original Hoek-Brown criterion used RMR classification system (Bieniawski, 1989), later in the generalised Hoek-Brown criterion the GSI classification was introduced (Hoek and Brown, 1997).

The original Hoek-Brown failure criterion (Hoek and Brown, 1980) was developed both for the intact rock and rock masses. The peak triaxial strength of a wide range of rock materials could be represented by expression:

$$\sigma_1 = \sigma_3 + \sqrt{m \cdot \sigma_3 \cdot \sigma_{ci} + s \cdot \sigma_{ci}^2} \quad (3.2)$$

where

- m and s are constants which depend on the properties of the rock,
- σ_1 and σ_3 are major and minor principal stresses at failure.

The unconfined compressive strength of rock masses is expressed as:

$$\sigma_{cm} = \sigma_c \cdot s^{\frac{1}{2}} \quad (3.3)$$

Hoek and Brown (1988a) presented the updated Hoek-Brown failure criterion where the concept of disturbed and undisturbed rock mass was introduced. The modified Hoek-Brown failure criterion for jointed rock masses, presented by Hoek et al. (1992), was a re-formulation that should predict a tensile strength of zero. The modified criterion can be written in the following form:

$$\sigma_1' = \sigma_3' + \sigma_c \left(m_b \frac{\sigma_3'}{\sigma_c} \right)^a \quad (3.4)$$

where

- m_b and a are constants for the broken rock.

A general form of the Hoek-Brown failure criterion was presented by Hoek et al. (1995). This failure criterion incorporates both the original and the modified criterion for fair to very poor rock masses, and the GSI classification was implemented instead of the RMR classification system. The generalised Hoek-Brown criterion is given by expression:

$$\sigma_1' = \sigma_3' + \sigma_c \left(m_b \frac{\sigma_3'}{\sigma_c} + s \right)^a \quad (3.5)$$

In the 2002 edition of the Hoek-Brown failure criterion (Hoek et al., 2002), the general expression (3.5) was used, but modifications of the m_b , s and a values were modified as follows:

$$m_b = m_i \exp\left(\frac{GSI-100}{28-14D}\right) \quad (3.6)$$

$$s = \exp\left(\frac{GSI-100}{9-3D}\right) \quad (3.7)$$

$$a = \frac{1}{2} + \frac{1}{6}(e^{-GSI/15} - e^{-20/3}) \quad (3.8)$$

The suggested value of the disturbance factor of is $D=0$ for undisturbed in-situ rock mass and $D=1$ for disturbed rock mass properties.

The effects of loading rate on the compressive strength and deformability of intact rocks have been recognized by several authors (Kumar, 1968; Farmer, 1983; Jaeger and Cook, 1979; Cristescu and Hunsche, 1998). A primary concern of the rate-dependent effect arises when the laboratory-determined properties of intact rock are applied to the design and stability analysis of rock under in-situ conditions. The strength and elastic properties obtained from laboratory testing under a relatively high loading rate, normally about 0.5–1.0 MPa per second tend to be greater than those of in-situ rocks during excavations or constructions. This may lead to a non-conservative analysis and design of the relevant geologic structures (Fuenkajorn et al., 2012).

Okubo et al. (1992), Ishizuka et al. (1993), Ray et al. (1999), Li and Xia (2000), Kohmura and Inada (2006) and Fuenkajorn et al. (2012) concluded from their experimental results that uniaxial compressive rock strengths tend to increase with strain and loading rates, respectively.

In flysch rock mass where weathering processes are emphasized, fresh rock mass transforms into residual soil, both strength failure criterion for soil and rock should be used. Implementation of failure criterion for these materials and its degradation with depth and weathering grade should be further investigated.

Experimental evidence (Kranz et al., 1982) indicated that rock under load shows a decrease in strength with time. Fakhimi and Fairhurst (1994) modelled the time dependent degradation of material strength by exponential friction and cohesion decay functions. Aydan et al. (1996) simulated the time dependent behaviour of squeezing rocks as the degradation of strength properties as a function of time by utilising information obtained from creep tests.

2.5. Deformability

The modulus of deformability is a widely used parameter and it best represents behaviour of a rock mass. During excavation stress, the state of rock mass is changed in accordance to in-situ state, and stress redistribution in a function of deformation modulus causes deformations of rock mass and its reinforcing system.

Deformability is characterized by a modulus describing the relationship between the applied load and the resulting strain. The fact that jointed rock masses do not behave elastically has prompted the usage of the term modulus of deformation rather than modulus of elasticity or Young's modulus (Palmström and Singh, 2001).

The commission of terminology, symbols and graphic representation of the International Society for Rock Mechanics (ISRM) gave the following definitions (ISRM, 1975):

- Modulus of elasticity or Young's modulus E : The ratio of stress to corresponding strain below the proportionality limit of a material,
- Modulus of deformation of a rock mass E_m : The ratio of stress p to corresponding strain during loading of a rock mass, including elastic and inelastic behaviour w_d – Figure 2.3.,
- Modulus of elasticity of a rock mass E_{em} : The ratio of stress p to corresponding strain during loading of a rock mass, including only the elastic behaviour w_e – Figure 2.3..

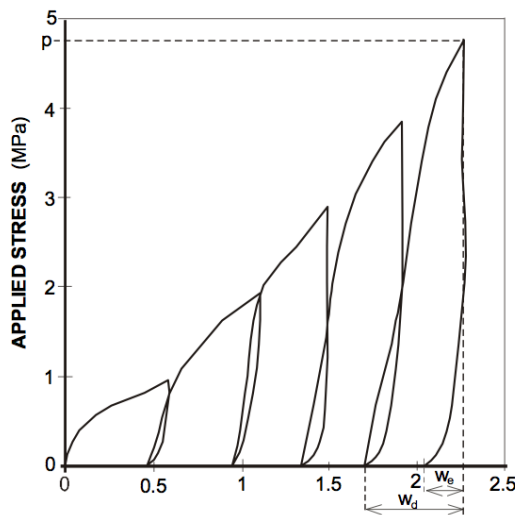


Figure 2.3 Typical stress vs. deformation curve recorded in a deformability test of a rock mass (Palmström and Singh, 2001)

The most accurate methods for determining deformation modulus of rock mass are direct in-situ measurement methods. These methods are mostly conducted in special test adits or drifts and initial preparation of these adits depends on local geological conditions. Following tests are mostly used to determine the deformation modulus of rock mass nowadays:

- Plate jacking test (PJT),
- Plate loading test (PLT),

- Radial jacking test or Goodman jack test.

In addition to these test types, the following in-situ deformation tests can be used:

- Flat jack test,
- Cable jacking test,
- Radial jack test,
- Dilatometer test,
- Pressure chamber.

In-situ measurement methods are quite time-consuming, expensive and difficult to conduct. Because of that the value of the modulus of deformation is often estimated indirectly from observations or relevant rock mass parameters that can be acquired easily and at low costs (Palmström and Singh, 2001). There are many correlations between rock mass classification systems and the modulus of deformation investigated by Bieniawski (1978), Serafim and Pereira (1983), Grimstad and Barton (1993), Clerici (1993), Palmström (1995), Hoek and Brown (1998b), Read et al. (1999), Barton (2000), Hoek et al. (2002) and many others.

Detailed comparison between in-situ tests and indirect estimates were researched by Palmström and Singh (2001) and it was found that the deformation modulus calculated from classification systems seems is valid only for the strongest rocks and that they give significantly higher values for weak rocks than the real values (Arbanas et al., 2005).

The effect of Poisson's ratio is one of the parameters used for the calculation of modulus value in an in-situ test. Sharma and Singh (1989) found that it is not much

variation in the values of the deformation modulus if the value of the Poisson's ratio is between 0.1 and 0.35.

It was found that elastic moduli E increase with increasing confining pressure (Maranini and Brignoli, 1999; Santarelli and Brown, 1989; Yang and Jiang, 2010). Yang and Jiang (2010) have performed short-term triaxial tests on sandstone and have confirmed earlier state that both the modulus of elasticity and deformation increase with increasing of confining pressure. Results are presented at Figure 2.4 and Table 2.7.

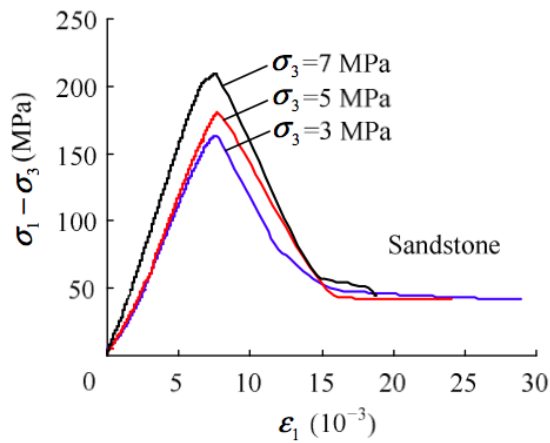


Figure 2.4 Typical short-term stress-strain curves of sandstone under different confining pressure (Yang and Jiang, 2010)

Table 2.7 Short-term mechanical parameters of sandstone under different confining pressure (Yang and Jiang, 2010)

σ_3 (MPa)	σ_c (MPa)	ε_{1c} (10^{-3})	E_S (GPa)	E_{S0} (GPa)	σ_r (MPa)
3	163.6	7.625	25.77	21.41	43.0
5	180.7	7.670	27.73	22.68	42.2
7	209.6	7.556	32.63	30.91	44.7

The results made by Fuenkajorn et al. (2012) indicate that the elastic modulus and failure stresses increase with the loading rates. They concluded that both Poisson ratio and elastic modulus tend to be independent of the confining pressures. This is in contrast with previously mentioned researches (Maranini and Brignoli, 1999; Santarelli and Brown, 1989; Yang and Jiang, 2010).

2.6. In-situ stress condition

Rock at any depth is subjected to stresses resulting from the weight of the overlying strata and from locked in stresses of tectonic origin. During the excavation the stress field is locally disrupted and a new set of stresses is induced in the surrounding rock. Knowledge of the magnitudes and directions of these in-situ and induced stresses is an essential component for excavation design (Grošić et al., 2013).

Measurements of vertical stresses confirmed assumption that the vertical stress is approximately equal to depth times unit weight of rock mass. Horizontal stresses of rock mass at specific depth are much more difficult to estimate than the vertical stresses.

There are two basic assumptions when estimating the state of stress at any depth z in a rock mass. The first one is the assumption of predicting a vertical stress component σ_v due to weight of overlaying rock mass. The second assumption is estimating horizontal stress component $\sigma_h = K_0 \sigma_H$ which is taken equal to coefficient K_0 multiplied by vertical stress σ_v .

Different expressions for the horizontal stresses in rock mass have been proposed in the literature by many authors: Terzaghi and Richart (1952), Talobre (1967), Brown and Hoek (1978), Herget (1988), Sheorey (1994) and others. Most of these

expressions were based on worldwide stress measurements in mining and civil engineering projects.

In many cases it is shown that horizontal stresses are equal or rather even several times greater than vertical stresses: Terzagi and Richart (1952), Isaacson (1957), Terzaghi (1962), Martinetti and Ribacchi (1980), Rummel et al. (1986), Cooling et al. (1988), Ribacchi (1988), Cristescu (1989), Hyett and Hudson (1989), Zoback (1992) and others. According to Aytmatov (1986), stress measurements conducted in different parts of the world have shown that the horizontal stresses exceed the vertical stresses in 65-70% of the cases.

In weak and highly fractured rock masses, that are accepted to behave as homogeneous and isotropic according to Bray (1967), horizontal stress can be obtained through one of the friction angle methods, such as the simplified form introduced by Jaky (1948).

3. CREEP AND TIME DEPENDENT BEHAVIOUR OF ROCK MASS

3.1. About rheology and creep mechanics

The term rheology was first introduced by E. C. Bingham and M. Reiner inspired by Heraclitus quote “*phanta rei*” that means “*everything flows*”, which was taken to be the motto of the subject. Rheology means the study of the deformation and flow of matter. This definition was accepted when the American Society of Rheology was founded on 29th of April 1929 at Columbus, Ohio (Reiner, 1964).

Two terms often used in rheology are: creep and time dependent behaviour. The term creep is time dependent behaviour of intact rock and is mostly used related to laboratory test of intact rock. On the other hand, the term time dependent behaviour is related with rock mass and its redistribution of stress and strains during time. Creep could be defined as irreversible deformation in time without fracturing and is observed mainly in soft rocks (Cristescu and Hunshe, 1998). Similar definitions were presented by Malan (1999). The term squeezing is connected with tunnels’ behaviour and originates from the pioneering days of tunnelling through the Alps in Europe. It refers to the reduction of the tunnel cross section that occurs as the tunnel is being advanced. Commission of the International Society for Rock Mechanics (ISRM) has described squeezing and the main features of this mechanism, it is agreed that “squeezing of rock” stands for large time dependent convergence during tunnel excavation (Barla et al., 2008).

There are three different phases in creep mechanics: primary, secondary and tertiary creep phase – presented at Figure 3.1. These three phases correspond to decreasing, stationary and increasing creep strain rate, respectively, and were introduced by Andrade (1910). After loading the specimen, there is instantaneous elastic strain followed by the primary creep phase. This phase is recoverable after unloading, but it is a delayed process. After the primary phase, the secondary or stationary creep phase is characterized by a constant creep strain rate. The secondary creep phase is the longest of the entire creep process and can be observed as a linear time strain rate. The tertiary creep phase is the final creep phase and indicates a time dependent deformation associated with crack growth and an increasing creep strain rate.

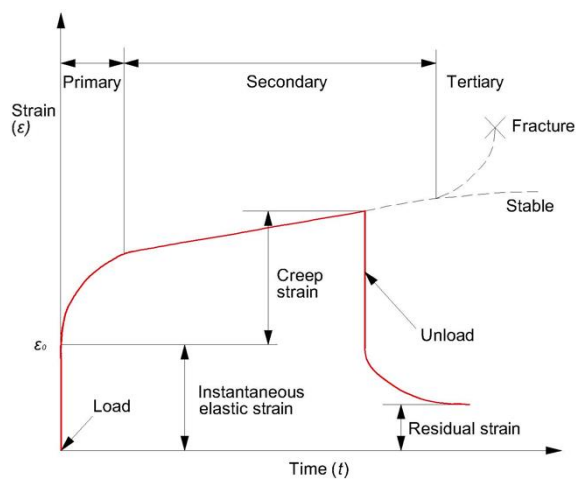


Figure 3.1 Time-strain curve and creep phases for specimen under constant load (Lama and Vutukuri, 1978)

There are several classification and definitions of strains of material that are presented as follows. Based on the small strain assumption and the work done, the total strain is the sum of the elastic and the viscoplastic strains, and can be presented as:

$$\varepsilon_{ij}^t = \varepsilon_{ij}^e + \varepsilon_{ij}^{vp} \quad (4.1)$$

where

- ε_{ij}^t is the second strain tensor of the total strain,
- ε_{ij}^e is the strain tensor of the elastic component,
- ε_{ij}^{vp} is the second strain tensor of the viscoplastic component.

Also, total strain can be presented as a sum of elastic strain and creep strain:

$$\varepsilon_t = \varepsilon_e + \varepsilon_c \quad (4.2)$$

where

- ε_t is total strain,
- ε_e is elastic strain,
- ε_c is creep strain.

By another classification the total strain is the sum of instantaneous strain and creep strain:

$$\varepsilon_t = \varepsilon_0 + \varepsilon_c \quad (4.3)$$

where

- ε_t is total strain,
- ε_0 is instantaneous strain,
- ε_c is creep strain.

When taking into account phases of creep strain, the total creep strain is the sum of primary, secondary and tertiary creep strain:

$$\varepsilon_{ct} = \varepsilon_{cp} + \varepsilon_{cs} + \varepsilon_{ca} \quad (4.4)$$

where

- ε_{ct} is total creep strain,
- ε_{cp} is strain of primary creep phase,
- ε_{cs} is strain of secondary creep phase,
- ε_{ca} is strain of tertiary creep phase.

Time of total creep strain can be divided into three phases as:

$$T_t = T_{cp} + T_{cs} + T_{ca} \quad (4.5)$$

where

- T_t is total time of strain,
- T_{cp} is time of primary creep strain,
- T_{cs} is time of secondary creep strain,
- T_{ca} is time of tertiary creep strain.

3.2. Laboratory tests of creep of intact rock

For the development of reliable laws and constitutive equations to describe creep of intact rock, appropriate laboratory tests should be performed. Most of these tests were developed individually by researchers to fulfil their needs. Standards, suggested methods, or recommendations for experimental procedures and their interpretation are given by several national and international commissions such as International Society for Rock Mechanics, American Society for Testing and Materials, German Geotechnical Society and others. Experimental techniques used in laboratory and their interpretations are presented as follows.

An overview of existing laboratory tests on rocks suitable for the determination of creep properties of intact rock are presented in detail and described by Cristescu and Hunshe (1998) in

Table 3.1.

Table 3.1 Table of laboratory tests on rocks suitable for the determination of creep properties of intact rock
(Cristescu and Hunshe, 1998)

TEST	PURPOSE
quasistatic tests: duration from one minute to several hours, control of stress rate or strain rate, uniaxial or triaxial	strength, deformation behaviour, volume change, elastic moduli, other (deformation) moduli
creep tests: duration hours to years, constant stress and temperature, uniaxial or triaxial	transient and stationary creep, volume change, creep fracture, tertiary creep
relaxation tests: stop of deformation at a certain strain, uniaxial, triaxial	stress relaxation, deformation and transient creep, recovery
stress drop tests: drop of stress difference after some strain, uniaxial and triaxial	deformation and transient creep, recovery, back-stress
direct tension tests: uniaxial or triaxial	tensile strength, deformation
indirect tension tests: Brazilian test, bending test, fracture toughness test	tensile strength, crack growth resistance
torsion test	strength, deformation
shear test	strength, deformation
hydrostatic compaction test	time dependent volume decrease, healing
permeability measurement	permeability
micro acoustic (AE)	crack formation and location, dilatancy
active sonic test	wave velocity, attenuation, dilatancy, healing
unloading, wave velocities	elastic behaviour

Uniaxial test is a common test for investigation of creep of intact rock. This test is carried out with stress or load control with certain rate of stress increase or strain increase. The sample is loaded by a piston and oil pressure in a cylinder controlled by servo control. Screw-driven test rigs are also commonly used instead of oil pressure. Displacements are measured by several LVDTs (Linear Variable Displacement Transducer) or strain gauges attached to the specimen. To monitor the applied stress a coaxial load cell between the sample and the frame base is placed. Oedometers or

dead loads with lever arm are also often used to perform these tests to keep the uniaxial stress constant. Specimens are usually cylindrical, but there are also uniaxial creep tests performed on prismatic specimens (Tomanović, 2009; 2012).

A Modified Point Load (MPL) testing technique is proposed to assess the time dependent properties of rock salt by Samsri et al. (2011). The test apparatus is similar to that of conventional Point Load Test, except that the loading points are cut flat to have a circular cross-sectional area instead of a half-spherical shape. These loading platens apply constant axial loads to the circular disk specimens.

Biaxial test of plate specimens are performed with combination of lever and the dead load system for applying vertical force, while the horizontal force is applied by means of two inter-connected jacks. In this way different ratios of vertical and horizontal pressure can be obtained. This device was used by Tomanović (2009; 2012) for creep testing of marls.

Triaxial tests are mostly used to obtain creep properties of rock. This test better reproduces the state of stress in which material is subjected in-situ. High-precision pumps control the confining pressure, deviatoric pressure and pore pressure while the pressure is automatically regulated by the computer and self-compensated flow pump. Oedometers or dead load with lever arm is also sometimes used to keep axial pressure constant.

At the beginning of the test the confining pressure is applied to the cylindrical sample by the oil hydraulic system, so the sample is set in the hydrostatic stress state. After the specific value of the confining pressure is reached, the axial deviatoric stress is applied and the stress level is maintained. The creep tests are carried out by a multi-step loading procedure. At the same time the axial and lateral deformation of the rock

are measured. To measure deformation of the specimen, strain gauges are commonly used. Strain gauges are attached to the surface of the specimen inside the membrane. Two full bridges are formed by the attached strain gauges to measure axial and circumferential strain. The disadvantage of strain gauges is the possibility to not adhere very well to the specimen.

Okubo et al. (2008) developed a transparent triaxial cell using acrylic resin. The cell was used to conduct strength and creep tests while the specimens were constantly photographed. Developing such cell enables to visually observe how specimen changes over time during strength and creep tests.

Based on the conventional triaxial compression test device, a temperature-controlled triaxial compression and creep test device was developed (Zhang et al., 2010) to investigate the influence of temperature on the mechanical behaviours of soft rocks.

In conventional triaxial compression test both confining and shear stresses vary with each increment of loading, but it is difficult to distinguish the effect of shear and volumetric stresses on the volumetric deformations, which include elastic, plastic and creep components. To avoid and separate the effects of volumetric and shear stress on the volumetric deformation, the pure shear stress path, which has been adopted in recent years to study the mechanical behaviour of rocks in the three-dimensional stress space, is used (Bernabe et al., 1994; Jeng and Huang, 1998; Weng et al., 2005; Hunsche and Albrecht, 1990; Cristescu, 1994; Tsai et al., 2008). In the pure shear stress path test the confining pressure is held constant by decreasing the cell pressure increments to one-half of the increment of the axial stresses.

Besides the conventional triaxial test, there is another technique for triaxial testing: true triaxial test. This test has a great advantage because all kinds of stress histories

can be simulated in very similar way to those that occur in nature. A true triaxial or polyaxial stress loading system was developed in the early 1990s at Imperial College London for determining the ultrasonic velocities and attenuation, fluid permeability and elastic properties of cubic rock specimens of 51 mm-side as they were loaded to failure (King et al., 1995; King, 2002). In 1996 ErgoTech Ltd., Glan Conwy, Wales, UK, modified the original system to accommodate 40 mm side cubic rock specimens (Jing et al., 2002). To enable high pore pressures to be employed, a unique pressure-sealing scheme was devised and a dedicated loading frame was constructed. In 2001 the system was again modified to replace the six ultrasonic transducer holders with those each containing four P-wave acoustic emission (AE) sensors, six of which strategically placed are employed as P-wave transmitters (King et al., 2011).

3.3. Creep of intact rock

In past decades creep of intact rock has been thoroughly investigated and studied by many authors: Phillips (1931), Pomeroy (1956), Bérest et al. (1979), Goodman (1984; 1989), Dusseault and Fordham (1993), Bernabe et al. (1994), Yu and Chern (1994), Cristescu (1989; 1994), Cristescu and Hunsche (1998), Yu (1998), Maranini and Brignoli (1999), Li and Xia (2000), Yahya et al. (2000), Fabre and Pellet (2006), Tsai et al. (2008), Yang and Jiang (2010), Zhang et al. (2012) and others.

Many experimental tests have confirmed various mechanisms of nucleation and growth of micro cracks in brittle rocks. Under compressive stresses, sliding wing cracks seem to be the principal propagation mode of micro cracks (Brace and Bombolakis, 1963; Nemat-Nasser and Horii, 1982; Olsson, 1995). Due to roughness of crack surfaces in geomaterials, crack sliding may induce an associated aperture that

is the origin of volumetric dilatancy in these materials (Wong, 1982; Nemat-Nasser and Obata, 1988).

Dilatancy boundary or compressibility/dilatancy surface represent a boundary between a domain where the volume decreases (compression) and a domain where it increases (dilatancy) under stress. At Figure 3.2 results of true triaxial test with creep phases and dilatancy boundary are presented. The influence of dilatancy boundary on the dilatancy is shown where the rate of volume increase depends on the distance from the dilatancy boundary and failure boundary. During the first two loading steps ($\tau = 3$ and 6 MPa) were below the dilatancy boundary and volume decreases, while at the next two loading steps ($\tau = 9$ and 11 MPa) were above the dilatancy boundary and volume significantly increases.

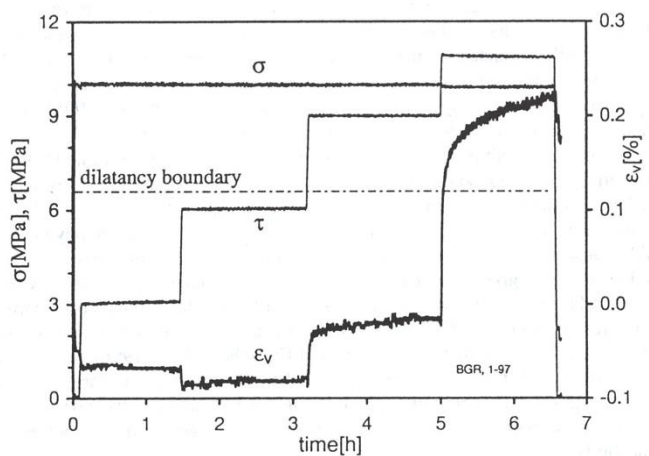


Figure 3.2 Dilatancy boundary and creep phases (Cristescu and Hunsche, 1998)

Experimental results (Bernabe et al., 1994; Jeng et al., 1998; Wang et al., 2005) suggest that rocks can exhibit nonlinear elastic deformation, and coupling between shear stress and elastic volumetric strains, e.g. shear dilation or shear contraction, is obvious. Microscopically, the nonlinear elastic deformation characteristics of rocks are possibly related to the opening and closing of the void space and the micro cracks

in rock during the loading–unloading processes (Cristescu, 2001). Most constitutive models for rocks assume that shear stress will not induce elastic volumetric strain, but this assumption does not conform to the experimental results, especially for weak rocks (Tsai et al., 2008). Tsai et al. (2008) have confirmed the coupling between the pure shear stress and the elastic volumetric behaviour, and described it by a regression function normalized by the confining pressure.

Influence of temperature on creep behaviour is presented at Figure 3.3. Strain vs. time and creep rate vs. time at four different temperature variations are shown for rock salt specimen under uniaxial compression. An increase of 10 K causes an increase of strain rate by about a factor of two.

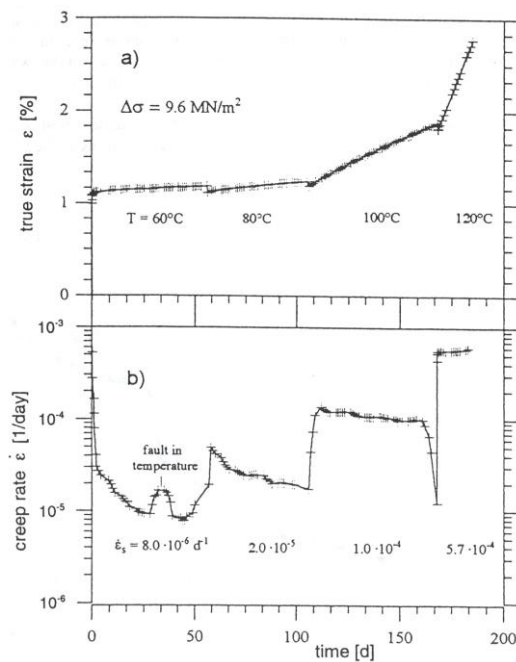


Figure 3.3 Uniaxial creep test with increasing the temperature (Cristescu and Hunsche, 1998)

Strain rate during laboratory tests has significant influence on deformability, strength and creep parameters of rock. If loading is applied at very low strain rate, the limit curve of the rock is obtained. This limit curve theory or concept was firstly introduced

by Bérest et al. (1979). This theory assumes that the loading rate is slow enough to allow the development of viscoplastic strains in real time. This curve is defined by the points reached at the end of each creep or relaxation test – Figure 3.4. For low levels of deviatoric stress, the delayed deformation stabilises asymptotically to a maximum value corresponding to the deformation reached at the same level of stress on the limit curve.

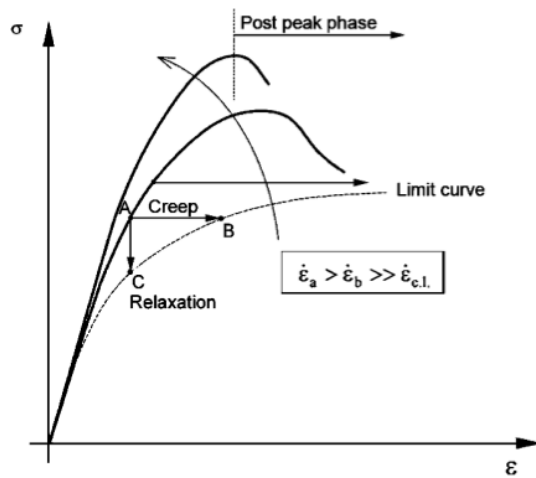


Figure 3.4 The limit curve and its links with creep path (AB) or relaxation path (AC) (Fabre and Pellet, 2006)

Experimental study on the creep behaviour of a porous chalk, named Pietra Leccese, was performed by Maranini and Brignoli (1999). They have concluded that creep contribution to rock deformation increases with confining pressure. At low confining pressure (from 0.0 to 10.0 MPa) samples show significant time dependent behaviour at high deviatoric stresses. At high confining pressure (ranging from 10.0 MPa to 30.0 MPa) creep influence is significant from the beginning of the test.

Fabre and Pellet (2006) have performed creep tests on argillaceous rocks, and among them, uniaxial creep tests have been performed on the Jurassic Mountains marl where multi-stage creep tests highlighted the existence of a stress threshold below which

viscoplastic deformations were stabilised. Depending on the applied deviatoric stress, this threshold is high and close to the rock strength under uniaxial compression.

Stress conditions have an important influence on rock mass deformability and creep parameters. Yang and Jiang (2010) concluded that deformation and elasticity modules of intact rock increase by increasing the adequate confining pressure.

In the conventional prediction of linear creep, creep parameters are assumed to be constant and independent of stress conditions. Creep laboratory tests provided by Goodman (1989), Yu and Chern (1994) and Tsai et al. (2008) have shown that intact rock exhibits non-linear behaviour and is dependent upon stress conditions. The stress strength ratio (SSR) was introduced to present a relationship between the strength of a material and the current stress state (Figure 3.5) and is defined by Yu (1998) as:

$$SSR = \frac{A}{B} = \frac{\frac{\sigma_1 - \sigma_3}{2}}{\frac{\sigma_{1f} - \sigma_3}{2}} = \frac{\sigma_1 - \sigma_3}{\sigma_{1f} - \sigma_3} \quad (4.6)$$

Goodman (1984) noted that if axial stress is lower than 40% of the uniaxial compressive strength, then time dependency is distinguished, and if it is lower than 60% of the uniaxial compressive strength, then the secondary creep phase will not be activated. If the SSR is lower than 0.5, the sample will exhibit an elastic response, and if the SSR is over 0.5, the primary creep stage will begin. When the SSR reaches 0.8, the secondary creep phase will become pronounced. Similar results were obtained by Yu (1998), and those results were implemented in a numerical non-linear creep model to predict the time dependent behaviour of weak rock masses. Creep parameters of intact rock are time dependent, and it is not realistic to keep those characteristics constant through time and independent of the stress state.

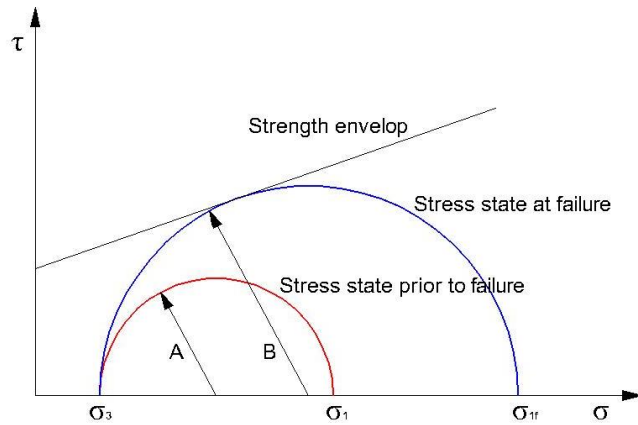


Figure 3.5 The definition of Stress Strength Ratio (SSR) (Yu, 1998)

Secondary creep phase, which is often observed on ice, salt or metallic alloys, is rarely observed during creep test on polycrystalline rocks and even some authors (Gonze, 1988; Dusseault and Fordham, 1993) have expressed doubts as to its existence. They have performed tests on brittle rocks and observed a transition from primary creep to tertiary creep without any stabilisation of the strain rate.

Based on performed triaxial tests by Zhang et al. (2012) it can be found that the steady creep rate increases nonlinearly with deviatoric stress. The effect of confining pressure on steady creep rate is significant. At the same deviatoric stress, if the confining pressure is higher, the steady creep rate is smaller. The impact of the confining pressure on steady creep rate is even more significant at a higher deviatoric stress – Figure 3.6.

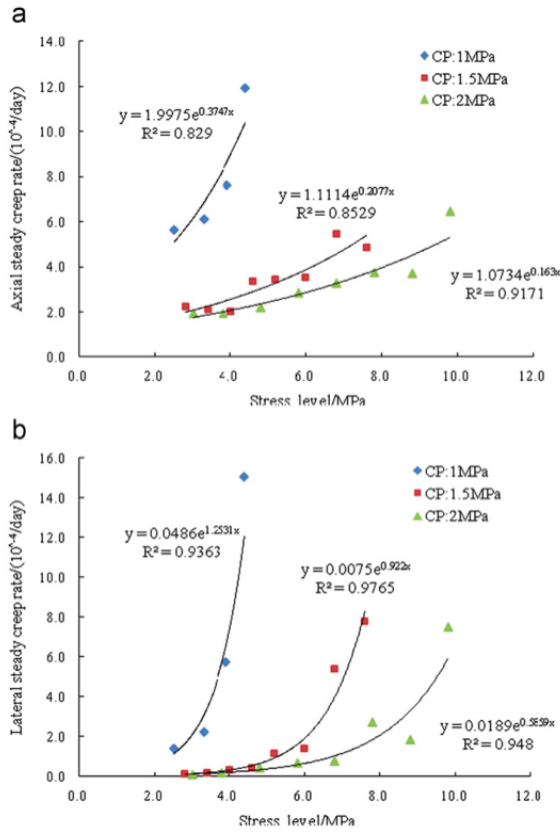


Figure 3.6 Deviatoric pressure vs. axial steady creep rate and vs. lateral steady creep rate (Zhang, 2012)

Tertiary creep of rock is absent before it reaches the failure stress level, showing only two typical stages of “primary creep” and “steady-state creep”. However, under the final failure stress level, tertiary creep is observed under different confining pressures - Figure 3.7.

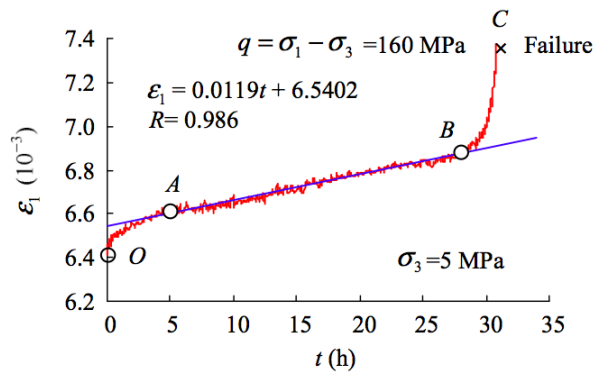


Figure 3.7 Characteristic strain-time creep curve (Yang and Jiang, 2010)

Creep properties of marl or flysch deposits or similar rocks have been researched by several authors: Bergues et al. (1998), Cristescu (1989), Cristescu and Hunsche (1998) and Tomanović (2006; 2009; 2012).

Detailed uniaxial, biaxial and triaxial creep tests of marl, which is a similar rock as flysch deposits at Draga valley, were performed by Tomanović (2006; 2009; 2012). Creep test description and results conducted by Tomanović (2006; 2009; 2012) are presented as follows. The block of marl rock was taken from “Potrlica” Mine in Montenegro at depth of 15-20 m and was of relatively regular dimensions of 380 x 90 x 80 cm. The tested marl contains about 48% CaCO_3 and the content of the insoluble remainder (clayey quartzite) is nearly 52%. Dominant mineral phases are represented with calcite (46-48%) and quartz (12-13%). The sample moisture was 8-11%, the uniaxial strength of the intact rock was about $\sigma_c=8.8$ MPa and the average volume weight was 18.8 kN/m^3 . To minimize and avoid the influence of moisture change and the humidity of the air in the surroundings, the specimens were coated by paraffin.

Uniaxial creep tests were performed on prismatic specimens of 15x15x40 cm each. A lever with dead load was used to ensure constant uniaxial force over time, and each of the devices was equipped with ring load cells. Test equipment is presented at Figure 3.8.



Figure 3.8 Devices for uniaxial creep tests (Tomanović, 2009)

Uniaxial creep tests were performed into three phases: loading, unloading and reloading to a higher level of stress. Total duration of test was 360 days (I phase: 180 days, II phase: 30 days and III phase: 150 days). After loading, the creep deformations were measured in the direction of the vertical (longitudinal) and horizontal specimen axes (on four unloaded sides of the specimen) by mechanical deformation meter with accuracy of 1/1000 mm. Measuring was performed at 1, 3, 6, 12 and 24 hours after loading, then after 3, 7 and 15 days, and in the remaining period every 30 days.

The results of these uniaxial creep tests at an axial stress of 2.0 MPa (25% of UCS) and 4.0 MPa (50% of UCS) are shown at Figure 3.9. Test results have showed the zone of intensive creep in the first 20 days after loading. After this period the creep strain increases linearly. It was also noticed that the creep strain increases with stress level. In unloading creep tests the reverse creep behaviour is obtained. The value of reverse creep strain is significant in comparison with instantaneous elastic strains. Most of reverse creep strain occurred in first 5 days of unloading.

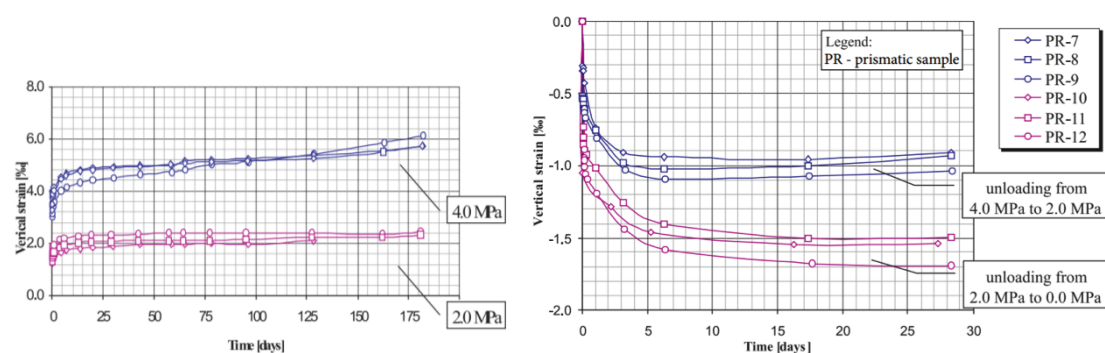


Figure 3.9 Uniaxial creep test results under different stresses (left) and comparative creep diagram after unloading in axial direction (right) (Tomanović, 2009)

Biaxial creep tests were performed on the plate specimens with dead load for uniaxial load and two inter-connected presses for horizontal load. The plate specimens were loaded under uniaxial and biaxial direction with load increments of 0.5 MPa in the

period of an hour to a vertical stress of 2.0 MPa (25% of UCS). The ratio of the horizontal and vertical stress of $K = 0.3, 0.5$ and 1.0 was varied. The measurement of creep strains were performed on the network of measuring spots 1, 6 and 24 hours after loading, then after 3 and 7 days and in the following period every 15 days.

Before performing biaxial creep tests of plate specimens, uniaxial creep tests were performed on marl specimens to compare results with uniaxial creep tests of prismatic specimens - Figure 3.9. The measured strains at same stress level are bigger on plate specimens than on prismatic ones. After 30 days of loading, the ratio between strains of plate and prismatic specimens is about 1.85. According to results presented at Figure 3.10 it could be noticed that with increasing of vertical creep strain horizontal strain reduces after certain time of loading, while vertical creep strain continues to increase.

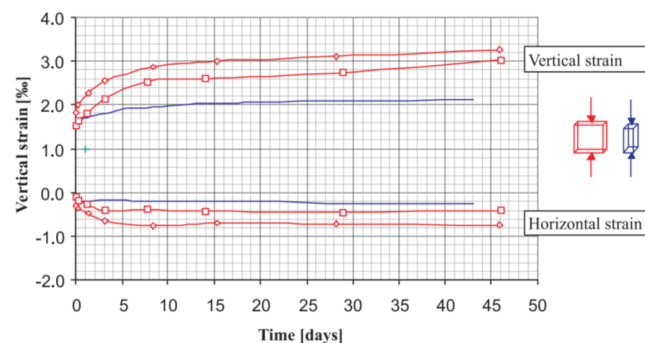


Figure 3.10 Diagram of creep uniaxial test of prismatic and plate specimens (Tomanović, 2009)

At biaxial creep tests of plate specimens with $K = 1.0$ the strain very slightly differs according to results of uniaxial creep tests on prismatic specimens - Figure 3.11a. The increase in the time strain was slightly bigger with the plate specimens compared to the prismatic specimens 10-15 days after loading. A larger increase of creep strains was a consequence of larger secondary creep with the plate specimens (secondary

creep becomes more important as the time passes, while primary creep had practically no further influence after a period of 10 days).

With a reduction of the relation K value, an increase of the initial and time dependent vertical strain was noted. The horizontal strain at biaxial tests showed fluctuations in the first 5-7 days after loading. In the further period the creep strain in the horizontal direction could be registered only for specimens loaded with $K = 1.0$.

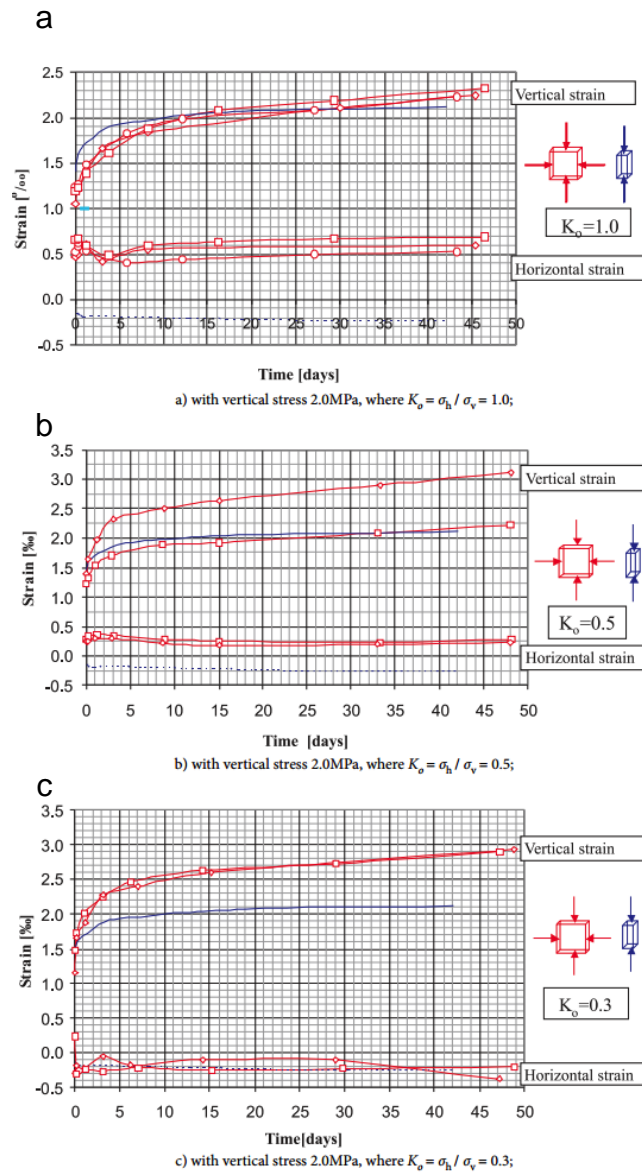


Figure 3.11 Diagram of creep biaxial test of plate specimens; (a) with vertical stress 2.0 MPa, where $K_0 = 1.0$; (b) with vertical stress 2.0 MPa, where $K_0 = 0.0$; (c) with vertical stress 2.0 MPa, where $K_0 = 0.3$ (Tomanović, 2009)

Triaxial tests were performed with different confining pressure in the standard Hook's cell with strain gauges and rosettes to measure strains in two directions. A conventional triaxial creep test helps to investigate the influence of the confining pressure. Lateral pressure in triaxial creep tests did not exceed the value of 50% UCS. Triaxial creep tests lasted for 7 days. Results of the triaxial creep test are presented at Figure 3.12. The full lines indicate the axial strain while the dashed lines indicated the tangential (horizontal) strain. It is shown that the radial deformation one day after loading preserves the obtained level, while the axial deformation indicates the presence of the influence of the confining pressure on the flow of time creep.

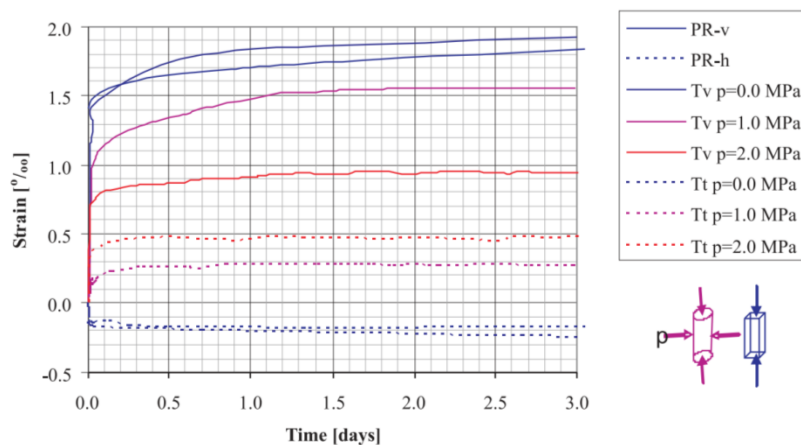


Figure 3.12 Diagram of creep triaxial test (Tomanović, 2009)

Tomanović (2012) has also obtained the dependence of the initial modulus of deformability of marls on the lateral pressure and found that even at domain of low stresses elastic modulus is stress-dependent. An expression is obtained by replacing the Young's modulus of elasticity E with the stress-dependent modulus of elasticity. Similar stress dependence of elastic modulus was observed on other types of rocks by

Maranini and Brignoli (1999), Santarelli and Brown (1989) and Yang and Jiang (2010).

3.4. In-situ creep test of rock mass

Creep properties of intact rock could significantly vary from creep properties of rock mass from which the specimens of rock are sampled. This is due to the high complexity and in-homogeneity of in-situ rock mass. To obtain creep parameters of in-situ rock mass, one of the in-situ creep test methods that encompass bigger volume of rock mass should be used. Field testing on a large volume of rock mass is often used as an alternative to overcome the size effect to some degree (Yu, 1998). Following tests are nowadays common in practice:

- The borehole dilatometer test,
- The plate loading test,
- The triaxial test.

The borehole dilatometer test is a simple and cost effective field test and is fairly common. The dilatometer consists of a cylindrical, radially expandable borehole probe used mainly to determine the short-term deformability of rock mass but with some modification is extended to the measurement of the creep properties of rock mass. The dilatometer probe basically consists of a portable membrane made of flexible material mounted on heat-treated, stainless steel ends. The data obtained during the tests are used to construct the pressure versus injected volume curves from which the deformability and/or creep parameters can be determined (Roctest, 2008). Typical borehole dilatometer equipment is presented at Figure 3.13.

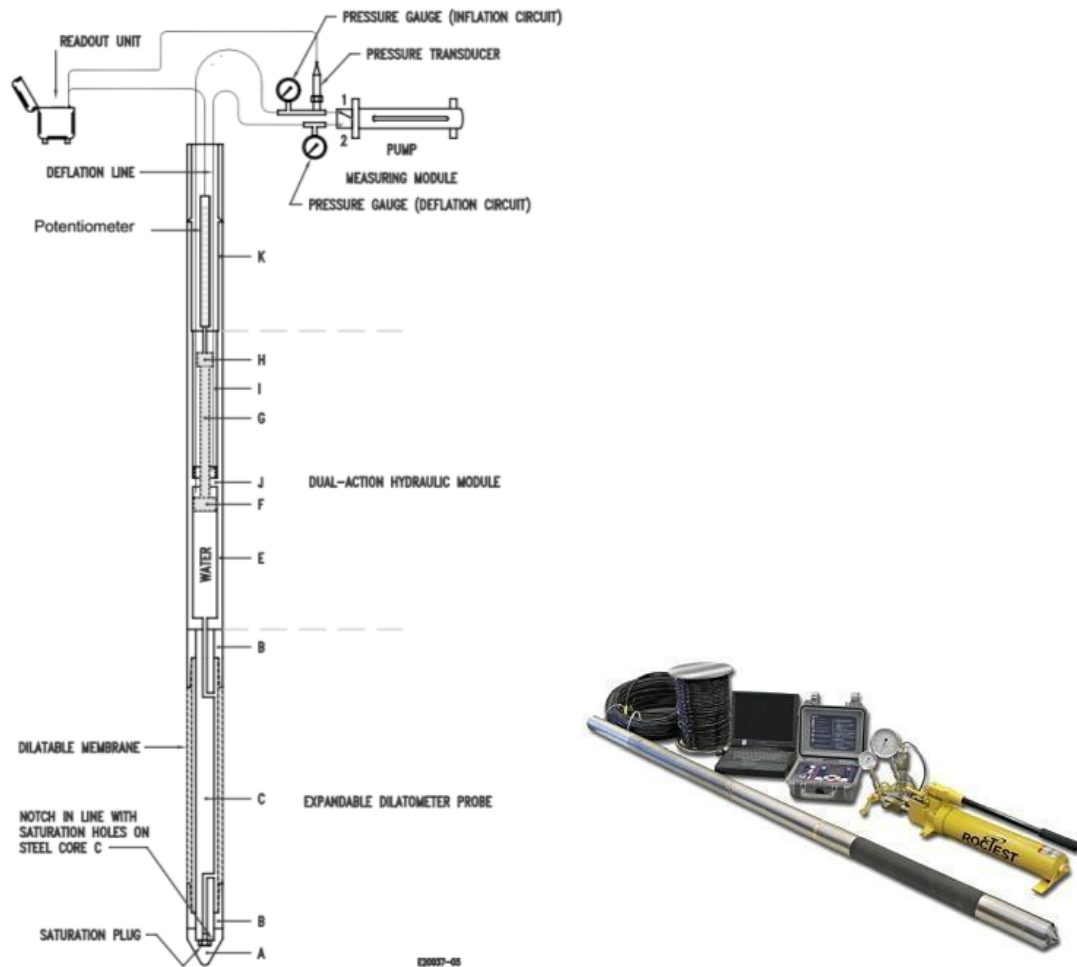


Figure 3.13 Typical borehole dilatometer test equipment (Roctest, 2008)

The general plot for a borehole dilatometer test under creep conditions is presented at Figure 3.14. The radial outward deformation is plotted against time at a fixed inner dilatometer pressure. Instantaneous deformation occurs immediately after loading and is denoted as u_0 . Further deformation denoted as u_B is defined as creep deformation and is represented as a sum of primary and secondary creep phase deformation.

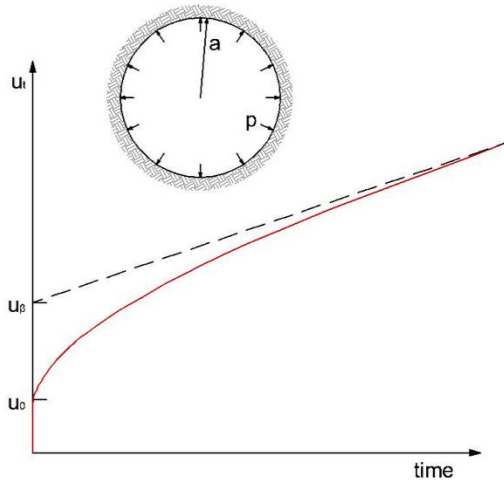


Figure 3.14 Radial deformation vs. time in the borehole dilatometer test (Goodman, 1989)

The radial deformation versus time relationship can be expressed through Burger's creep model as:

$$\bar{u}_r(t) = \frac{pa}{2} \left[\frac{1}{G_m} + \frac{1}{G_k} \left(1 - e^{-\frac{G_k t}{\eta_k}} + \frac{t}{\eta_m} \right) \right] \quad (4.7)$$

where

- $\bar{u}_r(t)$ is time dependent radial deformation,
- p is the applied radial pressure,
- a is the radius of the borehole,
- t is time of the test,
- G_m is the shear modulus of the spring in the Maxwell fluid,
- G_k is the shear modulus of the spring in the Kelvin solid,
- η_m is the viscosity coefficient of the dash pot in the Maxwell fluid,
- η_k is the viscosity coefficient of the dash pot in the Kelvin solid.

When $t = 0$ the instantaneous radial deformation can be expressed as:

$$\bar{u}_0 = \frac{pa}{2} \left(\frac{1}{G_m} \right) \quad (4.8)$$

The plate loading test is commonly used to determine creep properties of creep parameters of rock mass - Figure 3.15. The advantage of plate loading test is that larger volume of rock mass is encompassed than in the dilatometer borehole test, but the test is more expensive. The plate loading test is described by ASTM D4533-02 (ASTM, 2002). Results of this method are used to predict time dependent deformation characteristics of a rock mass resulting from loading. The test is conducted in an underground opening parallel or perpendicular to the anticipated axis of thrust. The two faces are rapidly loaded to the desired creep load, the load is maintained and the displacement of the plate is measured as a function of time (ASTM, 2002).

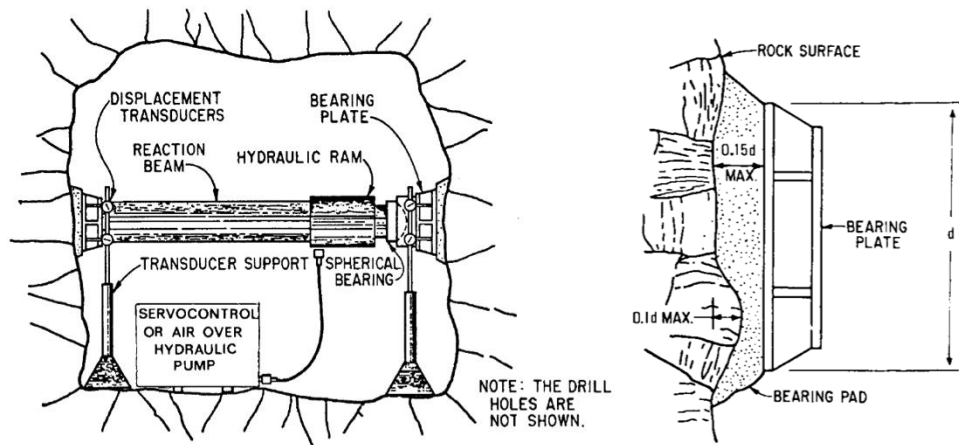


Figure 3.15 Typical rigid plate bearing test setup schematic (ASTM, 2002)

The settlement versus time relationship can be expressed through Burger creep model as:

$$\bar{u}(t) = \frac{1.70pa}{4} \left[\frac{1}{G_m} + \frac{t}{\eta_m} + \frac{1}{G_k} \left(1 - e^{-\frac{G_k t}{\eta_k}} \right) \right] \quad (4.9)$$

where

- $\bar{u}(t)$ is average time dependent plate settlement,
- p is the applied pressure on the plate,
- a is the radius of the plate,
- t is time of the test,
- G_m is the shear modulus of the spring in the Maxwell fluid,
- G_k is the shear modulus of the spring in the Kelvin solid,
- η_m is the viscosity coefficient of the dash pot in the Maxwell fluid,
- η_k is the viscosity coefficient of the dash pot in the Kelvin solid.

When $t = 0$ the instantaneous settlement of the plate can be expressed as:

$$\bar{u}_0 = \frac{1.70pa}{2} \left(\frac{1}{G_m} \right) \quad (4.10)$$

The disadvantage of the borehole dilatometer test and the rigid plate bearing test is the inability to determine the strength of rock mass, and without it is impossible to obtain *SSR* and its influence on deformability and creep behaviour of rock mass.

Carrying out an in-situ triaxial creep test may be a better method for obtaining the creep parameters of rock mass, but due to the high costs involved this method is seldom used (Yu, 1998). The test method was proposed in 1997 (Tani, 1999). The rock specimen is prepared at the bottom of a drill-hole. Axial and lateral strains are

measured in the centre hole and outer slit of the hollow cylindrical specimen. The outer cell is a hollow cylinder with its inner and outer sides being covered with rubber membranes. The rigid strong body of the outer cell is not needed because the surrounding rock mass takes all the reaction forces induced by the outer pressures (Okada et al., 2006). Test procedure of an in-situ triaxial test for rock masses is presented at Figure 3.16.

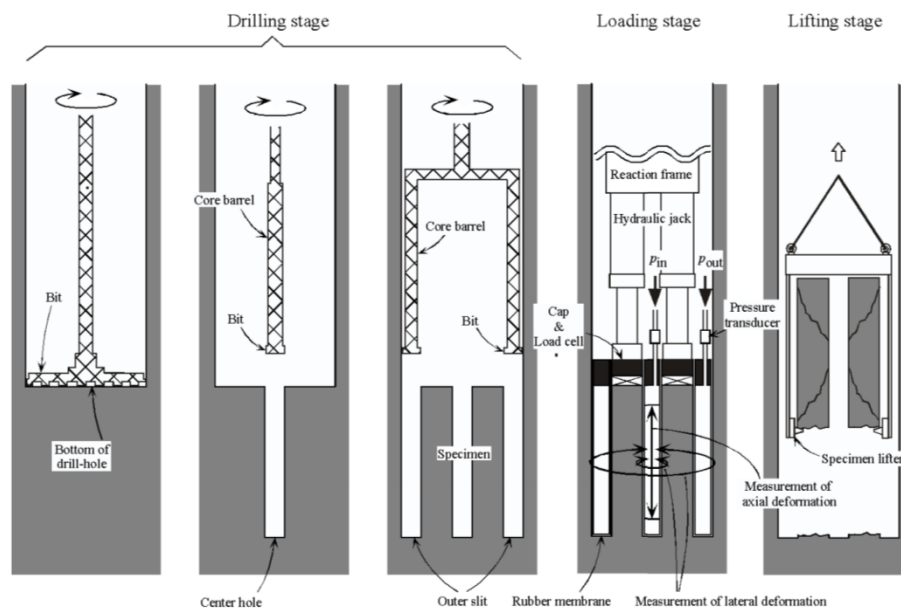


Figure 3.16 Test procedure of an in-situ triaxial test for rock masses (Tani et al., 2003)

The advantages of the triaxial in-situ test of rock mass is that deformation and strength properties are investigated together and directly, test results are not affected by stress relief and disturbance of the loading surface (Okada et al., 2006). In-situ triaxial tests can also be performed on prismatic rock specimens (blocks) with square cross section of 65 by 65 cm and 130 cm high (Yu, 1998).

3.5. Monitoring of rock-mass behaviour

To obtain relevant input parameters to research time dependent behaviour of rock mass, monitoring should be carried out during a time period of several years.

Monitoring begins with installing monitoring equipment at the beginning of the construction and lasts during the construction phase. Often, the monitoring period is extended to service period. Monitoring after the construction phase is often when time dependent behaviour of geotechnical construction is expected, but only in a short time period (up to 6 months).

There are two characteristic groups of geotechnical constructions. The first one encompasses underground structures such as road or railway tunnels, hydrotechnical tunnels, underground caverns, opening etc. The second group encompasses cuts that can be reinforced (engineered slopes) with rockbolts and/or sprayed concrete, or unreinforced. Cuts are parts of roads, motorways, railways, open pits or quarries. Even though these two groups have extremely different stress-strain conditions, both of them should be monitored during a time period to detect and to understand time dependent behaviour.

Monitoring of time dependent behaviour for different projects of underground structures is mostly consisting of geodetic measuring of tunnel convergence and displacement (Guan et al., 2008; Barla et al., 2008; Likar et al., 2006; Malan, 1999).

For monitoring of time dependent behaviour of slopes and cuts, usually the geodetic measurement, (Feng et al., 2003) or even extensometers (Kodama et al., 2009) and/or inclinometers are used.

These monitoring techniques, except measurements of inclinometers or extensometers, provide displacements of only one point of the structure that is positioned on the visible surface. The lack of these techniques is that there is no information about displacements of rock mass below the surface. Measuring the displacements of the damaged zone around excavation gives incorrect response of

time dependent behaviour of rock mass. For simulating and back analysing time dependent behaviour of rock mass the monitoring technique that can measure time dependent behaviour of rock mass, and not only behaviour of surface, should be used. Inclinometers and extensometers are proposed to provide a quality monitoring of time dependent behaviour.

3.6. Time dependent behaviour of rock mass

Time dependent behaviour of rock mass has been studied in detail by many authors, both for the underground geotechnical structures (Cristescu et al., 1987; Guan et al., 2008; Barla et al., 2008; Likar et al., 2006; Malan, 1999; Yu, 1998) or for slopes (Kodama et al., 2008; Feng et al., 2003; Bozzano et al., 2012; Apuani et al., 2007).

According to the results from laboratory or in-situ tests and the experiences from engineering practice, many rheological models have been proposed to predict the time dependent behaviour of rock mass. Guan et al. (2008) divided these models into two categories: the classic viscoplastic models and the viscoplastic-damaged models. The constitutive laws in the classic viscoplastic models try to relate the current strain rate to the current stress (and/or stress rate) directly. The relationship between the deviatoric strain rate and the deviatoric stress (and/or stress rate) can be schematically represented by a series of spring, dashpot and plastic slider that are connected in parallel and/or in series. Some of this models are represented by Burger viscoplastic or viscoelastic model, the Bingham model, the power law Mohr-Coulomb model etc. (Hudson and Harrison, 1997; Itasca Consulting Group, 2011).

The constitutive laws in the viscoplastic-damaged models are based on the principle of strain and energy equivalence and are derived from a standard thermodynamic dissipation potential. Many researchers have contributed their pioneering works on

this issue (Pellet et al., 2005; Bhandari and Inoue, 2005; Shao et al., 2006). The dissipation potential consists of two independent potentials, which correspond to the strain softening (i.e. plasticity) process and the damaging process, respectively. When these two potentials are well defined, by applying the normality rule, the plastic strain rate and the damage evolution rate can be formulated as the potential's first-order difference with respect to the current stress and the thermodynamic force, respectively (Guan et al., 2008).

Guan et al. (2008) proposed the Burger-deterioration rheological model, and its framework is the same as the classic Burger-Mohr-Coulomb model, but it assumes that the cohesion c and the friction angle φ will decrease with time, regardless of whether the loss of strength is caused by cycle loading fatigue, by clay mineral hydration or by some other reasons. It is assumed that the loss of strength is controlled by its current stress state and that there exists a threshold to initiate this kind of strength deterioration and a lower limit to circumscribe the strength deterioration, as presented in following equations.

$$\frac{dc}{dt} = -\omega_c R \quad (R \geq R_{thr}, c \geq c_{res}) \quad (4.11)$$

$$\frac{d\varphi}{dt} = -\omega_\varphi R \quad (R \geq R_{thr}, \varphi \geq \varphi_{res}) \quad (4.12)$$

$$R = \frac{\sigma_1 - \sigma_3}{2ccos\varphi + (\sigma_1 + \sigma_3)sin\varphi} \quad (4.13)$$

In these equations, the parameter R is named as stress coefficient and indicates the distance from the current stress state to the Mohr-Coulomb failure envelope. When the stress coefficient is greater than a certain threshold R_{thr} , the rock strength initiates to deteriorate. The multipliers ω_c and ω_φ are two deterioration ratios that scale the

increments of cohesion c and friction angle φ by some certain proportions. Residual cohesion c_{res} and residual friction angle φ_{res} can be estimated from conventional triaxial tests. The Burger-deterioration model was implemented in the numerical codes to account for the delayed deformation that occurred after construction of Ureshino Tunnel Line 1 in Nagasaki, Japan (Guan et al., 2008). Time dependent behaviour was modelled for a time period of 5 years and simulation results of tunnel convergence were compared with measured ones - Figure 3.17.

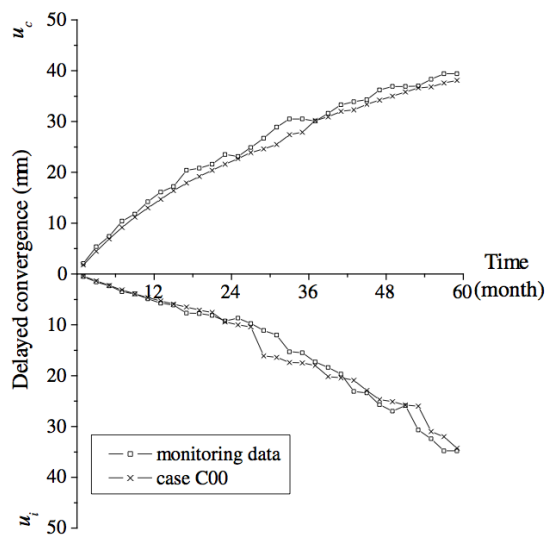


Figure 3.17 Comparison of simulation and measured data for convergence of Ureshino Tunnel Line 1, Nagasaki (Guan et al., 2008)

The deterioration model proposed by Guan et al. (2008) is able to account for the delayed deformation mechanics after the tunnel was put into use and can be applied to predict the further deformation of rock mass and help the maintenance of the tunnel in the future (Guan et al., 2008).

Guan et al. (2009) proposed a rheological parameter estimation technique by using error back propagation neural network (BN) and genetic algorithm (GA). It is proved

that the proposed technique can provide an optimal estimation of the rheological parameters that can help to predict the long-term deformations of tunnels.

Time dependent behaviour of large size tunnels in weak rock masses of very poor quality which exhibit squeezing behaviour were studied in detail by Barla et al. (2008). In order to describe time dependent behaviour of the Saint Martin La Porte access adit (Lyon-Turin Base Tunnel), detailed time dependent numerical simulations were performed using several constitutive models: viscoelastic-plastic (CVISC) model (an analogical model which couples, in series, the Burger viscoelastic model with a plastic flow rule, based on the Mohr-Coulomb yield criterion), elastic-viscoplastic (VIPLA) model (based on the Perzyna's overstress theory) and a more complex elastic-plastic-viscoplastic (SHELVIP) model (stress hardening elastic viscous plastic model derived from Perzyna's overstress theory by adding a time dependent plastic component (Perzyna, 1966; Lemaitre and Chaboche, 1996; Debernardi, 2008; Itasca, 2011)).

These three constitutive models (CIVISC, VIPLA, and SHELVIP) have been adopted in order to analyse the tunnel response in terms of convergence monitored during excavation. The purpose of the study was to see how three different constitutive models with three different levels of complexity reproduce the time dependent deformations of the tunnel in different cross sections – Figure 3.18.

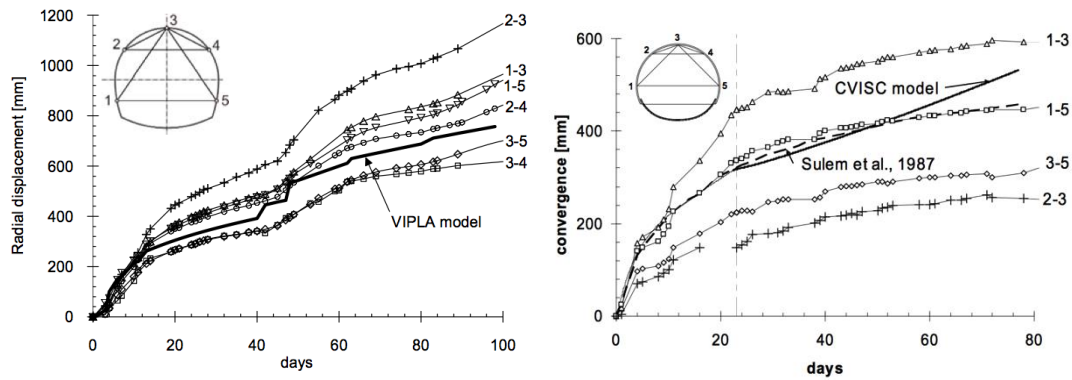


Figure 3.18 Comparison of simulation and measured data for convergence of Saint Martin La Porte access adit (Lyon-Turin Base Tunnel) (Barla et al., 2008)

Likar et al. (2006) have performed time dependent back analysis of Trojane tunnel (Slovenia) excavation at four cross sections. Displacements consisted of initial displacement, unlined displacement and lined tunnel displacement, and were calculated based on equations performed by Goodman (1989) for Burger viscoelastic model. Comparison between measured and calculated vertical displacements of roof measuring point in cross sections is presented at Figure 3.19.

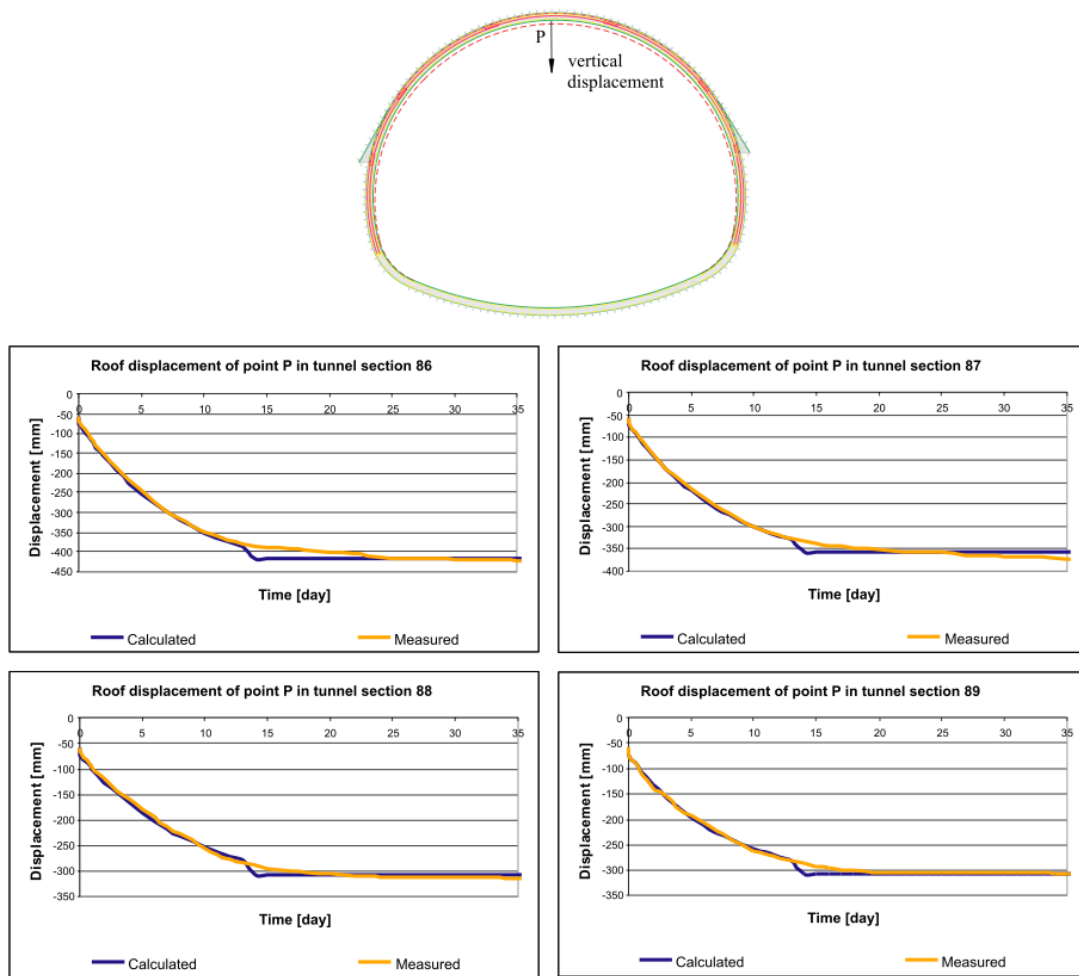


Figure 3.19 Comparison of measured and calculated displacements of roof measuring point for Trojane tunnel at four cross sections (Likar et al., 2006)

Measurement and interpretation of long-term deformation of a rock cut at the Ikura limestone quarry in Japan was performed by Kodama et al. (2009). The Ikura limestone quarry is an open-pit mine located at Niimi City in Okayama prefecture, Japan. Two near-horizontal extensometers were installed with their anchor sets at 5, 10, 25, 50, 75 and 100 m from the surface and monitoring was carried out for a time period of 7 years. The relative displacements along both extensometers gradually increased by time, with the rate of relative displacement being greatest in the early stages of measurements and gradually decreasing thereafter to become more or less constant after certain period of time – Figure 3.20.

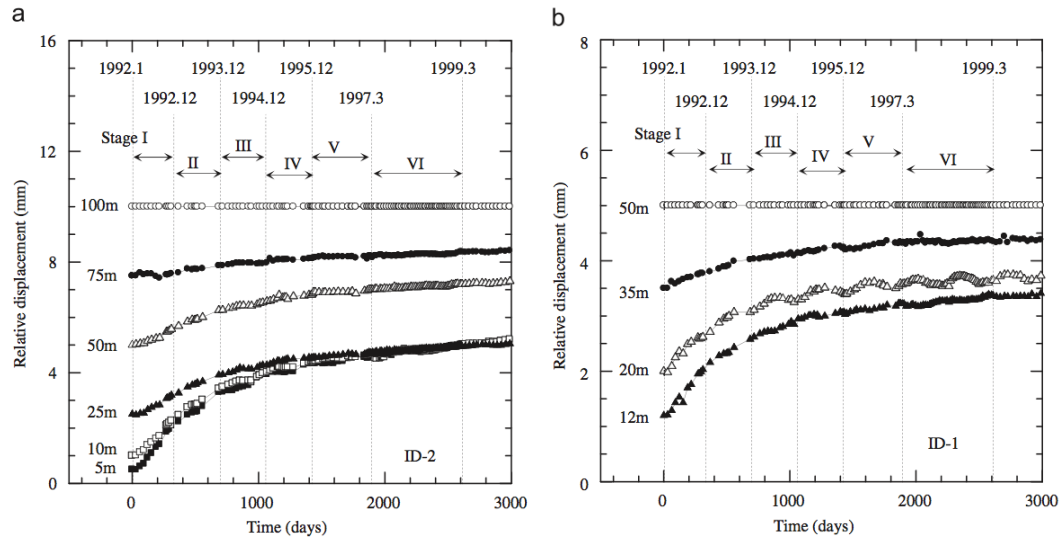


Figure 3.20 Relative displacement at Ikura limestone quarry measured by extensometers ID-2 (a) and ID-1 (b) for a period of more than 7 years (Kodama et al., 2009)

Deformability parameters of rock mass were obtained by back analysis. During numerical modelling Poisson ratio ν varied from 0.0 to 0.4 and Young's modulus E was back calculated and obtained values that varied from 0.3 to 1.6 GPa. It was shown that relative displacements and Young's modulus E strongly depend on Poisson's ratio – Figure 3.21.

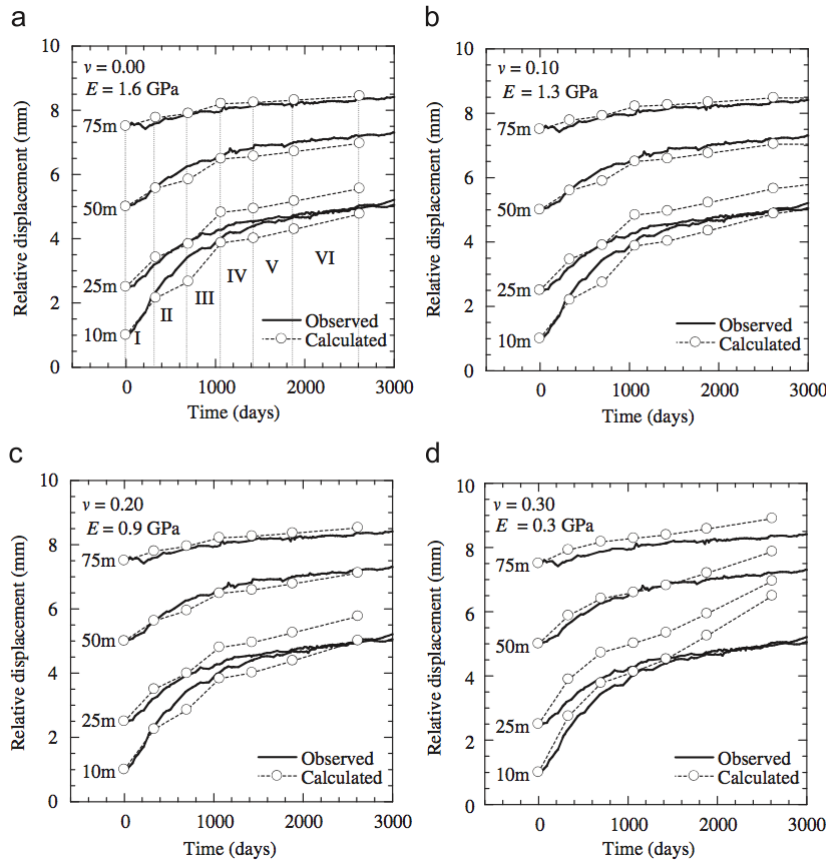


Figure 3.21 Comparison of measured and calculated relative displacements for extensometer ID-2 at Ikura quarry (Kodama et al., 2009)

Even if long-term deformations were measured during the time period of 7 years and deformations continue to occur after excavation had ceased, numerical simulations were conducted only with usage of elasto-plastic model. Time dependent behaviour of rock cut was not simulated through visco-elastic nor visco-plastic models.

Creep modelling in excavation analysis of a high rock slope of the Three Gorges ship lock in China due to excavation unloading was investigated by Feng et al. (2003). For a hard but jointed rock mass the dominant part of creep deformation is usually produced from numerous discontinuities. These rock mass joint conditions were simulated by a discrete element model that consisted of block and contact joints, modelled with spring and the Kelvin element in series (visco-elastic model) while the

rock block was modelled with spring element (elastic model). Joint discretization for the south slope is presented at Figure 3.22.

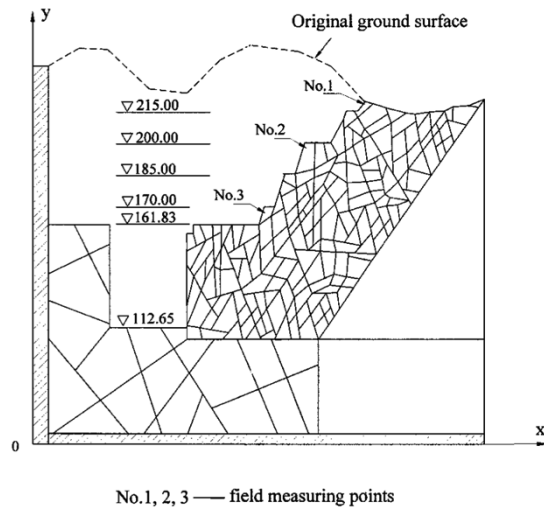


Figure 3.22 Joint discretization for cross section for the south slope of Three Gorges (Feng et al., 2003)

Joint stiffness was obtained from field and laboratory tests. Field tests for joint stiffness were conducted in drainage adits at different elevations. Normal and shear loads were imposed with compression plates, corresponding displacements were measured and the load-displacement relationships were obtained. Determination of viscous parameter for the Kelvin model was obtained from back analysis from the field measurements of the displacement histories of the slope. Comparison of displacements between numerical results and field measurements are presented at Figure 3.23.

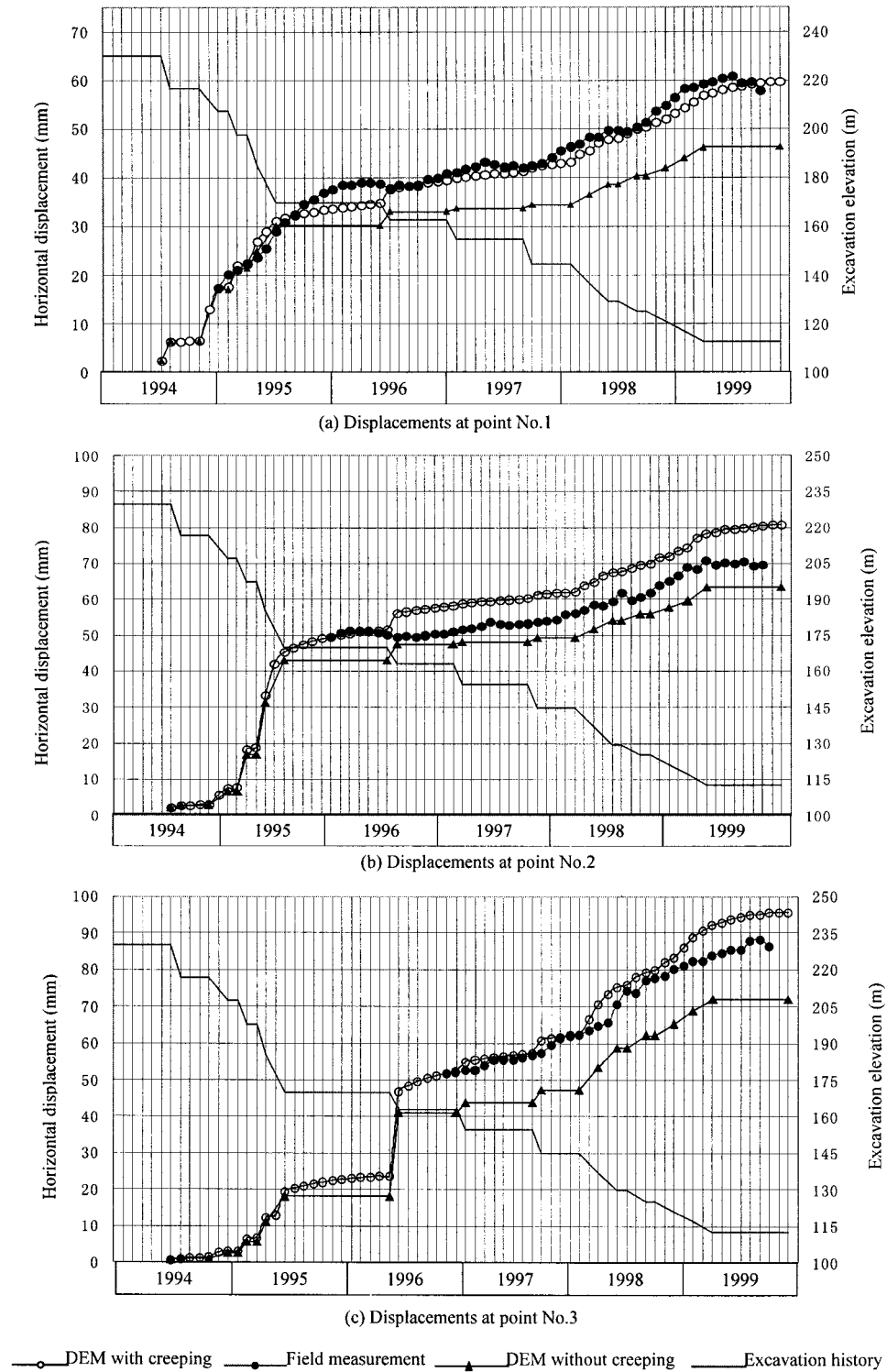


Figure 3.23 Comparison of displacements between numerical results and field measurements for the south slope

(Feng et al., 2003)

The research had confirmed that the proposed model is applicable to analysis of creep deformation of jointed rock mass slopes, and indicates that the creep behaviour must be taken into account in deformation analysis of a jointed rock mass slope.

Analysis of time dependent behaviour of development of a deep-seated gravitational slope deformation (DSGSD) was carried out by numerical modelling using elastic-visco-plastic Burger model (Apuani et al., 2007). Studied DSGSD is located in the Central Italian Alps in the San Giacomo Valley. The modelling has been performed by simulating the melting of an ancient glacier.

Time dependent stress-strain analysis of a rock landslide at Santa Trade in Italy was performed using Burger model and back analysis to define the values of the rheological parameters for jointed gneiss (Bozzano et al., 2012). Performed numerical simulation demonstrated the reliability of visco-plastic rheology for simulating the rock mass creep.

Time dependent behaviour of rock mass is a common research topic in rock mass engineering but most of these researches are focused of time dependent behaviour of underground structures. In this field most researches have been conducted in past decades. On the other hand, time dependent behaviour of cuts was investigated in only a few studies, which were mostly focused on time dependent behaviour of high rock mass cuts. These cuts were made of jointed but quality rock mass. Also, most of time dependent behaviour or slopes are usually referred to a time phase of a rock mass slide due to, or before a failure. Time dependent behaviour of rock mass cuts or weak rock mass cuts has not yet been thoroughly researched.

3.7. Time dependent behaviour of reinforced cuts

Time dependent behaviour of reinforced systems has not been thoroughly researched by many authors. For tunnel linings researches were performed by Cristescu et al. (1987), Goodman (1989) and Yu (1998), and for rockbolts researches are rare and absent. Most of time dependent behaviour of rock mass is focused on time dependent behaviour of underground structures and thus the pressure on tunnel linings.

In time dependent behaviour of rock mass at a certain moment of construction phase, a rock mass surface becomes stress free due to excavation. One of the major parameters involved in the rock support interaction time dependent analysis is the time of application of the support after the excavation. If this time is too short, then the support may fail due to overloading; if this time is too long, then a failure of the rock mass is possible due to excessive deformation (Cristescu et al., 1987).

One of the consequences of time dependent behaviour of reinforced rock mass is transformation and redistribution of stresses and thus an increases load on the reinforcing system and the reduced stability of the structure, which in extreme cases may even lead to collapse (Likar et al., 2006).

Cristescu et al. (1987) performed an analysis of the rock support interaction for two kinds of non-linear support, and a rock behaving according to a linear viscoelastic constitutive equation. It was shown that the stress evolution in the lining is caused by the pressure exerted by the rock, which is also the influence of the lining on the creep process in rock. Analysis performed by Cristescu et al. (1987) could allow the optimisation of a reinforcing system.

Time dependent behaviour of reinforcement systems should be more thoroughly investigated to design reinforcement systems for loads and pressures that are activated after construction phase over time.

4. MODELING OF TIME DEPENDENT BEHAVIOUR OF ENGINEERED SLOPES

4.1. Numerical modelling and finite difference method

It is not possible to obtain analytical mathematical solutions for most of engineering problems; such solutions can be obtained only for certain simplified situations. For engineering problems involving complex material, supporting structure properties and boundary conditions, the engineer resorts to numerical methods that provide approximate, but acceptable, solutions (Desai and Abel, 1971). One of these numerical methods is the finite difference method that was developed simultaneously with increasing use of high-speed computers and with the growing emphasis on numerical methods for engineering analysis.

The finite difference method is perhaps the oldest numerical technique used for the solution of sets of differential equations, given initial values and/or boundary values (Desai and Christian, 1977). In the finite difference method, every derivative in the set of governing equations is replaced directly by an algebraic expression written in terms of the field variables (e.g., stress or displacement) at discrete points in space; these variables are undefined within elements (Itasca, 2011).

4.2. FLAC software

For numerical modelling of time dependent behaviour of engineered slopes FLAC software v7.0 has been used. FLAC uses the finite difference method and an explicit time-marching method to solve algebraic equations and performs a Lagrangian analysis. FLAC was developed by Dr. Peter Cundall in 1986 specifically to perform engineering analysis. The program has been used primarily for analysis and design in

mining engineering and underground construction but also for slope and foundation analysis. Brief description of FLAC software is presented as follows (Itasca, 2011).

FLAC uses dynamic equations of motion in formulation to solve a static solution of the problem. The general calculation sequence is presented at Figure 4.1. This explicit dynamic solution scheme first invokes the equations of motion to derive new velocities and displacements from stress and forces. Then strain rates are derived from velocities, and new stresses from strain rates. One loop of the cycle occupies one timestep and neighbouring elements cannot affect one another during the period of calculation. The advantage of this explicit method is that no iteration process is necessary when computing stresses from strains in an element. In implicit method every element communicates with every other element during one solution step and several cycles of iteration are necessary before compatibility and equilibrium are obtained.

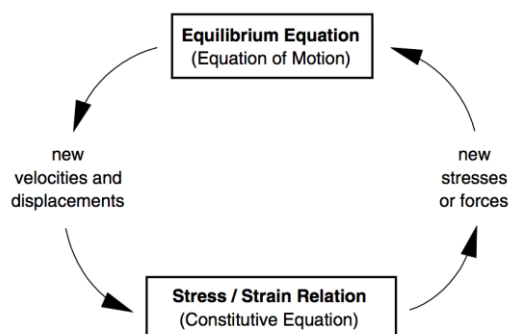


Figure 4.1 Basic explicit calculation cycle in FLAC (Itasca, 2011)

The incremental displacements are added to the coordinates so that the grid deforms with the material it represents. This is termed a “Lagrangian” formulation, in contrast to a “Eulerian” formulation, in which the material moves and deforms relative to a fixed grid. The constitutive formulation at each step is a small-strain one, but is equivalent to a large-strain formulation over many steps.

The solid body in FLAC is divided (discretized) into a finite difference mesh composed of quadrilateral elements. Internally, FLAC subdivides each element into two overlaid sets of constant-strain triangular elements.

4.3. Modelling of material response and reinforcing system

In order to set up a numerical model to simulate a geotechnical engineering problem and its response, the following components and steps must be specified:

- Defining model geometry,
- Discretization of model to regions and forming a grid mesh according to geotechnical unit position – grid generation,
- Defining boundary conditions and calculating the in-situ stresses,
- Choice of constitutive model and material properties,
- Loading and sequential loading – changing the stress conditions and setting a new stress distribution that induces response of the model through strains and/or loads at reinforcing system,
- Interpretation of the results.

General solution procedure is presented at Figure 4.2.

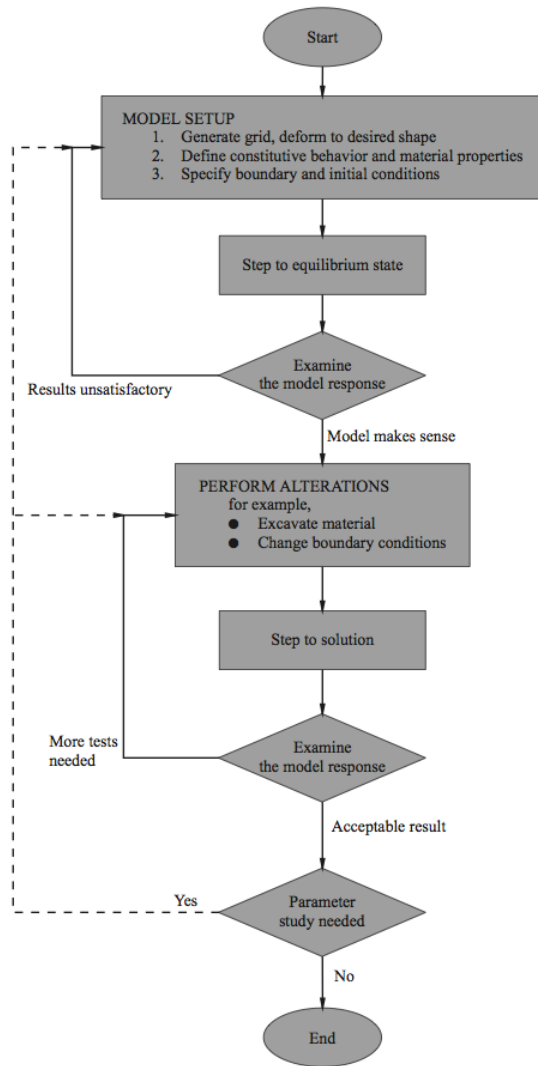


Figure 4.2 General solution procedure in FLAC (Itasca, 2011)

First step of numerical modelling is the grid generation and grouping zones or regions that present distribution and spreading of geotechnical units. The grid defines the geometry of the problem. Geotechnical units are a group of materials with same or similar deformability and strength properties that are determined by geotechnical investigation results. Zones or regions of the grid are shaped to present geotechnical unit distribution and other geological ground conditions such as faults or weak zones. This step is usually named as discretization in terms of numerical modelling.

Boundary conditions are applied as pinned boundary conditions along the bottom of the model and roller boundary conditions applied to the sides. To prescribe pinned boundary condition on the bottom, a fixed gridpoint velocity in the x- and y-direction is used. To prescribe roller boundary condition a fixed gridpoint velocity in x-direction is used.

In-situ stress condition is modelled by using an elastic constitutive model with applying gravitational loading to the model. The model is brought to an initial equilibrium state. The calculation for the initial equilibrium state starts from a zero stress state. After gravitational loading is finished and in-situ stress state is reached the strains should be reset before continuing with the next step of numerical modelling.

There are several different types of calculation that can be performed by FLAC software: instantaneous stress-strain calculation (elastic or elasto-plastic), creep or time dependent behaviour, dynamic calculation, thermal calculation and other. Based on the calculation type, the constitutive or user-defined model and associated properties are assigned to grid.

There are numerous constitutive models built-in in FLAC software: null, elastic-isotropic, elastic-transversely isotropic, Druker-Prager plasticity, Mohr-Coulomb plasticity, ubiquitous-joint, strain-hardening/softening, bilinear strain-hardening/softening ubiquitous-joint, double-yield, modified Cam-clay, Hoek-Brown plasticity, Cysoil and simplified Cysoil.

A brief description of mostly used models is presented as follows. Null model represents material that is removed or excavated from the model. The elastic-isotropic model is valid for homogenous, isotropic, continuous materials that exhibit linear

stress-strain behaviour. The Mohr-Coulomb plasticity model is used for materials that yield when subjected to shear loading, but the yield stress depends on the major and minor principal stresses only; the intermediate principal stress has no effect on the yield. The Hoek-Brown plasticity model is an empirical relation that is a non-linear failure surface representing the strength limit for isotropic intact rocks and rock masses. A modified version of the Hoek-Brown model provides an alternative plastic flow rule given in terms of dilation angle.

Also, several creep models have been implemented in FLAC: a classical viscoplastic model, a two-component power law, a reference creep formulation (the WIPP model) for nuclear-waste isolation studies, a Burger creep viscoplastic model combining the Burger creep model and the Mohr-Coulomb model, a WIPP-creep viscoplastic model combining the WIPP model and the Drucker-Prager model and a crushed-salt constitutive model.

In numerical analysis of engineered slopes for the construction phase the Mohr-Coulomb model will be used. For time dependent numerical analysis Burger elasto-plastic model will be used.

4.4. Mohr-Coulomb model

The failure envelope for Mohr-Coulomb model corresponds to a Mohr-Coulomb criterion (shear yield function) with tension cutoff (tensile yield function). The shear flow rule is nonassociated, and the tensile flow rule is associated.

In the FLAC software implementation of this model, principal stresses σ_1 , σ_2 , σ_3 are used, the out-of-plane stress σ_{zz} being recognized as one of these. The principal

stresses and principal directions are evaluated from the stress tensor components, and ordered as:

$$\sigma_1 \leq \sigma_2 \leq \sigma_3 \quad (4.1)$$

The corresponding principal strain increments $\Delta e_1, \Delta e_2, \Delta e_3$ are decomposed as:

$$\Delta e_i = \Delta e_i^e + \Delta e_i^p \quad i=1,3 \quad (4.2)$$

where

- Δe_i^e is elastic part,
- Δe_i^p is plastic part of an increment.

The plastic components are non-zero only during plastic flows. The incremental expression of Hook's law in terms of principal stress and strain has the form:

$$\Delta \sigma_1 = \alpha_1 \Delta e_1^e + \alpha_2 (\Delta e_2^e + \Delta e_3^e) \quad (4.3)$$

$$\Delta \sigma_2 = \alpha_1 \Delta e_2^e + \alpha_2 (\Delta e_1^e + \Delta e_3^e) \quad (4.4)$$

$$\Delta \sigma_3 = \alpha_1 \Delta e_3^e + \alpha_2 (\Delta e_1^e + \Delta e_2^e) \quad (4.5)$$

$$\alpha_1 = K + \frac{4G}{3} \quad (4.6)$$

$$\alpha_2 = K - \frac{2G}{3} \quad (4.7)$$

The failure criterion may be represented in the plane (σ_1, σ_3) as illustrated at Figure 4.3.

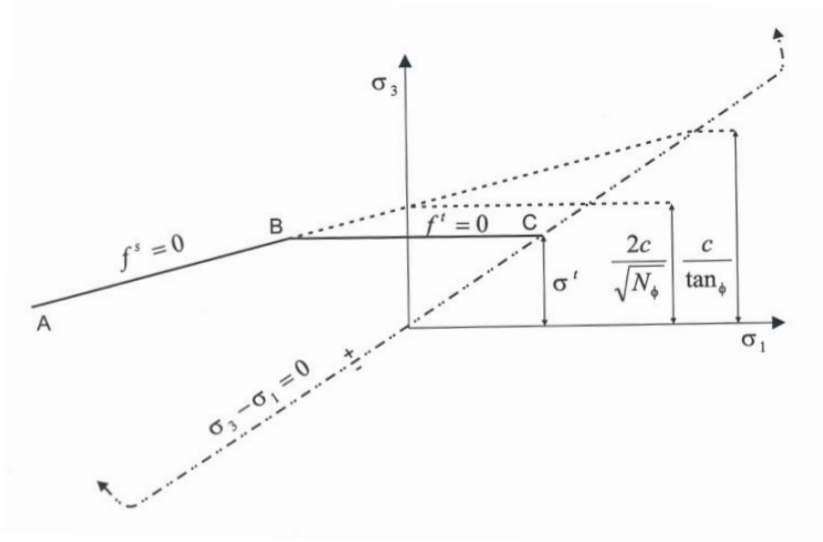


Figure 4.3 Mohr-Coulomb failure criterion in FLAC (Itasca, 2011)

The failure envelope is defined from point A to point B by the Mohr-Coulomb yield function:

$$f^s = \sigma_1 - \sigma_3 N_\phi + 2c\sqrt{N_\phi} \quad (4.8)$$

and from point B to point C by a tension yield function of the form:

$$f^t = \sigma^t - \sigma_3 \quad (4.9)$$

where

- ϕ is the friction angle,
- c is cohesion,
- σ^t is the tensile strength.

Expression N_ϕ is defined as:

$$N_\phi = \frac{1+\sin\phi}{1-\sin\phi} \quad (4.10)$$

From above equations it should be noted that only the major and minor principal stresses are active in the shear yield formulation while the intermediate principal stress has no effect. For a material with friction, $\phi \neq 0$ and the tensile strength of the material cannot exceed the value σ_{max}^t given by:

$$\sigma_{max}^t = \frac{c}{\tan \phi} \quad (4.11)$$

The shear potential function g^s corresponds to a nonassociated flow rule and has the form:

$$g^s = \sigma_1 - \sigma_3 N_\psi \quad (4.12)$$

where

- ψ is the dilation angle

and

$$N_\psi = \frac{1+\sin \psi}{1-\sin \psi} \quad (4.13)$$

The associated flow rule for tensile failure is derived from the potential function g^t with

$$g^t = -\sigma_3 \quad (4.14)$$

The flow rules for Mohr-Coulomb model are given a unique definition in the vicinity of an edge of the composite yield function in three-dimensional stress space by application of a technique for the case of a shear-tension edge (Figure 4.4).

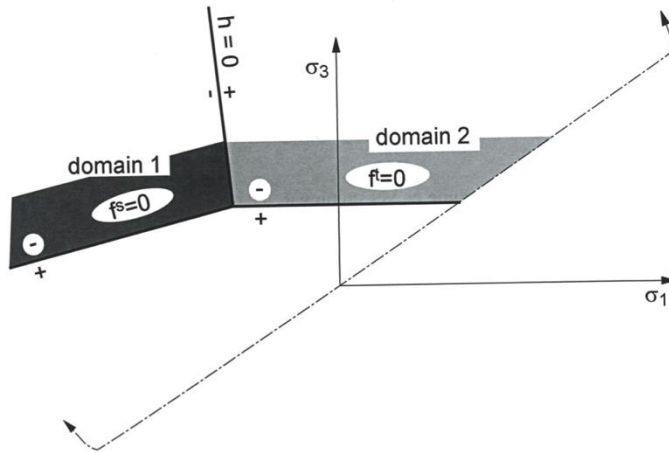


Figure 4.4 Domains used in the definition of the flow rule in Mohr-Coulomb model (Itasca, 2011)

4.5. Burger elasto-plastic model

The Burgers-creep viscoplastic model in FLAC is characterized by a visco-elasto-plastic deviatoric behaviour and elasto-plastic volumetric behaviour. The visco-elastic and plastic strain-rate components are assumed to act in series. The visco-elastic constitutive law corresponds to a Burgers model (Kelvin cell in series with a Maxwell component), and the plastic constitutive law corresponds to a Mohr-Coulomb model (Figure 4.5).

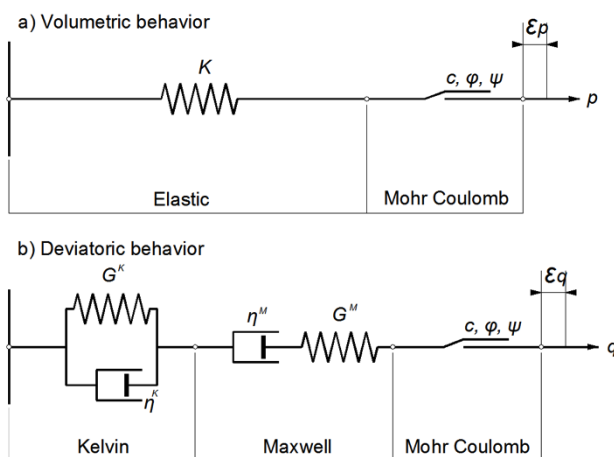


Figure 4.5 Sketch of Burger viscoplastic Mohr-Coulomb model: (a) volumetric behaviour, and (b) deviatoric behaviour

As a notation convention symbols S_{ij} and e_{ij} are used to denote deviatoric stress and strain components:

$$S_{ij} = \sigma_{ij} - \sigma_0 \delta_{ij} \quad (4.15)$$

$$e_{ij} = \epsilon_{ij} - \frac{e_{vol}}{3} \delta_{ij} \quad (4.16)$$

where

$$\sigma_0 = \frac{\sigma_{kk}}{3} \quad (4.17)$$

and

$$e_{vol} = \epsilon_{kk} \quad (4.18)$$

Kelvin, Maxwell and plastic contributions to stresses and strains are labelled using the superscripts $.^K$, $.^M$ and $.^p$ respectively. The model deviatoric behaviour may be described by following relations of strain rate partitioning

$$\dot{e}_{ij} = \dot{e}_{ij}^K + \dot{e}_{ij}^M + \dot{e}_{ij}^p \quad (4.19)$$

Kelvin

$$S_{ij} = 2\eta^K \dot{e}_{ij}^K + 2G^K e_{ij}^K \quad (4.20)$$

Maxwell

$$\dot{e}_{ij}^M = \frac{\dot{S}_{ij}}{2G^M} + \frac{S_{ij}}{2\eta^M} \quad (4.21)$$

Mohr-Coulomb

$$\dot{e}_{ij}^p = \lambda \frac{\partial g}{\partial \sigma_{ij}} - \frac{1}{3} \dot{e}_{vol}^p \delta_{ij} \quad (4.22)$$

$$\dot{e}_{vol}^p = \lambda \left[\frac{\partial g}{\partial \sigma_{11}} + \frac{\partial g}{\partial \sigma_{22}} + \frac{\partial g}{\partial \sigma_{33}} \right] \quad (4.23)$$

Volumetric behaviour is given by expression:

$$\dot{\sigma}_0 = K(\dot{e}_{vol} - \dot{e}_{vol}^p) \quad (4.24)$$

In the equations and expressions above, the properties K and G are the bulk and shear modules, respectively, and η is the dynamic viscosity. The parameter λ is non-zero during plastic flow only, which is determined by application of the plastic yield condition $f=0$. The Mohr-Coulomb yield envelope is a composite of shear and tensile criteria. The yield criterion is $f=0$, and in the principal axes, the formulation of shear yielding and tensile yielding are presented in following equations:

$$f = \sigma_1 - \sigma_3 \frac{1+\sin\phi}{1-\sin\phi} + 2c \sqrt{\frac{1+\sin\phi}{1-\sin\phi}} \quad (4.25)$$

$$f = \sigma^t - \sigma_3 \quad (4.26)$$

The potential function g for shear and tension failure is presented as:

$$g = \sigma_1 - \sigma_3 \frac{1+\sin\phi}{1-\sin\phi} \quad (4.27)$$

$$g = -\sigma_3 \quad (4.28)$$

4.6. Reinforcing system

For modelling of the reinforcing system in FLAC software there are several built-in structural elements that are used in numerical analysis: beam, liner, cable, pile, rockbolt, strip element and support member.

Cable element is a one-dimensional axial element that may be anchored at a specific point in the grid (point-anchored) or grouted so that the cable element develops forces

along its length as the grid deforms. In these numerical analyses cable elements will be used to model rockbolt as a part of reinforcing system of engineered slope.

The cable element is assumed to be divided into a number of segments of length L with nodal points located at each segment end. A one-dimensional constitutive model is adequate for describing the axial behaviour of the reinforcing element and the axial stiffness is described in terms of the reinforced cross-section area A and Young's modulus E .

The tensile yield-force limit and the compressive yield-force limit can be assigned to the cable as presented at Figure 4.6.

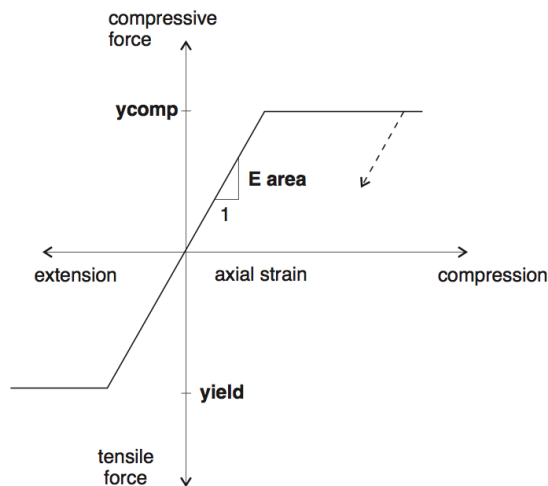


Figure 4.6 Cable material behaviour for cable elements (Itasca, 2011)

In evaluating the axial forces that develop in the reinforcement, displacements are computed at nodal points along the axis of the reinforcement - Figure 4.7.

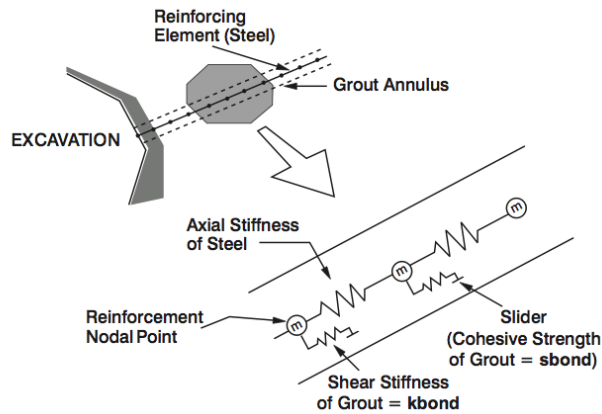


Figure 4.7 Conceptual mechanical representation of fully bonded reinforcement which accounts for shear behaviour of the grout annulus (Itasca, 2011)

Shear forces contributed through shear interaction along the grout annulus are computed from axial forces in the reinforcement. The shear behaviour of the grout annulus is represented as a spring-slider system located at the nodal points – Figure 4.7. The maximum shear force that can be developed in the grout is a function of the cohesive strength of the grout and the stress-dependent frictional resistance of the grout.

Sprayed concrete will be modelled using beam structural element. Beam elements are two-dimensional elements with three degrees of freedom (x-translation, y-translation and rotation). Beam elements can be jointed together with one another and/or the grid. Beam elements are used to represent a structural member, including effects of bending resistance and limited bending moments.

4.7. Observational method and back analysis

Construction of a significant geotechnical structure is a complex engineering endeavour requiring careful and extensive technical and financial planning, involving rational optimisation of various possible solutions to frequently conflicting objectives,

requirements and environmental conditions. Not always well-known and understood natural ground conditions are often the cause of large cost and time overruns, or fortunately less often, construction failures. Therefore, dealing with geotechnical risk, created by construction in natural ground, attracts great interest among geotechnical engineers (Savits-Nossan, 2006).

There are two design approaches found in present day geotechnical practice. In the first, a conventional approach, the design is completed prior to beginning of the construction phase. This design is based on pessimistic and unfavourable approach and monitoring and observations during construction phase are used only as tool for verification the design assumptions. Instrumentation and monitoring could be used during construction phase but they play a passive role and are used to check original predictions from the design. In the second design approach, so called observational method is used to avoid these conservative assumptions about ground conditions, and monitoring plays a very much active role in both the design and construction. Monitoring is used here to allow planned modifications. This approach was recognized by Terzaghi and Peck (1967) as the observational procedure.

The formal ingredients and name of this method was laid down by Peck in his Rankine lecture (Peck, 1969). Observation methods were studied in detail by many researchers: Peck (1969), Powderham (1994; 1998; 2002), Powderham and Nicholson (1996) and others.

To the observational method in geotechnical engineering back analysis procedure is very well tied. The term back-analysis involves a procedure where different parameters and hypotheses of a trial problem are varied in order for results of the analysis to match a predicted performance as much as possible (Vardakos, 2007).

Cividini et al. (1981; 1983) gave an insightful review of back analysis principles and aspects, including examples. Their probabilistic analysis shares the concept presented by Eykhoff (1974) in parameter identification. Back analysis method was studied in detail by many researches: Gioda (1985), Gioda and Sakurai (1987), Sakurai and Abe (1981), Sakurai and Takeuchi (1983), Sakurai et al. (1985) and others.

According to Cividini et al. (1981), there are two different ways to conduct back analysis: the inverse approach and the direct approach. For the inverse approach, the formulation is the reverse of that in ordinary stress analysis, even though the governing equations are identical. According to this approach, the number of measured values should be greater than the number of unknown parameters, but it is unclear whether the method could be applied in geotechnical problems in which the measured values contain a scattering. The direct approach to back analysis is based on an iterative procedure of correcting the trial values of unknown parameters by minimizing the error function, and because of that, this approach is often called minimization method. Gioda and Maier (1980) pointed out that an advantage of direct approach methods is that they may be applied to non-linear back analysis problems without having to rely on a complex mathematical background. Cividini et al. (1981) stated that standard algorithms of mathematical programming might be adopted for numerical solutions.

Iterative solutions require quite time-consuming computations so, since early 1990s, Artificial Neural Networks (ANN) has been applied successfully to geotechnical engineering and has improved and accelerated performance of back analysis methods.

4.8. Methodology

Numerical analysis and the results of the analysis in this paper will be presented for the models established at the cuts of Adriatic Motorway near the City of Rijeka. The geological settings of the Draga Valley steep slopes is composed of limestone rock masses, and at the bottom of the valley there are deposits of Palaeogene flysch deposits, which mainly consist of siltstones, with rare layers of sand, marl, and breccia. Numerical analysis will be performed in two phases: a construction phase and a service period.

The monitoring equipment installed before the start of construction included vertical inclinometers and horizontal extensometers installed in pairs on several cross sections for the observation of the construction behaviour used in numerical analysis. The installed rockbolts were tested using pull-out tests, and the results of those tests made it possible to include the real stiffness values of the installed anchors in numerical analysis.

The results of the horizontal displacement measurements at the vertical inclinometer show that most of the displacement occurred in the upper part of the cut, i.e., in layers that are characterised as residual soil (RS) to moderately weathered flysch rock mass (MW). The maximum horizontal displacement occurred at the top of the inclinometers, and the main part of these displacements occurred during the construction time period. Realised displacements during the service period are significant and should not be neglected in the consideration of cut support stability analysis.

It is evident that most of the instantaneous displacements and time dependent displacements occurred in the upper part of the cut that consists of residual soil (RS)

and moderately weathered flysch rock mass (MW). A significant decrease of these displacements is observed as a function of the depth of the weathering profile of the flysch rock mass. Time dependent displacements in the slightly weathered (SW) to fresh flysch rock mass (F) were not present and will not be considered and analysed in this research.

According to geotechnical field investigation results, the representative models are consisted of several geotechnical units with same or similar geotechnical properties. Disposition and thickness of these geotechnical units have been determined on the basis of geophysical measurements results and have been confirmed by geotechnical drilling logs. According to the seismic refraction method that utilized the refraction of seismic waves on geologic layers and rock/soil units, the numerical model is consisted of several geotechnical units with similar geotechnical properties. In the upper layer, where the difference between parameters is pronounced with depth, grouping has been defined with smaller longitudinal seismic wave velocities. On the other hand, where the difference between parameters is not significantly pronounced with depth, grouping of the geotechnical units at the lower half of the model has been defined with greater longitudinal seismic wave velocities. Each model used for numerical analysis will be grouped into 6 geotechnical units.

To obtain deformability and creep properties of these units the direct approach to back analysis has been used in numerical modelling. Direct approach is based on an iterative procedure of correcting the trial values of unknown parameters by minimising the error function. Back analysis of the behaviour of engineered slopes in the flysch rock mass has been performed using a trial and error method to obtain the deformability and creep parameters of geotechnical units in the numerical model.

Calibration of the numerical model have been carried out from the bottom, where no or very small displacements are measured, toward the surface, where larger displacements are measured.

Verification of numerical modelling has been based on comparison of simulation data (obtained from numerical analysis) and measured data (obtained from measurement results). Comparison has been directed on horizontal displacements at vertical inclinometer since these are the most significant indicator of displacements of reinforced cuts in the construction phase and in the service period. From the diagram of horizontal displacements per depth of vertical inclinometers the weathering profile of flysch rock mass is clearly visible. Verification and calibration of numerical modelling have been carried out on several points through the upper part of the cut where most of the displacements occur; in every 1.0 to 3.0 m.

Numerical analyses have been performed in two phases: construction phase and service period. For initial deformability and strength parameters in construction phase the values obtained from geotechnical investigation works and previously performed numerical analysis on this will be used. The Mohr-Coulomb model has been used for modelling residual soil (RS) to moderately weathered rock mass (MW). To estimate initial geotechnical properties of slightly weathered (SW) and fresh rock mass, a methodology proposed by Marinos and Hoek (2001) for estimating the GSI for these geological formations has been used.

The engineered slope has been modelled using the linear elastoplastic Mohr-Coulomb model. Rockbolts in the model has been defined as structural cables, with the stiffness obtained from in situ pull-out tests. Sprayed concrete at excavation face has been modelled using beam structural element. Analyses have been carried out in several

stages, which represent excavation stages. After each stage, rockbolts and support construction installation have been included in the model.

The back stress-strain numerical analysis of the cut reinforced construction described above provided probable deformability parameter values: shear modulus, G , and bulk modulus, K , referring to the Mohr-Coulomb elastoplastic model.

The service period analyses have been carried out using the initial stress and strain states in the model obtained from construction phase modelling. The soil and rock mass layers in the cut have been modelled using the Burger-Mohr-Coulomb model for upper layers, denoted as RS, CW, HW, MW and SW, whereas the lower layers in the cut, denoted as F, have been modelled with the classic elastoplastic Mohr-Coulomb model and have not been processed as time dependent.

The determination of the Burger model parameters for each geotechnical unit was the most challenging part of the numerical analysis. Because of numerous uncertainties, the simplified method for parameter estimation in the first iteration has been used: the shear modulus of the Maxwell unit, G_M , in the Burger model are referred to as a shear modulus, G , in the elastoplastic model obtained from a back analysis carried out from the construction phase. The shear modulus of the Kelvin unit, G_K , that controls primary creep are set to be several times higher than the shear modulus of the Maxwell unit, G_M .

The creep parameters of the viscosity of the Kelvin unit, η_K , and the Maxwell unit, η_M , will be taken using the specific ratio R ; where $\eta_M/\eta_K=R$. In time dependent stress-strain numerical modelling Bozzano et al. (2012) used ratio $R=0.1$, Likar et al. (2006) $R=7,769$, Apuani et al. (2007) $R=1.0$, Barla et al. (2008) $R=6.57$. Yu (1998) used ratio $R=100$ for validation of creep code in uniaxial compression case, $R=202.9$ for

numerical analysis of the circular tunnel under hydrostatic stress field – example from Goodman (1989), $R=30-100,000$ from curve fitting of the axial strain vs. time curves in laboratory triaxial creep tests of model material, $R=73.3-1e7$ from laboratory triaxial creep test for fault zone material, $R=73.3-1e7$ from laboratory triaxial creep test for very weak sandstone. Ratio of $R=100$ has been used through numerical back analysis. Using these relationships in the parameter selection, the number of parameters that should be determined in the creep back analysis has been considerably reduced.

The back stress-strain analysis of the reinforced cut construction should provide real deformability and creep parameters. This initial set up parameters has been used to perform time dependent behaviour for prediction of behaviour of reinforced slope for a long period of time (up to 25 years). These analyses should also obtain time dependent behaviour of reinforcing elements – rockbolts.

5. APPLICATION – THE ADRIATIC MOTORWAY CASE STUDY

5.1. Outline of the project

One of the most challenging sections of the Adriatic motorway along the Croatian Adriatic coast was constructed in the Draga Valley near the City of Rijeka (Figure 5.1) during the period from 2004 to 2006. The Adriatic Motorway section is only 6.8 km long, but from geological, geotechnical and construction points of view, this is a very complex transportation structure with 3 junctions, 2 tunnels, and several viaducts.

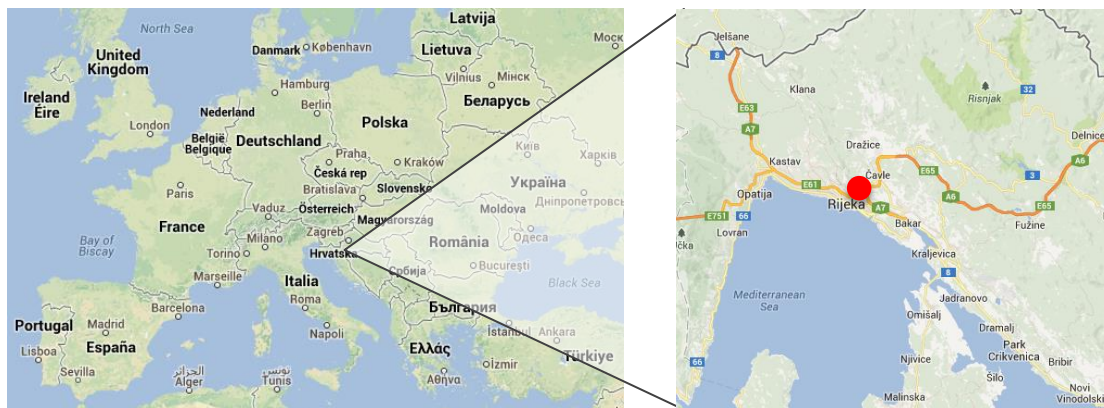


Figure 5.1 Location of the Adriatic Motorway near the City of Rijeka, Republic of Croatia

The Draga Valley is gradually descending from the Orehovica area (60 m.a.s.l.) to the Martinšćica Bay (30 m.a.s.l.). From this location the terrain gradually raises again to the Sv. Kuzam saddle (224 m.a.s.l.) and then descends to the Bakar Bay. The width of the valley significantly varies from 400 to 500 m in Draga Valley to 100 m on Sv. Kuzam saddle.

Construction work and technology of reinforcing of cuts were presented in detail by Arbanas et al. (2008a) and Brunčić et al. (2008). During the construction of the Adriatic Motorway, on the major part of the road, the cutting in flysch rock mass is designed and executed, and the cut stability is ensured using rock bolts and appropriate reinforcing system such as multi-layered sprayed concrete layers and reinforced concrete structures. Due to the low strength properties of flysch rock mass and its very low deformability modulus, an extra attention was dedicated to the technology of the construction.

According to executed geotechnical field investigations, use of rock mass reinforcement system was specified in slightly weathered to fresh rock mass, while in weaker parts of rock mass the change of geometry is specified. Construction works on flysch rock mass reinforcing showed for the need of additional analysis of interaction between rockbolts and surrounding rock mass.

Because of steep slopes it was not possible to select a stable geometry on the most cuts in the flysch rock mass without rock mass reinforcement or applying of support system. The reinforcement system was designed in two phases. The first phase consisted of rockbolt reinforcement system and multi-layered sprayed concrete to enable stable excavation of the cuts with relatively low factors of safety. In the second phase, a stiff concrete retaining construction was applied to fix relatively soft primary reinforcement system.

The primary reinforcement systems were performed by excavation in the horizontal and vertical phases, of 2.5 to 3.0 m height, and a successive construction of a three-layered sprayed concrete support system reinforced by self-drilling rockbolts from top to bottom of the excavation. A cut in the flysch rock mass without the applied support

system has seem to be extremely unstable, so the working phases were taken as very short. It means that the same day after the excavation was performed, the sprayed concrete and rockbolts were installed. Simultaneously with reinforcement, the shallow drainage boreholes were drilled to allow dissipation and lowering of potential ground water behind the cuts – Figure 5.2a.

The secondary reinforcement systems included construction of stiff strip footing, concrete pillars, and a concrete beam on the toe of the cut. The fronts of the constructions were closed with prefabricated concrete elements that connected strip footing with head concrete beam – Figure 5.2b.

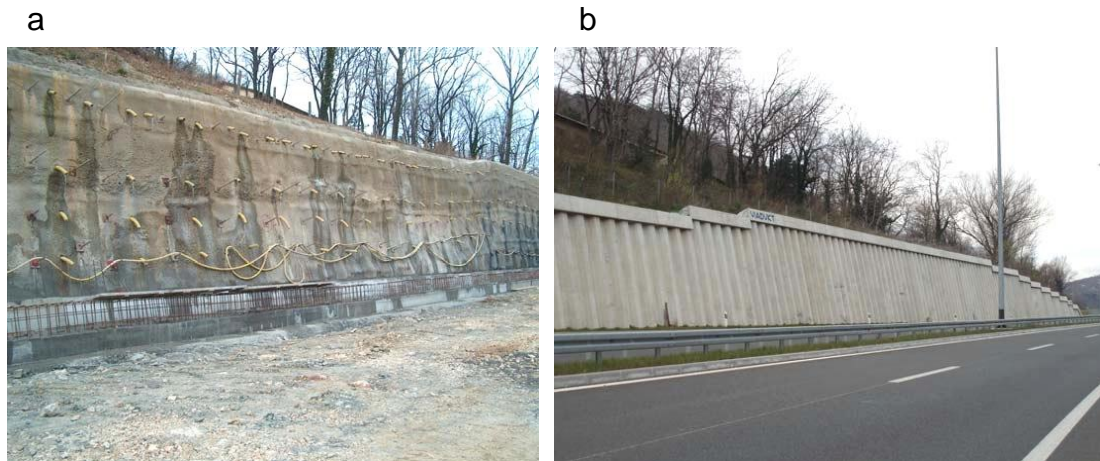


Figure 5.2 Reinforced cut in flysch rock mass at km 2+440; (a) during construction phase and (b) after finished secondary lining

During the cut construction a detailed monitoring system was established which included measuring of deformation in horizontal deformeters and vertical inclinometers, observations of geodetic marks, load measuring in rockbolts and engineering geological mapping of cuts. In this way the necessary data for the stress-strain back analysis of the real behaviour of excavated and reinforced rock mass was obtained. An active design procedure was established which made possible the changes required in the rock mass reinforcement system in cuts. The measurements

were performed after any construction stage, as well as in the long period after completing of the reinforcing system construction.

This active design approach allowed the designer to change the reinforcement system during construction work based on rock mass conditions and monitoring results, and to observe the time dependent behaviour of the engineered slope during the service period.

Numerical stress-strain back analyses have been performed on two different models established at chainages in km 2+380 and km 2+440. Similar geological conditions were present also on additional two reinforced cuts, km 0+560 and 1+880, but numerical back analysis were not performed on them. At km 0+560 shallow sliding occurred during construction time and the measured results were not applicable. At km 1+880 there were not enough detailed results of geotechnical investigation works to set up an acceptable numerical model.

5.2. Geological overview

The geological setting of the Draga Valley is very complex. The Cretaceous and Palaeogene limestone is located at the top of the slope, while the Palaeogene flysch crops are located at the lower part of the slope and in the bottom part of the Draga Valley where the motorway route is situated. As opposed to limestone rock mass outcrops at the top of the valley, the flysch rock mass is completely covered by colluvial deposits, residual soils and talus breccias (Arbanas et al., 1994). Schematic engineering-geological situation plan of the Draga Valley and its cross section is presented at Figure 5.3.

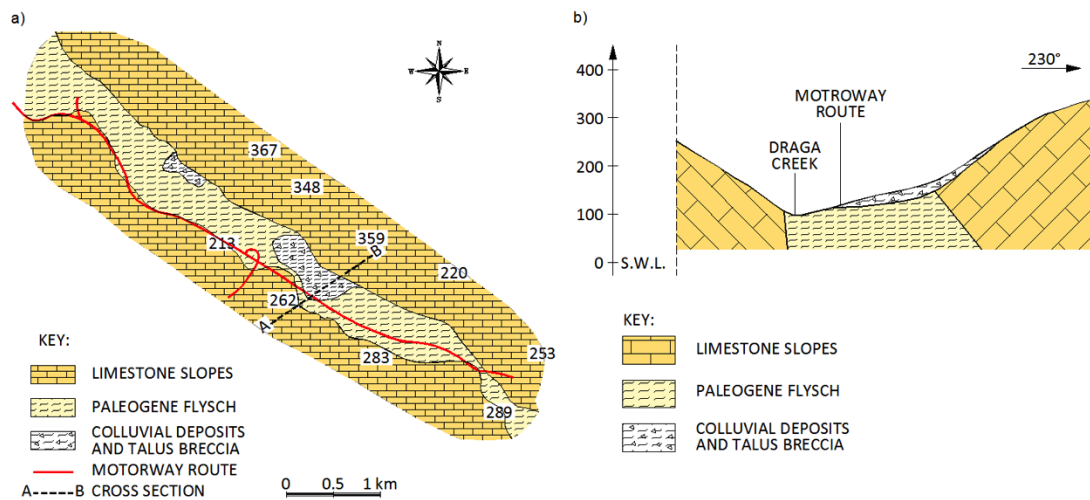


Figure 5.3 (a) Schematic engineering-geological map of the Draga Valley; (b) Schematic engineering-geological cross-section of the Draga Valley (Arbanas et al., 1994)

According to Arbanas et al. (1994) the flysch rock mass is covered with slope superficial deposits, which tend to slide and denude the slope. The characteristic geological profile consists of clay cover made after the disintegration of a flysch rock mass (RS) or brought gravitationally from hypsometrically higher parts of the slope, a layer of weathered flysch rock mass with variable characteristics that depend on the weathering stage (CW, HW, and MW), which significantly increases with depth, and the fresh flysch zone as a bedrock (SW and F).

5.3. Weathering profile of flysch rock mass in Draga Valley

Weathering profile and its geological and geotechnical properties were investigated by Grošić and Arbanas (2013). The flysch rock mass in Draga Valley is mainly composed of a siltstone rock mass, which exhibits a visual transition from a completely weathered (CW) yellow coloured zone, through highly weathered (HW) and moderately weathered (MW), to the slightly weathered (SW) deposits and fresh rock mass (F) that are grey to blue – Figure 5.4. In the zone of the completely weathered siltstone, the rock mass is completely disintegrated, but the original

structure of the rock mass is still intact. The layers of fresh siltstone have no visible weathering marks except for the colour change on the main discontinuity surfaces.

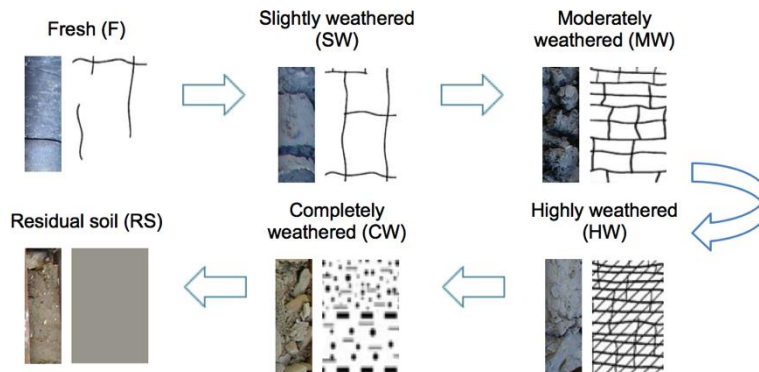


Figure 5.4 Process and grades of weathering in flysch rock mass (Grošić and Arbanas, 2013)

The weathering profile determination was based on geotechnical investigation results, which consisted of drilling with core sampling, geophysical investigations, and laboratory tests. The depth of the weathering profile of the flysch rock mass with a complete transition from residual soil (RS) to fresh rock mass (F) was identified as ranging from 5.0 to 8.0 m.

Determination of the geotechnical properties of the flysch rock mass during the geotechnical field investigations was difficult. During drilling, it was difficult to obtain undisturbed samples because of rock mass disintegration. Sudden degradation and disintegration of slightly weathered (SW) to fresh (F) siltstone occurred after removing geostatic loads and exposing the core to air and water. The consequence of these processes in the siltstone was that a very small number of undisturbed samples were taken for laboratory uniaxial strength tests.

According to Grošić and Arbanas (2013), there are other significant problems and unknowns when dealing with a heterogeneous flysch rock mass, which include

vulnerability to weathering and sudden degradation and disintegration. These uncertainties include the following:

- The influence of weathering on reducing the strength criterion,
- The time dependence of weathering on reducing the strength criterion,
- The decrease in the deformation characteristics' values regarding the duration of the weathering process.

5.4. Geotechnical conditions

Detailed geotechnical and geological studies of a flysch rock mass in the Draga Valley are presented by Arbanas et al. (1994; 2007; 2008a; 2008b) and Grošić and Arbanas (2013), Brunčić (2008), Brunčić et al. (2009). Geotechnical field investigations consisted from core drilling, engineering geological mapping of terrain, geophysical investigations and laboratory and in-situ tests. Geotechnical field investigations performed at researched location are presented at Figure 5.5.

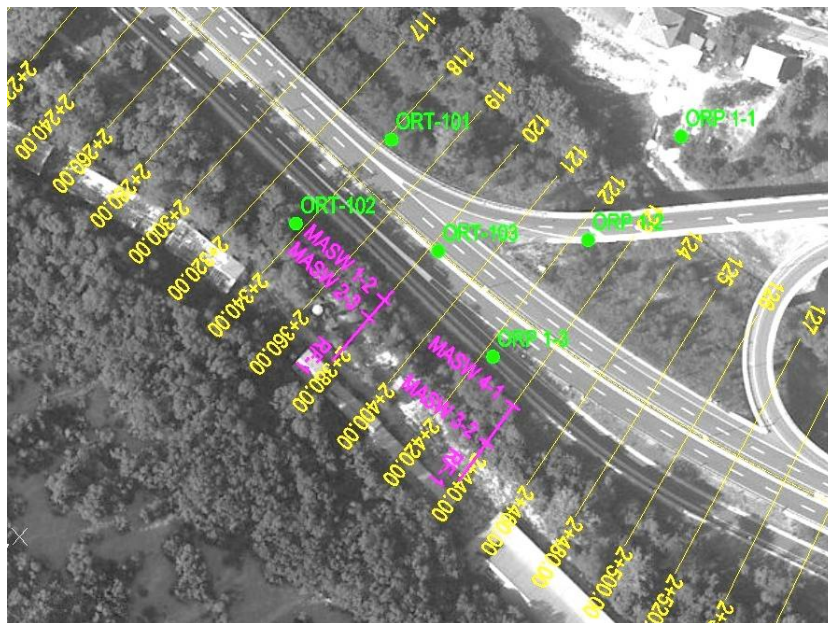


Figure 5.5 Situation plan of Adriatic Motorway (from km 2+300 to 2+500) with position of geotechnical investigation works: geotechnical core drilling (green) and geophysical investigations (magenta)

Geotechnical core drilling at this micro location was performed during the design phase in years 1977 and 1990. Continuously with drilling engineering geological logging of boreholes were performed and documented in engineering geological report (Croatian Geological Survey, 1990). Boreholes ORT-101, ORT-102, ORT-103, ORP 1-1, ORP 1-2 and ORP 1-3 were situated near researched profiles and were taken as representative for further research.

According to borehole logs three geotechnical units were determined:

- Delluvial deposits (*dl*) – superficial deposit,
- Weathered flysch (*rp*) – superficial deposit,
- Flysch ($E_{2,3}$) - bedrock

Deluvial deposits (*dl*) are made of clay and silt with fragments, mid plasticity and yellow to brown colour. Soil particles are angular to sub-angular. Weathered flysch (*rp*) is made of fragments of weathered silty sandstone and siltstone with sand particles, yellow-brown colour. Flysch ($E_{2,3}$) is made of siltstone and sandstone, homogeneous structure, grey to grey-brown colour.

According to performed granulometry laboratory tests residual soil is made of silty clay to sandy silt. Samples of siltstones were crushed, immersed and dried before granulometry and have shown that they consist of 35 to 75% of clay particles, 5 to 65% of silt particles and 0 to 30% of sand particles. According to performed laboratory tests density of superficial deposit (delluvial deposits and weathered flysch) vary from 1,840.0 to 1,980.0 kg/m³, cohesion from 14.0 to 41.5 kPa and internal friction angle from 16 to 27° (Arbanas et al., 1994).

The uniaxial strength of slightly weathered (SW) to fresh (F) siltstones obtained from uniaxial tests varied from 8 to 32 MPa. Obtaining undisturbed samples in completely (CW) to moderately weathered (MW) siltstone rock masses was not possible for the uniaxial test, so the Point load tests (PLTs) were conducted immediately after drilling and sampling to avoid further weathering and strength reduction in the samples. A disadvantage of PLTs is the large dispersion of test results, which occurs especially in weak flysch rock masses, but the use of this method is recommended when there is a lack of more reliable testing or a lack of appropriate representative samples and in combination with detailed descriptions of tested samples from the flysch rock mass. Test results of PLTs on fresh (F) siltstone samples showed that the representative uniaxial strength of these materials varies from 10 to 15 MPa, and in extreme cases, this value reached up to 20 MPa. The representative uniaxial strength of moderate (MW) to slightly weathered (SW) samples showed values <2 MPa. These values obtained from PLTs are uncertain and unacceptable for engineering analysis without adequate precautions.

During the classification of rock mass in period of geotechnical investigation works and in period of construction phase, a great dispersion of obtained information was noticed. The complex structure of these materials, resulting from their depositional and tectonic history, means that they cannot easily be classified in terms of widely used rock mass classification systems. A methodology for estimating the Geological Strength Index and the rock mass properties for these geological formations is presented by Marinos and Hoek (2001). This methodology is presented by Hoek, Marinos and Benissi (Hoek et al., 1998), Hoek and Marinos (2000), Marinos and Hoek (2000; 2001) and Marinos (2004).

During construction phase, engineering geological mapping of open cuts were continuously performed along the Adriatic Motorway. Table 5.1 summarizes photo documentation during the construction phase and the results of engineering geological mapping of open cuts with GSI estimation according to the methodology introduced by Marinos and Hoek (2001). GSI classification estimation was carried out in cross sections 0+560, 2+380, 2+440, 3+980, 4+360, 4+520, 4+600 and 5+280. GSI values varied from 21 to 37 and flysch rock mass was placed in groups C, D and E - Table 5.2.

Table 5.1 Photodocumentation of open cuts with GSI estimation (Brunčić, 2008)

1. km 0+560 (GSI=25; Group E)



2. km 2+380 (GSI=30; Group D)



3. km 2+380 (GSI=25; Group E)



4. km 2+440 (GSI=25; Group C)



5. km 3+980 (GSI=24; Group E)



6. km 3+980 (GSI=21; Group E)



7. km 3+980 (GSI=37; Group C)



8. km 3+980 (GSI=33; Group D)



9. km 4+360 (GSI=28; Group D)



10. km 4+360 (GSI=35; Group D)



11. km 4+360 (GSI=30; Group D)



12. km 4+520 (GSI=35; Group C)



13. km 4+600 (GSI=32; Group D)






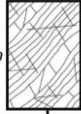

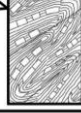
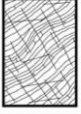

14. km 4+600 (GSI=28; Group D)



15. km 5+280 (GSI=35; Group C)



Table 5.2 GSI estimate for flysch rock mass at Adriatic Motorway (modified form Marinós and Hoek, 2001 and Brunčić, 2008)

GSI FOR HETEROGENEOUS ROCK MASSES SUCH AS FLYSCH (Marinos, P and Hoek, E, 2000)		SURFACE CONDITIONS OF DISCONTINUITIES (Predominantly bedding planes)		COMPOSITION AND STRUCTURE		
From a description of the lithology, structure and surface conditions (particularly of the bedding planes), choose a box in the chart. Locate the position in the box that corresponds to the condition of the discontinuities and estimate the average value of GSI from the contours. Do not attempt to be too precise. Quoting a range from 33 to 37 is more realistic than giving GSI = 35. Note that the Hoek-Brown criterion does not apply to structurally controlled failures. Where unfavourably oriented continuous weak planar discontinuities are present, these will dominate the behaviour of the rock mass. The strength of some rock masses is reduced by the presence of groundwater and this can be allowed for by a slight shift to the right in the columns for fair, poor and very poor conditions. Water pressure does not change the value of GSI and it is dealt with by using effective stress analysis.		VERY GOOD - Very rough, fresh unweathered surfaces	GOOD - Rough, slightly weathered surfaces	FAIR - Smooth, moderately weathered and altered surfaces	POOR - Very smooth, occasionally slickensided surfaces with compact coatings or fillings with angular fragments	VERY POOR - Very smooth slickensided or highly weathered surfaces with soft clay coatings or fillings
 <p>A. Thick bedded, very blocky sandstone The effect of pelitic coatings on the bedding planes is minimized by the confinement of the rock mass. In shallow tunnels or slopes these bedding planes may cause structurally controlled instability.</p>		70	60	A		
 <p>B. Sandstone with thin inter-layers of siltstone</p>			50	B		
 <p>C. Sandstone and siltstone in similar amounts</p>				C		
 <p>D. Siltstone or silty shale with sandstone layers</p>				D		
 <p>E. Weak siltstone or clayey shale with sandstone layers</p>				E		
<p>C, D, E and G - may be more or less folded than illustrated but this does not change the strength. Tectonic deformation, faulting and loss of continuity moves these categories to F and H.</p>						
 <p>F. Tectonically deformed, intensively folded/faulted, sheared clayey shale or siltstone with broken and deformed sandstone layers forming an almost chaotic structure</p>						
 <p>G. Undisturbed silty or clayey shale with or without a few very thin sandstone layers</p>						
 <p>H. Tectonically deformed silty or clayey shale forming a chaotic structure with pockets of clay. Thin layers of sandstone are transformed into small rock pieces.</p>						

➡ : Means deformation after tectonic disturbance

→ : Means deformation after tectonic disturbance

The strength parameters are found to decrease as the weathering stage of the siltstone flysch rock mass increases, but the existing GSI estimation does not include the weathering grade as an influencing parameter that could affect the correction of the GSI value. This effect suggests the need for further evaluation of the GSI concept in regard to different weathering categories of rock masses vulnerable to fast weathering processes.

Geophysics investigations involved seismic refraction and the downhole seismic survey method conducted during field investigations in the design phase (Geofizika, 1991). Based on performed geophysical investigation, following lithological-seismological classification was presented according to P-wave velocities:

- 350 – 650 m/s clay and rock fragments
- 1000 – 1800 m/s siltstone, degraded, moderately to highly weathered
- 1800 – 2600 m/s siltstone, fresh to slightly weathered

Ratio between V_P and V_S for degraded and weathered siltstone varies from 2.5 to 2.7 and the Poisson ratio varies from 0.4 – 0.42. In slightly weathered to fresh flysch rock mass V_P/V_S ratio vary from 2.2 to 2.5 and Poisson ratio varies from 0.37 to 0.40. Dynamic modulus of elasticity varies from 2.0 to 4.0 GPa for weathered siltstones and from 4.0 to 8.0 GPa in slightly weathered to fresh flysch rock mass.

Additional geophysics investigations were performed during year 2013 (Gearheo, 2013) at km 2+380 and 2+440 to obtain the thickness of the weathering profile of flysch and to investigate the distribution of shear waves velocities through the weathering profile. Seismic refraction (profiles RF 1 and RF 2 presented at Figure 5.6) and a multichannel analysis of the surface wave method (profiles MASW 1-2, MASW 2-3, MASW 3-2 and MASW 4-1 presented at and Figure 5.8) were carried out at a length of 35 m with 24 channels and distances between geophones of 1.5 m.

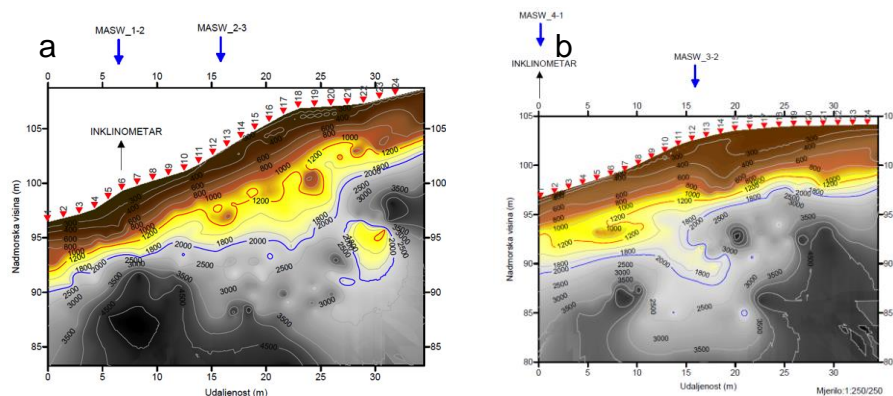


Figure 5.6 Results of geophysical investigation – seismic refraction; (a) profile RF-1 at km 2+380; (b) profile RF-2 at km 2+440 (Gearheo, 2013)

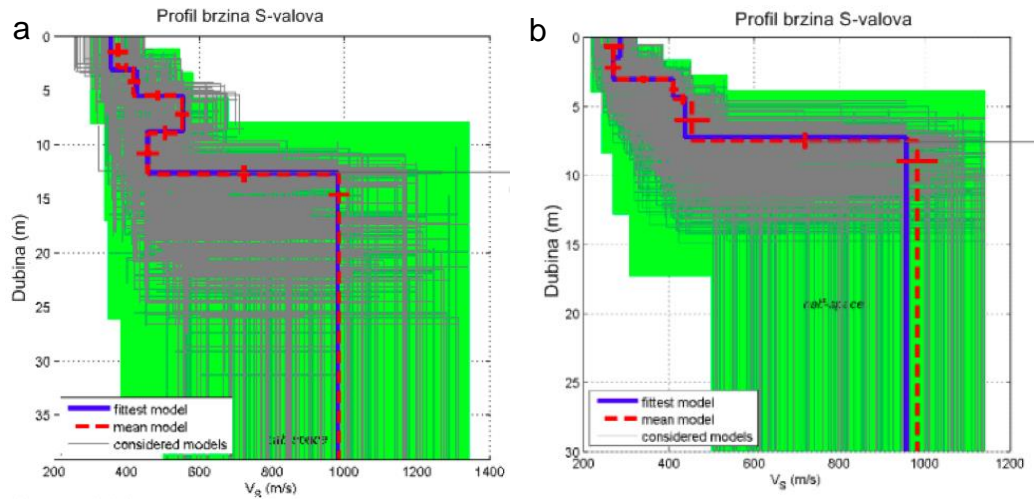


Figure 5.7 Results of geophysical investigation – MASW; (a) profile MASW 1-2 at km 2+380; (b) profile MASW 2-3 at km 2+380 (Geoarheo, 2013)

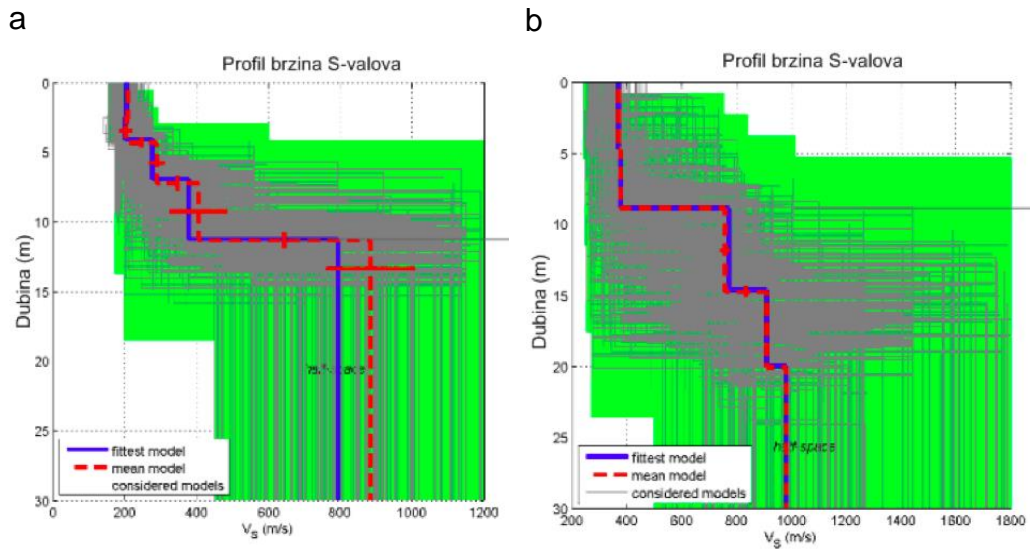


Figure 5.8 Results of geophysical investigation – MASW; (a) profile MASW 3-2 at km 2+440; (b) profile MASW 4-1 at km 2+440 (Geoarheo, 2013)

Geophysics results were correlated with investigation drilling results and laboratory test results, and it was observed that at longitudinal seismic wave velocities over 2,000.0 m/s, slightly weathered (SW) to fresh flysch rock (F) is present. Similar results were measured during field investigations at some other locations with same geological properties (Geofizika, 1991).

Based on performed geotechnical field investigations and laboratory tests, geotechnical models at chainage km 2+380 and 2+440 were determined and selected for further research. Geotechnical cross sections used for modelling are presented at Figure 5.9.

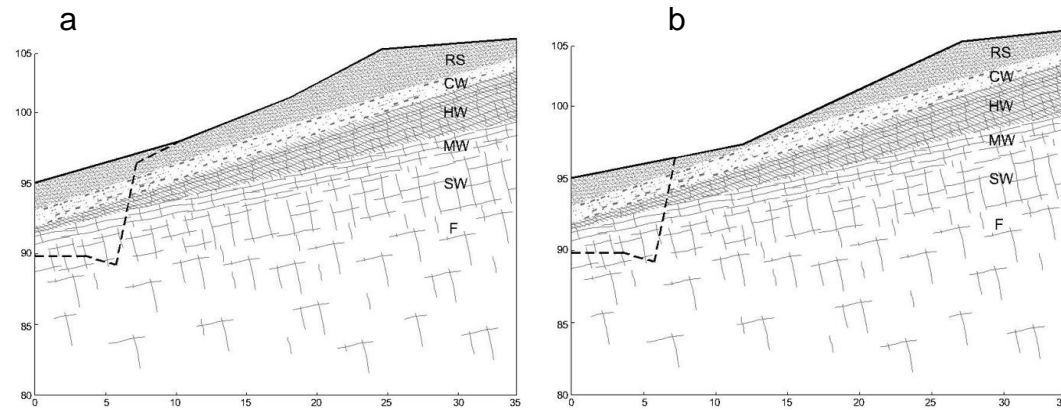


Figure 5.9 Geotechnical cross sections used for numerical analysis; (a) cross section at chainage km 2+380; (b) cross section at chainage km 2+440

The results of geotechnical field investigations have shown that it is not possible to precisely determine the disposition of the different grades of the weathering profile (from RS to F), but it is possible to determine the depth and the location of the fresh flysch rock mass. Geophysical investigations in correlation with other geotechnical field investigations such as engineering geological core determination and classification, and laboratory tests or in-situ tests made it possible to determine the borders of the slightly weathered (SW) and the fresh (F) flysch rock mass. This border also denotes the thickness of the weathering profile of the flysch rock mass, which is an important parameter for numerical analysis.

5.5. Monitoring data and interpretation

During the construction of the Adriatic Motorway route in the Draga Valley, a significant amount of monitoring equipment was installed and numerous

measurements were conducted. The monitoring by the installed equipment was conducted during the construction period and has continued during service period of several years. Most of the monitoring equipment was installed during the years 2004 and 2005.

The monitoring equipment included vertical inclinometers and horizontal deformeters installed in pairs, as shown in a cross sections at chainage km 2+380 and 2+440 (Figure 5.10). Depth of the vertical inclinometers is 15.0 m and length of the horizontal deformeters is 12.0 m. The cross sections at chainage km 2+440.0 and km 2+380 were chosen as a representative cross sections used for the observation of construction behaviour and for numerical back analysis.

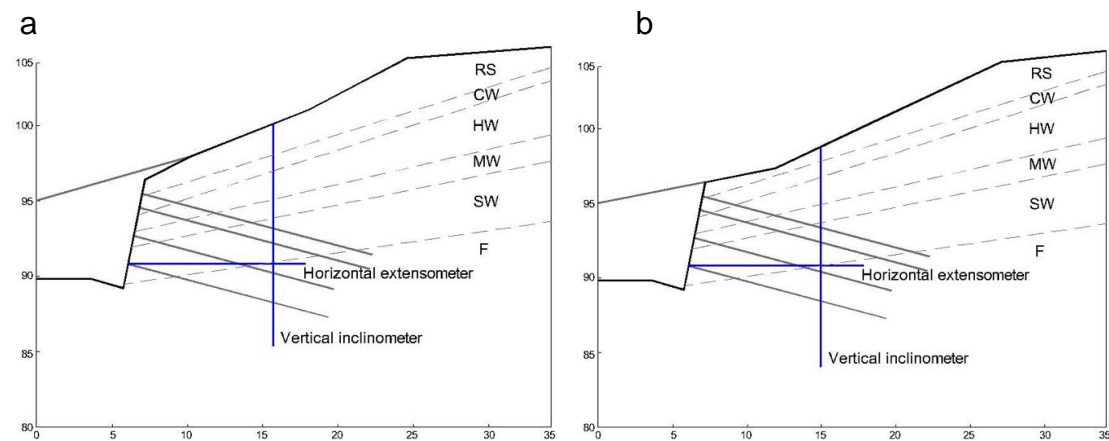


Figure 5.10 Cross sections with monitoring equipment; (a) cross section at chainage km 2+380; (b) cross section at chainage km 2+440

Before the construction began, the vertical inclinometer casings were installed several meters above of the top of the future cut for horizontal displacement monitoring. The horizontal deformer casings were installed in the lower part of the construction area (about 1.5 m above the bottom) after excavation of the cut.

Geodetic benchmarks were also installed as additional control points at the cut construction but their measuring accuracy was significantly lower than those from

inclinometers or deformeters and because of that they were not taken into account for back analysis. The installed anchors were tested using pull-out tests, the results of which indicate the stiffness of the installed anchors, used in numerical models.

The results of the horizontal displacement measurements at the vertical inclinometer casing at the chainage km 2+380 (Figure 5.11 and Figure 5.12) show that most of the displacement occurred in the upper part of the cut, i.e., in layers that are characterized as residual soil to moderately weathered flysch rock mass. A maximum horizontal displacement of 5.4 mm occurred at the top of the inclinometer casing, with the main portions of these displacements occurring during construction (3.6 mm). Displacements that occurred during the service phase (1.8 mm) are significant and reached up to 50% of displacements that occurred during the construction period. With depth increasing horizontal displacement of service period is gradually reduced till depth of 7.0 m where it reaches zero. From plot of horizontal displacement vs. depth (Figure 5.12) it could be seen that displacements have progressively increased at depth of 7.0 m and from 3.0 till 2.0 m that indicates significant change in material properties.

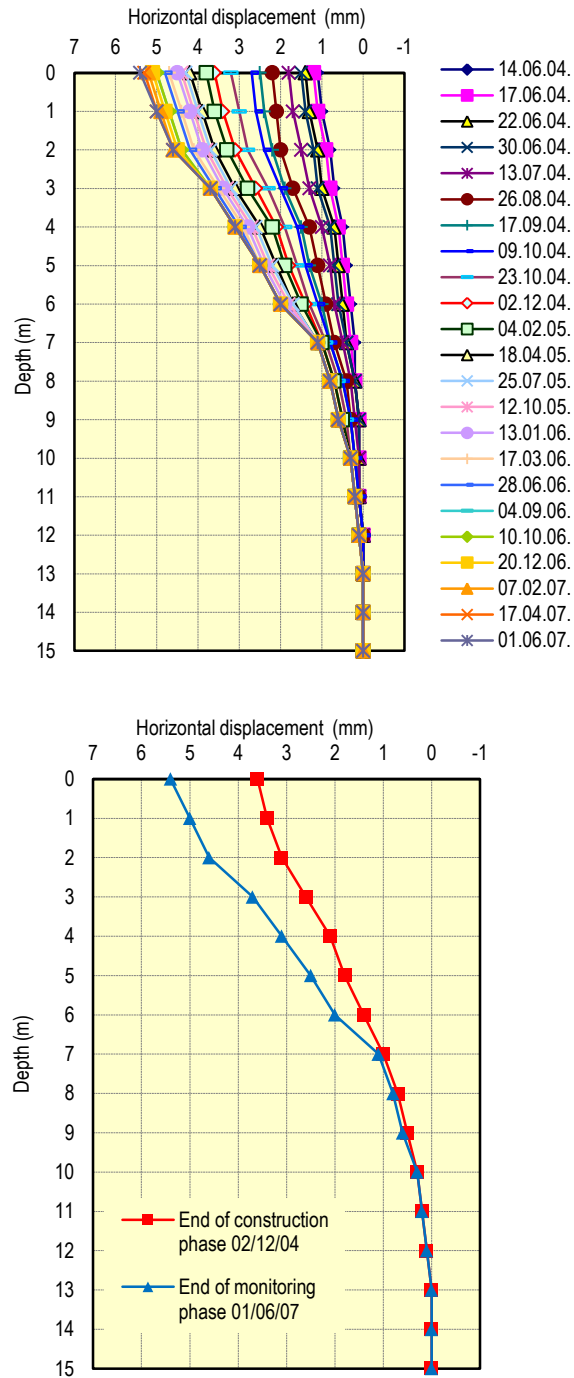


Figure 5.11 Horizontal displacement vs. depth measured at vertical inclinometer at km 2+380

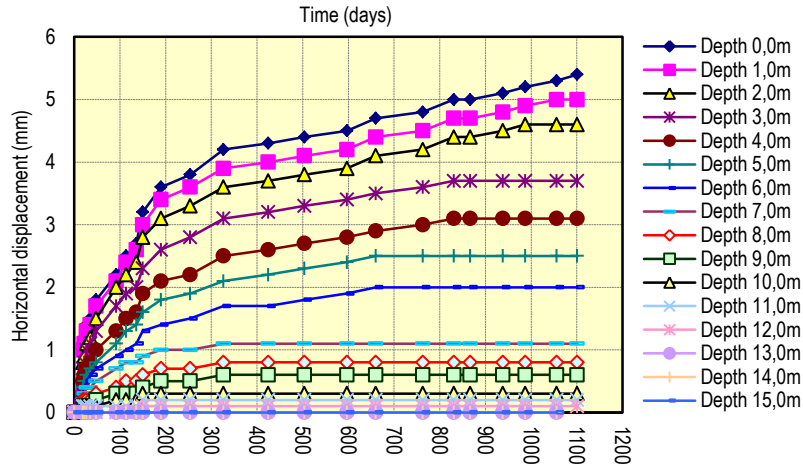


Figure 5.12 Horizontal displacement vs. time measured at vertical inclinometer at km 2+380

After excavation of the cut the horizontal deformer was installed and was measuring horizontal displacement during service phase for 3 years (1,100 days) presented at Figure 5.13 and Figure 5.14. A maximum horizontal displacement of 1.97 mm occurred at the surface of the cut and is reduced along surface distance.

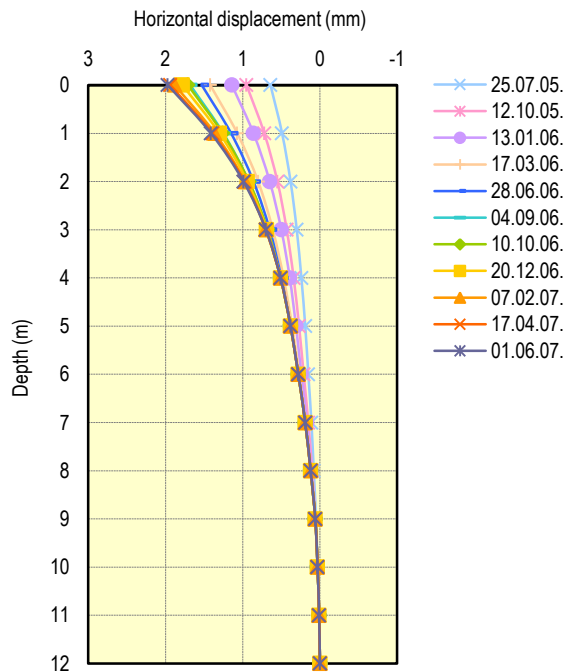


Figure 5.13 Horizontal displacement vs. distance measured at horizontal deformer at km 2+380

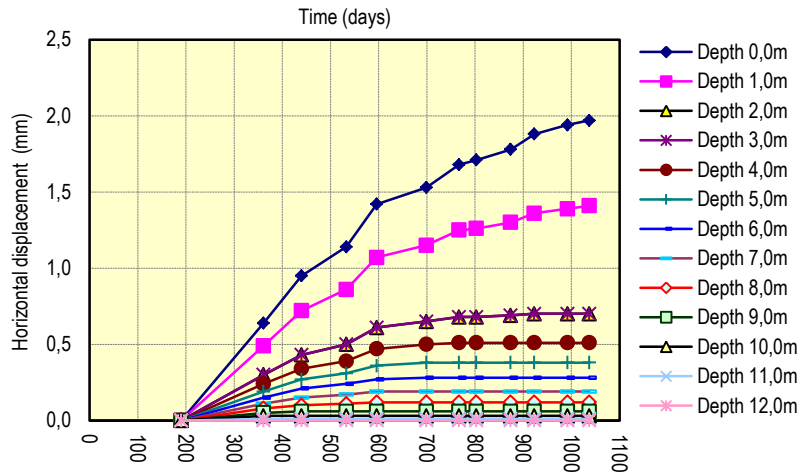


Figure 5.14 Horizontal displacement vs. time measured at horizontal deformer at km 2+380

Similar trend of displacement values and disposition was observed at km 2+440. The results of the horizontal displacement measurements at the vertical inclinometer casing at the chainage km 2+440 (Figure 5.15 and Figure 5.16) show that most of the displacement occurred in the upper part of the cut, i.e., in layers that are characterized as residual soil to moderately weathered flysch rock mass. A maximum horizontal displacement of 6.0 mm occurred at the top of the inclinometer casing, with the main portions of these displacements occurring during construction (3.9 mm). Displacements that occurred during the service phase (2.1 mm) are significant and reached up to 54% of displacements that occurred during the construction period. With depth increasing horizontal displacement of service phase is gradually reduced till depth of 8.0 m where it reaches zero. From plot of horizontal displacement vs. depth (Figure 5.16) it could be seen that displacements have progressively increased at depth of 7.0 m and at 3.0 m that indicates significant change in material properties.

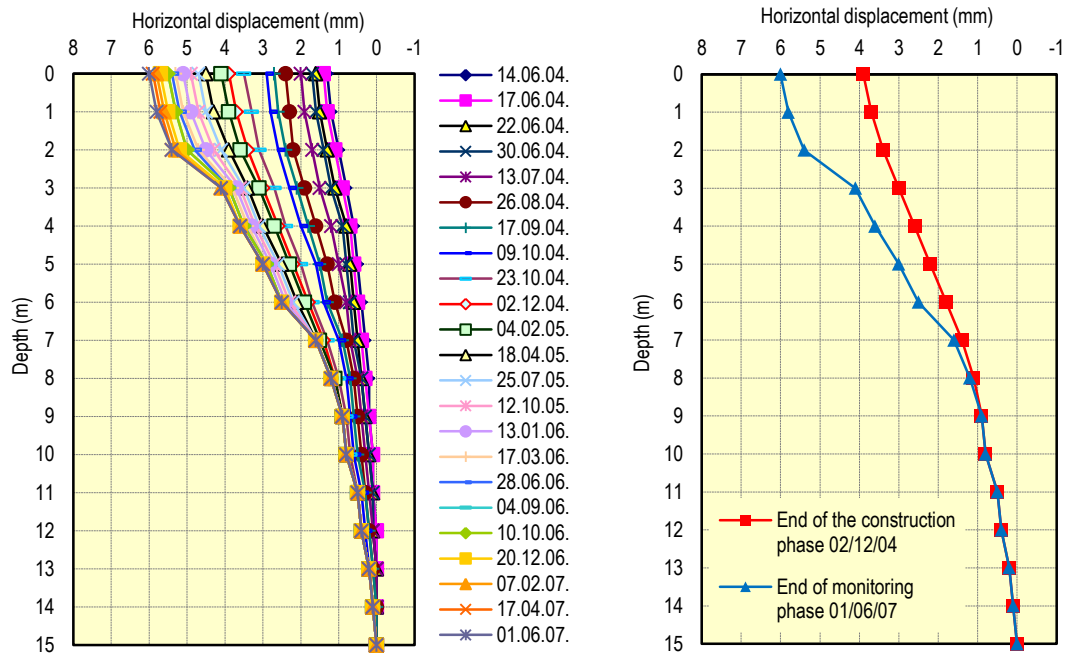


Figure 5.15 Horizontal displacement vs. depth measured at vertical inclinometer at km 2+440

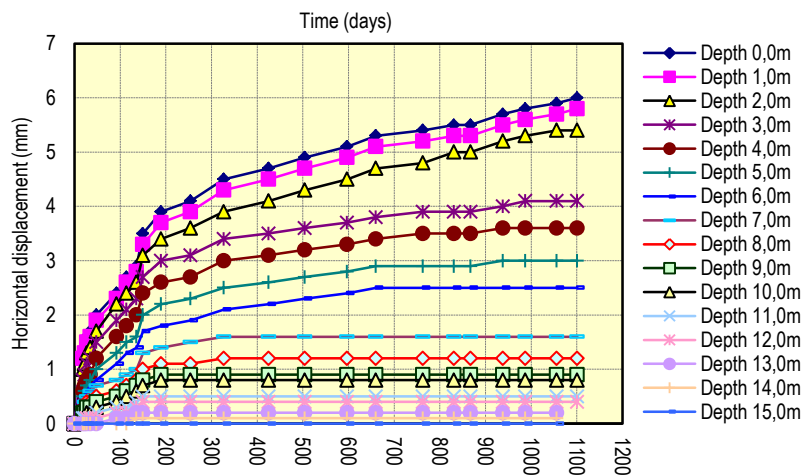


Figure 5.16 Horizontal displacement vs. time measured at vertical inclinometer at km 2+440

After excavation of the cut the horizontal deformer was installed and was measuring horizontal displacement during service phase for 3 years (1,100 days) presented at Figure 5.17 and Figure 5.18. A maximum horizontal displacement of 2.21 mm occurred at the surface of the cut and is reduced along surface distance.

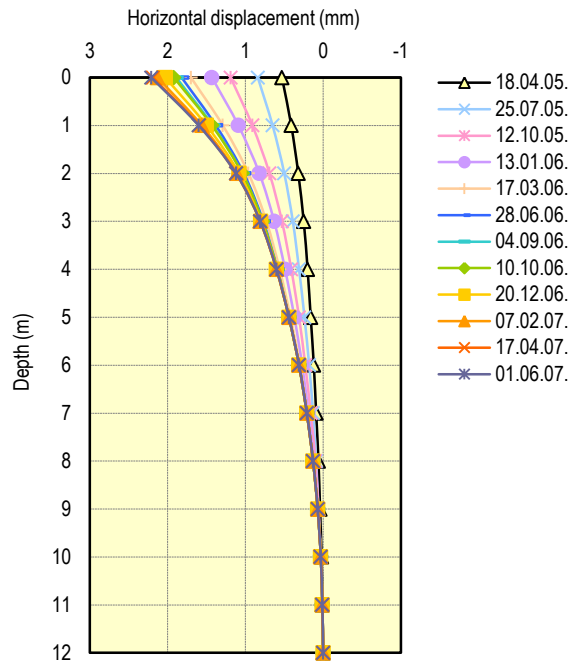


Figure 5.17 Horizontal displacement vs. distance measured at horizontal deformeter at km 2+440

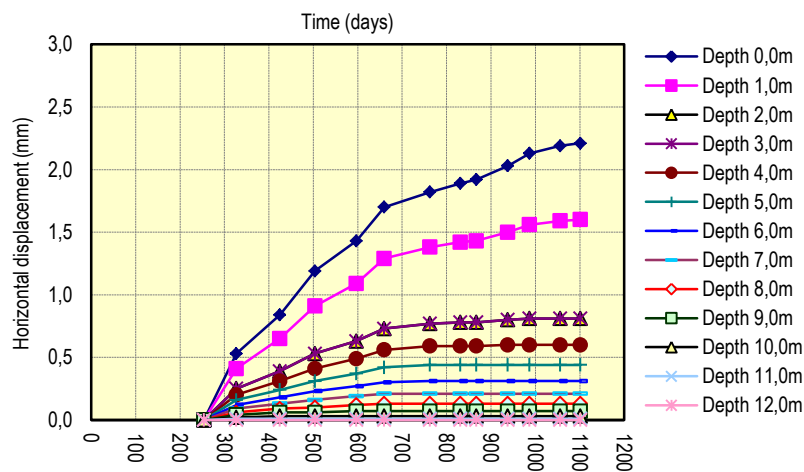


Figure 5.18 Horizontal displacement vs. time measured at horizontal deformeter at km 2+440

5.6. Numerical back analysis of construction phase – cross section at km 2+380

Numerical back analyses have modelled the stages following the construction of the reinforced cut – excavation and reinforcement system. Numerical back analyses of the

construction phase were divided into two different stages: in-situ phase and construction phase.

Initial finite difference was modelled of 100 zones in the i-direction and 33 zones in the j-direction, which represents 50.0 m wide and 28.25 m high model in nature. Elastic material model was assigned for in-situ phase analysis. Boundary conditions for the model were assigned as a pinned boundary condition on the bottom and a fixed-gridpoint velocity in the x-direction along the left and right boundaries. Gravitational load was specified as a global setting in the model with the value of 9.81 m/sec^2 . Finite difference grid used for numerical modelling is presented at Figure 5.19.

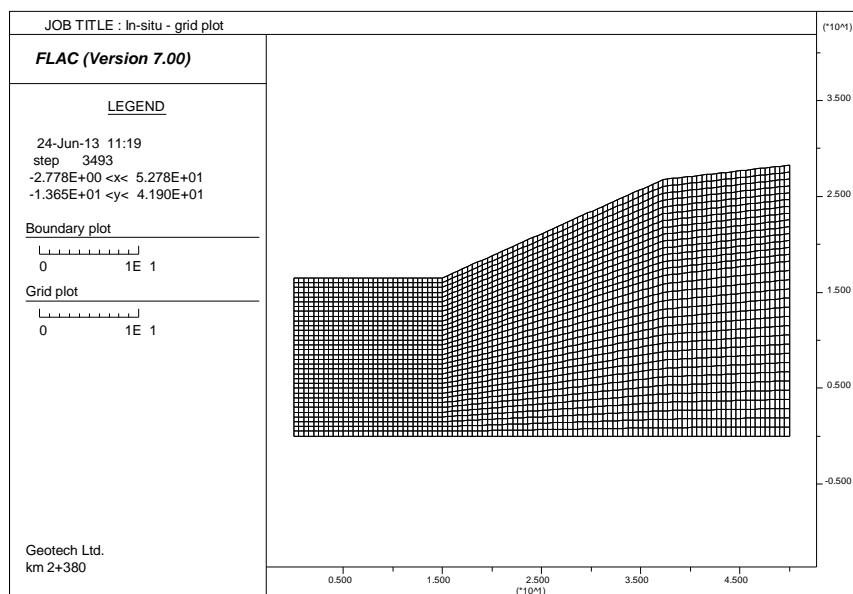


Figure 5.19 Cross section km 2+380 –finite difference grid used for numerical analysis

The first stage is in-situ phase in which the analysis begins at an initial equilibrium state prior to excavation. The initial stress state was found for the given soil conditions, assuming that the ratio of effective horizontal stress to effective vertical stress is 0.5.

For the in-situ phase one uniform geotechnical unit was used to obtain an initial equilibrium state – elastic model that represents stress-strain behaviour. For the in-situ phase analysis elastic model was used with shear modulus of 1.0×10^9 Pa, Poisson ratio of 0.38 and density of $2,000 \text{ kg/m}^3$.

According to laboratory tests and geotechnical field investigations the model was divided into 6 different geotechnical units with similar geotechnical properties. Each of these units represents same or similar soil conditions and weathering grade; from residual soil at the surface to the fresh flysch rock mass at the bottom of the model. Thickness and disposition of each geotechnical unit was mostly determined by geophysical investigations – seismic refraction and MASW in-situ tests. In the upper layer, where the difference between parameters is pronounced with depth, grouping was defined with smaller longitudinal seismic wave velocities. On the other hand, where the difference between parameters is not significantly pronounced with depth, grouping of the geotechnical units at lower half of model was defined with greater longitudinal seismic wave velocities. Geotechnical unit thickness, depth and associated longitudinal seismic wave velocities are summarized in

Table 5.3. The model used for numerical analysis with user-defined groups of geotechnical units is presented at Figure 5.20.

Table 5.3 Cross section km 2+380 – longitudinal wave velocities, thickness and weathering grade of geotechnical units

Description	Symbol	Unit	GU 1	GU 2	GU 3	GU 4	GU 5	GU 6
Longitudinal wave velocity	v_p	m/s	0-400	400-800	800-1200	1200-2000	2000-3000	>3000
From depth	d_{top}	m	0.00	1.60	3.60	4.60	6.75	9.00
To depth	d_{bottom}	m	1.60	3.60	4.60	6.75	9.00	bottom
Thickness	-	m	1.60	2.00	1.00	2.15	2.25	vary
Weathering grade	-	-	RS/CW	CW/HW	HW/MW	MW/SW	SW/F	F

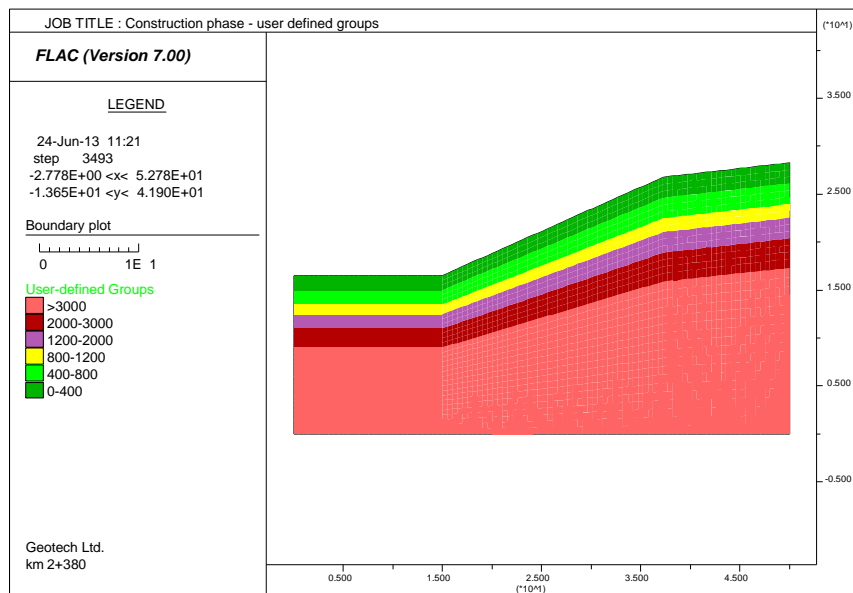


Figure 5.20 Cross section km 2+380 – user-defined groups used for construction phase back analysis

Numerical back analyses have modelled the stages following the construction of the reinforced cut – excavation and rockbolts and sprayed concrete installation. Reinforcements of the cut are simulated in four excavation stages, and after each rockbolt and sprayed concrete were installed – Figure 5.21.

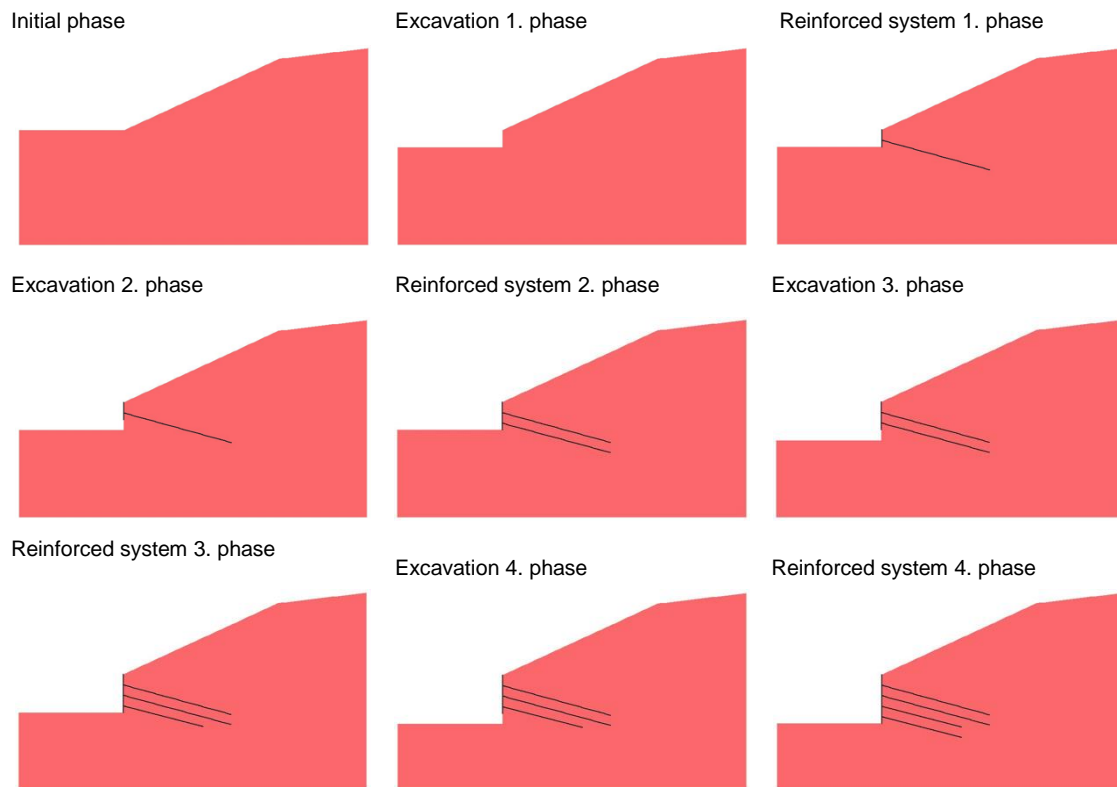


Figure 5.21 Cross section km 2+380 – construction phases used in back analysis

Increments of excavation were modelled by deleting elements of model after which the model was stepped to equilibrium for each phase. Before accessing the next excavation phase, the reinforcing system (beam elements representing the shotcrete face support and cable elements representing the rockbolts) was introduced. This procedure was repeated four times following the construction stages of reinforced cut.

Reducing three-dimensional problem with regularly spaced reinforcement to two-dimensional problems involves averaging the reinforcement effects in three dimensions over the distance between the reinforcement. The engineered slope was modelled using the linear elastoplastic Mohr-Coulomb model. Rockbolts in the model were defined as structural cables, with the stiffness obtained from in-situ pull-out tests. The beam elements and cable elements were assumed to be homogenous, isotropic, linear elastic material with properties shown in Table 5.4.

Table 5.4 Cross section km 2+380 – Properties of rockbolts and shotcrete

Property	Symbol	Value	Unit
<i>Rockbolt properties</i>			
Type of structural element	-	Cable element	-
Rockbolt length	L	9.0 to 15.0	m
Horizontal distance between rockbolts	d	1.80	m
Modulus elasticity of steel	E _c	200E6	kN/m ²
Rockbolt yield force	F _{y,k}	400	kN
	S _{bond}	100	kN/m
	K _{bond}	7.285E6	kN/m/m
<i>Shotcrete properties</i>			
Type of structural element		Beam element	
Modulus elasticity of shotcrete	E	30E6	kN/m ² /m
Moment of inertia	I	281.25E-6	m ⁴ /m
Surface of cross section	A	150E-3	m ² /m

Numerical code used for back analysis of construction phase at km 2+380 is presented in *Appendix 1*.

5.7. Numerical back analysis of service period – cross section at km 2+380

The major difference between creep and other constitutive models in FLAC is the concept of problem time in the simulation. For creep runs, the problem time and timestep represent real time; for static analysis in the other constitutive models, the timestep is an artificial quantity, used only as a means of stepping to a steady-state condition (Itasca, 2011). The timestep in numerical back analysis is controlled by FLAC to change automatically.

The service period analysis was carried out using the initial stress and strain states in the model obtained from construction phase modelling. The soil and rock mass layers in the engineered cut was modelled using the Burger-Mohr-Coulomb model for upper layers, denoted as RS, CW, HW, and MW, whereas the lower layers in the cut, denoted as SW and F, was modelled with the classic elastoplastic Mohr-Coulomb model and was not processed as time dependent (Figure 5.22).

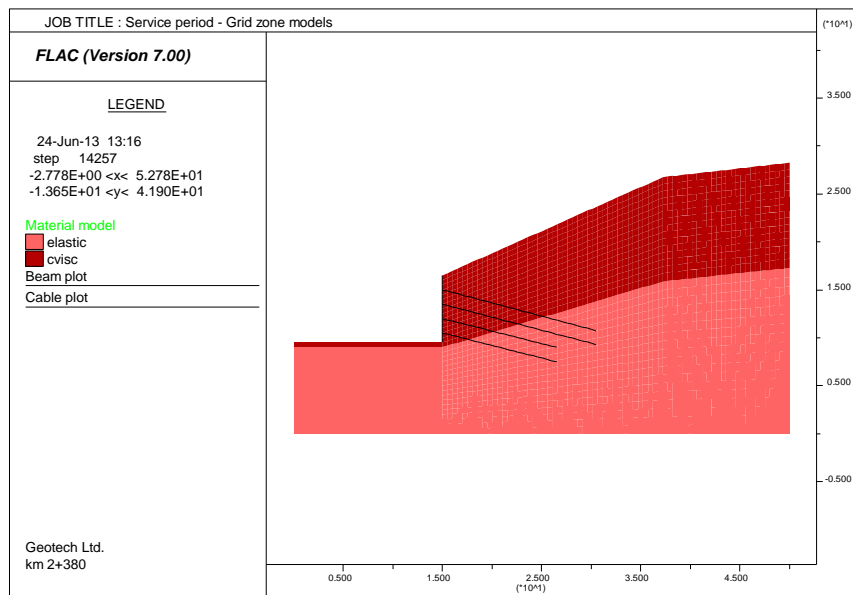


Figure 5.22 Cross section km 2+380 – Grid zone models used for numerical back analysis for service period

The determination of the Burger model parameters for each geotechnical unit was the most challenging part of the numerical analysis. Because of numerous uncertainties, the simplified method for parameter estimation in the first iteration was used: the shear modulus of the Maxwell unit, G_M , in the Burger model was referred to as a shear modulus, G , in the elastoplastic model obtained from a back analysis carried out from the construction phase. The shear modulus of the Kelvin unit, G_K , that controls primary creep, was set to be several times higher than the shear modulus of the Maxwell unit, G_M . The creep parameters of the viscosity of the Kelvin unit, η_K , and

the Maxwell unit, η_M , were taken as the specific ratio $R=100$; $\eta_M/\eta_K=R$, as it explained previously.

Disposition and thickness of geotechnical units are identical to construction phase analysis – Figure 5.23.

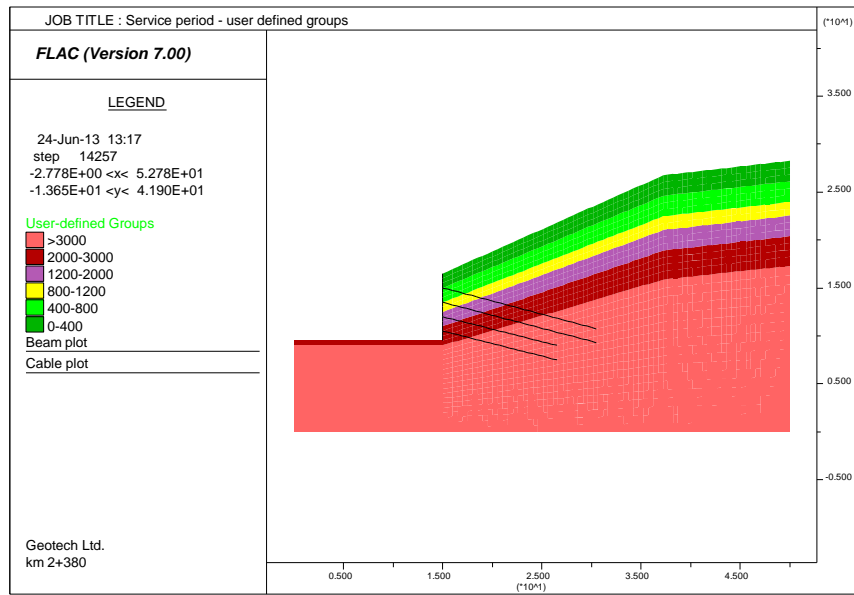


Figure 5.23 Cross section km 2+380 – user-defined groups used for numerical back analysis for service period

Numerical code used for back analysis of service period at km 2+380 is presented in *Appendix 1*.

5.8. Numerical back analysis of construction phase – cross section at km 2+440

Numerical back analyses have been performed with similar methodology as for cross section at km 2+380.

Initial finite difference was modelled out of 100 zones in the i-direction and 33 zones in the j-direction that represent a 50.0 m wide and 28.75 m high model in nature. Elastic material model was assigned for in-situ phase analysis. Boundary conditions

for the model were assigned as a pinned boundary condition on the bottom and a fixed-gridpoint velocity in the x-direction along the left and right boundaries. Gravitational load was specified as a global setting in the model with the value of 9.81 m/sec^2 . Finite difference grid used for numerical modelling is presented at Figure 5.24.

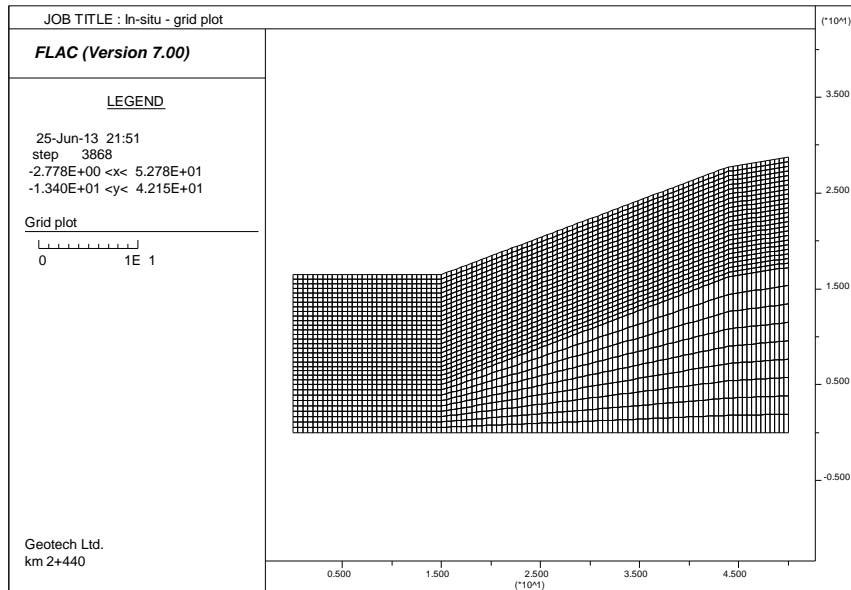


Figure 5.24 Cross section km 2+4400 –finite difference grid used for numerical analysis

The first stage is in-situ phase in which the analysis begins at an initial equilibrium state prior to excavation. The initial stress state was found for the given soil conditions, assuming that the ratio of effective horizontal stress to effective vertical stress is 0.5.

For in-situ phase one uniform a geotechnical unit was used to obtain an initial equilibrium state – elastic model that represents stress-strain behaviour. For in-situ phase analysis an elastic model was used with shear modulus of $1.0\text{e}9 \text{ Pa}$, Poisson ratio of 0.38 and density of $2,000 \text{ kg/m}^3$.

According to laboratory tests and geotechnical field investigations the model was divided into 6 different geotechnical units with similar geotechnical properties. Each of these units represents same or similar soil conditions and weathering grade; from residual soil at the surface to the fresh flysch rock mass at the bottom of the model. Thickness and disposition of each geotechnical unit was mostly determined by geophysical investigations – seismic refraction and MASW in-situ tests. In the upper layer, where the difference between parameters is pronounced with depth, grouping was defined with smaller longitudinal seismic wave velocities. On the other hand, where the difference between parameters is not significantly pronounced with depth, grouping of the geotechnical units at the lower half of model was defined with greater longitudinal seismic wave velocities. Geotechnical unit thickness, depth and associated longitudinal seismic wave velocities are summarized in Table 5.5. The model used for numerical analysis with user-defined groups of geotechnical units is presented at Figure 5.25.

Table 5.5 Cross section km 2+440 – longitudinal wave velocities, thickness and weathering grade of geotechnical units

Description	Symbol	Unit	GU 1	GU 2	GU 3	GU 4	GU 5	GU 6
Longitudinal wave velocity	v_p	m/s	0-400	400-800	1200	2000	3000	>3000
From depth	d_{top}	m	0.00	0.70	3.00	4.25	8.00	11.25
To depth	d_{bottom}	m	0.70	3.00	4.25	8.00	11.25	bottom
Thickness	-	m	0.70	2.30	1.25	3.75	3.25	vary
Weathering grade	-	-	RS/CW	CW/HW	HW/MW	MW/SW	SW/F	F

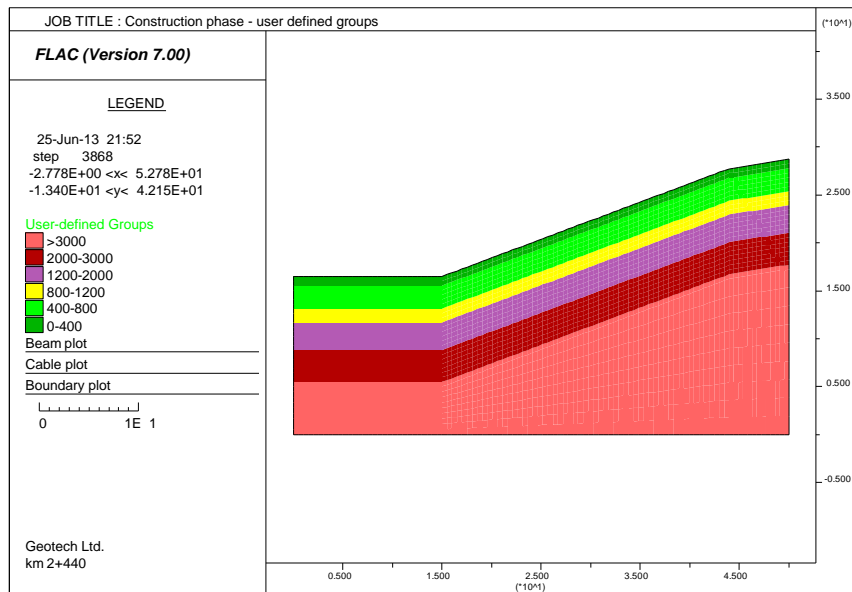


Figure 5.25 Cross section km 2+440 – user-defined groups used for construction phase back analysis

Numerical back analyses have modelled the stages following the construction of the reinforced cut – excavation and rockbolts and the sprayed concrete installation. Reinforcements of the cut are simulated in four excavation stages and after each rockbolt and sprayed concrete were installed – Figure 5.26.

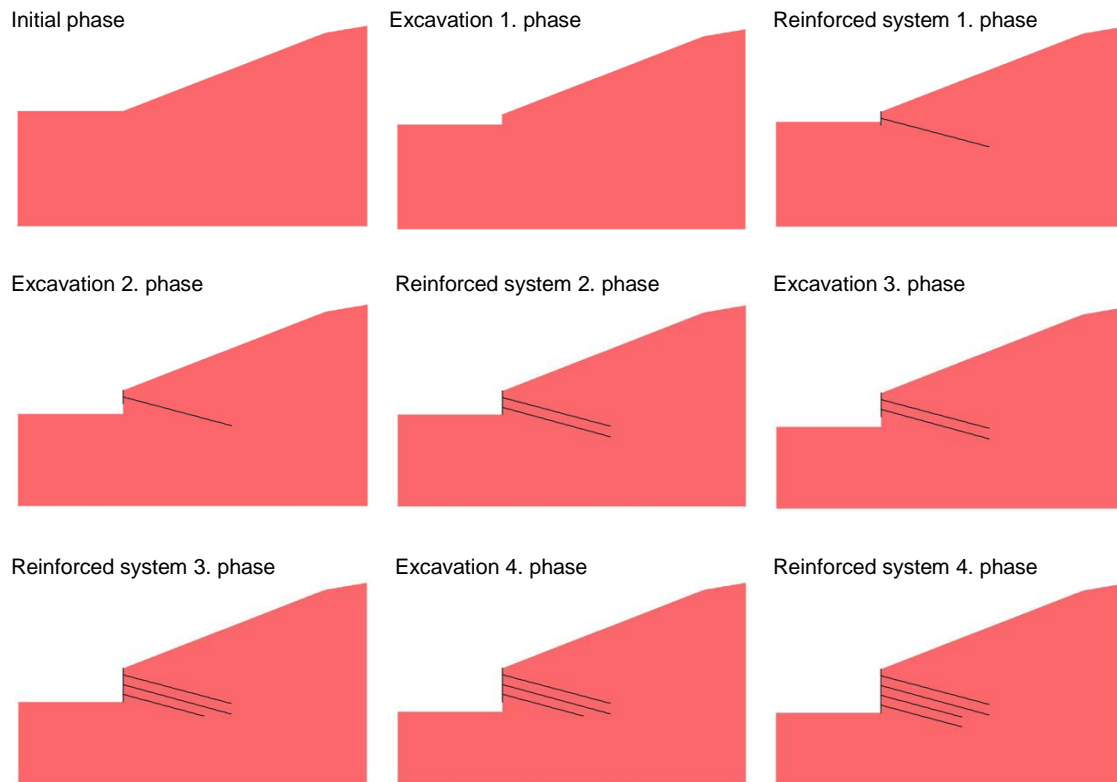


Figure 5.26 Cross section km 2+4400 – construction phases used for back analysis

Increments of excavation were modelled by deleting elements of the model after which the model was stepped to equilibrium for each phase. Before accessing the next excavation phase, the reinforcing system (beam elements representing the shotcrete face support and cable elements representing the rockbolts) was introduced. This procedure was repeated four times following the construction stages of reinforced cut.

Reducing three-dimensional problems with regularly spaced reinforcement to two-dimensional problems involves averaging the reinforcement effects in three dimensions over the distance between the reinforcement. The engineered slope is modelled using the linear elastoplastic Mohr-Coulomb model. Rockbolts in the model were defined as structural cables, with the stiffness obtained from in-situ pull-out tests. The beam elements and cable elements were assumed to be homogenous, isotropic, linear elastic material with properties shown in Table 5.6.

Table 5.6 Cross section km 2+440 – Properties of rockbolts and shotcrete

Property	Symbol	Value	Unit
<i>Rockbolt properties</i>			
Type of structural element	-	Cable element	-
Rockbolt length	L	9.0 to 15.0	m
Horizontal distance between rockbolts	d	1.80	m
Modulus elasticity of steel	E _c	200E6	kN/m ²
Rockbolt yield force	F _{y,k}	400	kN
	S _{bond}	100	kN/m
	K _{bond}	7.285E6	kN/m/m
<i>Shotcrete properties</i>			
Type of structural element		Beam element	
Modulus elasticity of shotcrete	E	30E6	kN/m ² /m
Moment of inertia	I	281.25E-6	m ⁴ /m
Surface of cross section	A	150E-3	m ² /m

Numerical code used for back analysis of construction phase at km 2+440 is presented in *Appendix 2*.

5.9. Numerical back analysis of service period – cross section at km 2+440

Numerical back analyses have been performed with similar methodology as for cross section at km 2+380.

The service period analyses were carried out using the initial stress and strain states in the model obtained from construction phase modelling. The soil and rock mass layers in the engineered cut were modelled using the Burger-Mohr-Coulomb model for upper layers, denoted as RS, CW, HW, and MW, whereas the lower layers in the cut,

denoted as SW and F, were modelled with the classic elastoplastic Mohr-Coulomb model and was not processed as time dependent (Figure 5.27).

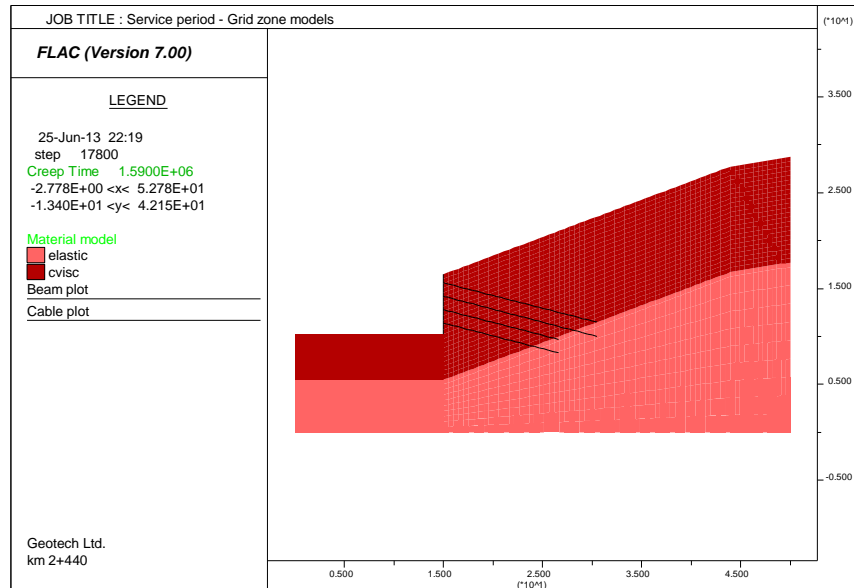


Figure 5.27 Cross section km 2+440 – Grid zone models used for numerical back analysis for service period

Disposition and thickness of the geotechnical unit was identical to the construction phase analysis – Figure 5.28.

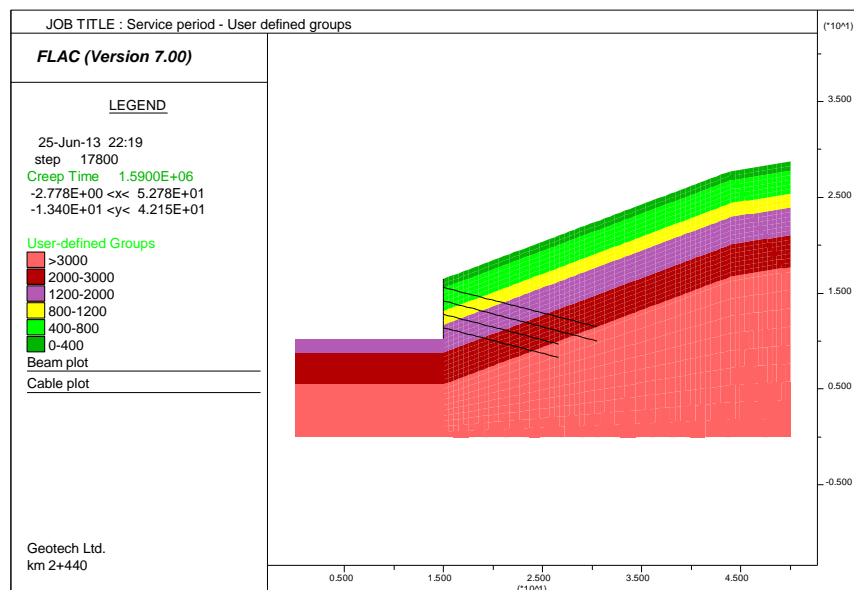


Figure 5.28 Cross section km 2+440 – user-defined groups used for numerical back analysis for service period

Numerical code used for back analysis of service period at km 2+440 is presented in *Appendix 2*.

6. RESULTS OF THE NUMERICAL BACK ANALYSIS AND INTERPRETATION

6.1. Results of construction phase analysis – cross section at km 2+380

In the in-situ phase the analysis begins as an initial equilibrium state prior to excavation. For the in-situ phase, one uniform geotechnical unit was used to obtain an initial equilibrium state – elastic model that represents stress-strain behaviour.

Total vertical stress contours at equilibrium state are presented at Figure 6.1 and total horizontal stress condition is presented at Figure 6.2.

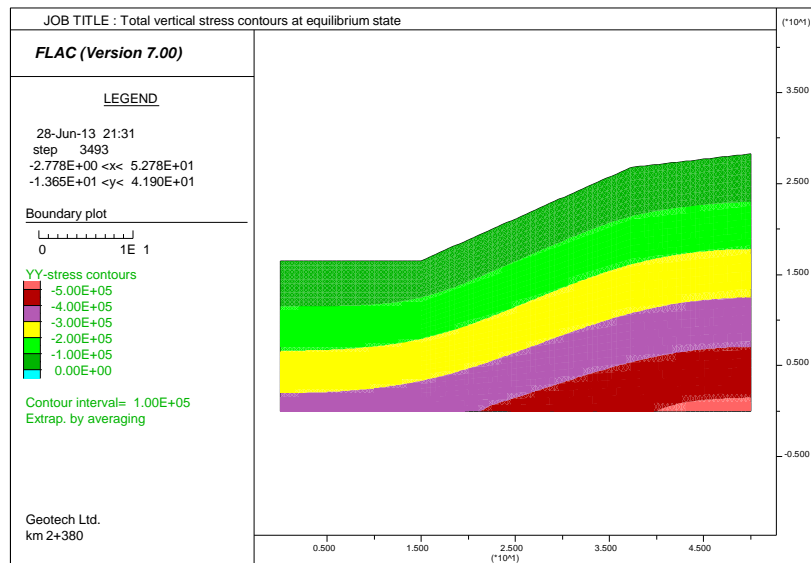


Figure 6.1 Cross section at km 2+380 – total vertical stress contours at equilibrium state

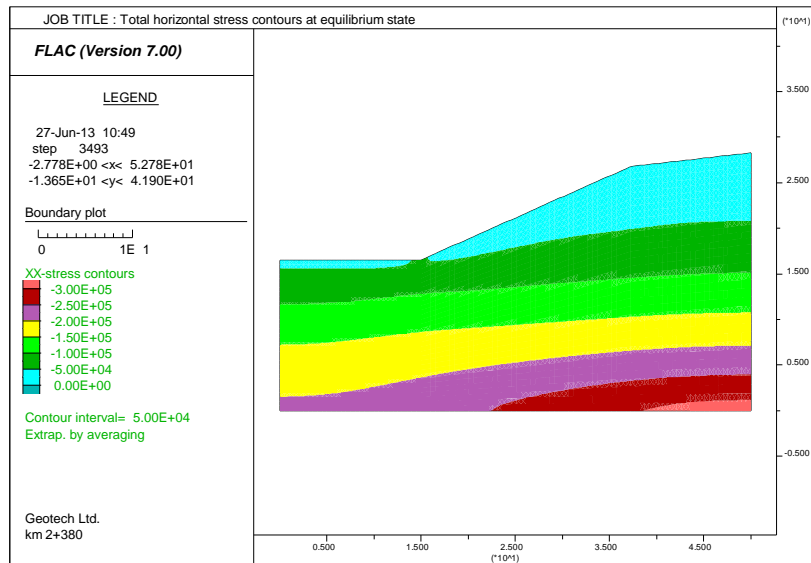


Figure 6.2 Cross section at km 2+380 – total horizontal stress contours at equilibrium state

Numerical back analyses have modelled the stages following the construction of the reinforced cut – excavation and rockbolts and the sprayed concrete installation. Reinforcements of the cut were simulated in four excavation stages and after each, a reinforced system was installed – Figure 5.21. Geotechnical unit thickness, depth and associated longitudinal seismic wave velocities are summarized in

Table 5.3 and the model used for numerical analysis with user-defined groups of geotechnical units is presented at Figure 5.20. Rockbolts in the model were defined as structural cables, with the stiffness obtained from in-situ pull-out tests and the shotcrete is modelled as liner beam elements. Properties of the beam elements and cable elements are presented in Table 5.4.

Deformability parameters obtained from numerical back analysis and are presented in

Table 6.1.

Table 6.1 Cross section km 2+380 – deformability parameters of geotechnical units obtained from construction phase back analysis

Description	Symbol	Unit	GU 1	GU 2	GU 3	GU 4	GU 5	GU 6
Longitudinal wave velocity	v_p	m/s	0-400	400-800	800-1200	1200-2000	2000-3000	>3000
Weathering grade	-	-	RS/CW	CW/HW	HW/MW	MW/SW	SW/F	F
Model	-	-	cvisc	cvisc	cvisc	cvisc	cvisc	elastic
Cohesion	c	kPa	15	25	25	50	75	75
Friction angle	ϕ	°	28	32	32	32	32	32
Mass density	γ	kg/m ³	2,000	2,000	2,000	2,000	2,000	2,150
Poisson coefficient	ν	-	0.38	0.38	0.38	0.38	0.38	0.38
Shear modulus	G	Pa	5.0E+05	2.0E+06	3.5E+06	1.5E+07	5.0E+07	1.0E+08

Total vertical stress contours at the end of the construction phase are presented at

Figure 6.3 and total horizontal stress contours are presented at Figure 6.4.

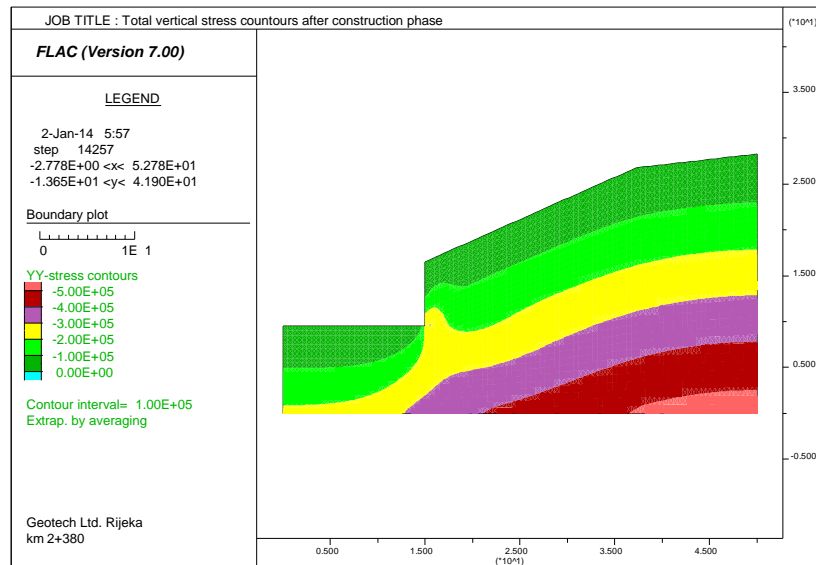


Figure 6.3 Cross section at km 2+380 – total vertical stress contours after construction phase

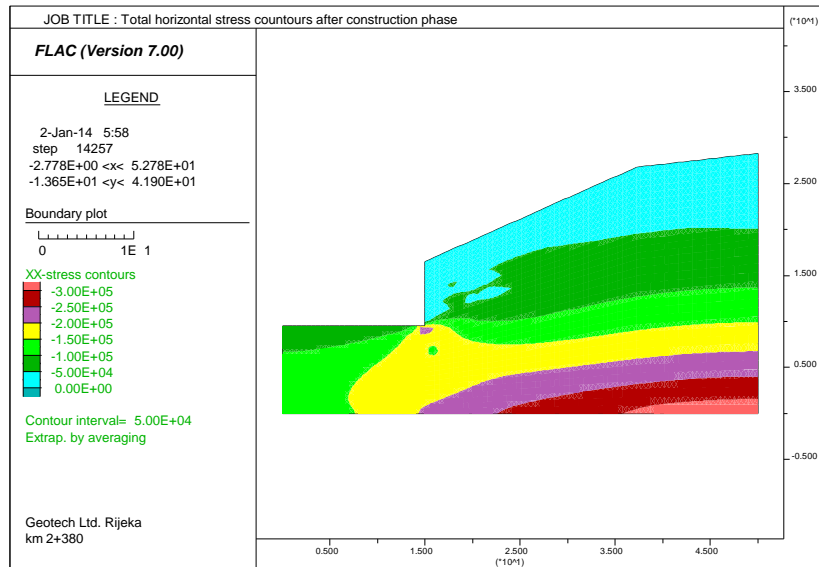


Figure 6.4 Cross section at km 2+380 – total horizontal stress contours after construction phase

Axial forces realized in rockbolt in the construction phase are presented at Figure 6.5. Maximum force (135.5 kN) was realized in upper rockbolt, while in the second and third row the forces were 103.8 kN and 60.4 kN respectively. At the bottom rockbolt null force was activated since it was installed after final excavation of the model. Most part of the forces were realised into first half length of the rockbolt, while in other parts the forces were minimalized.

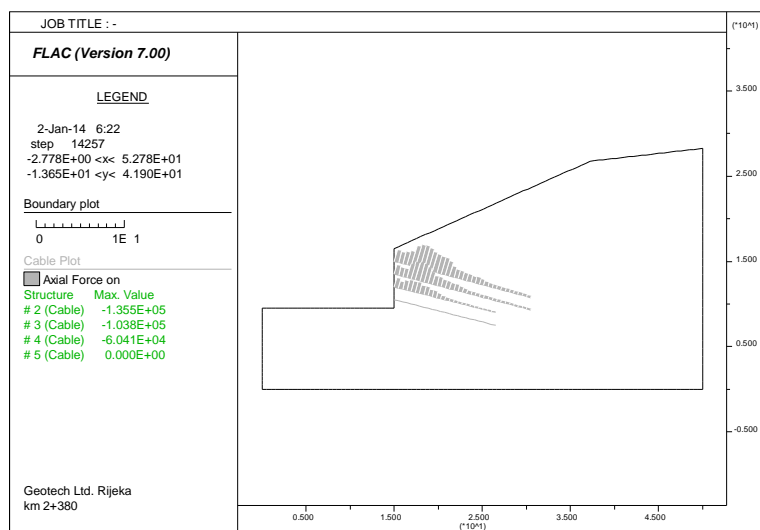


Figure 6.5 Cross section at km 2+380 – axial forces in rockbolts after construction phase

Displacement vectors after the construction phase (Figure 6.6) have shown that maximum displacements were realized in the upper part of the cut in residual soil or completely weathered flysch. Local plasticity was noticed in this part of the model, which can be the cause of this behaviour.

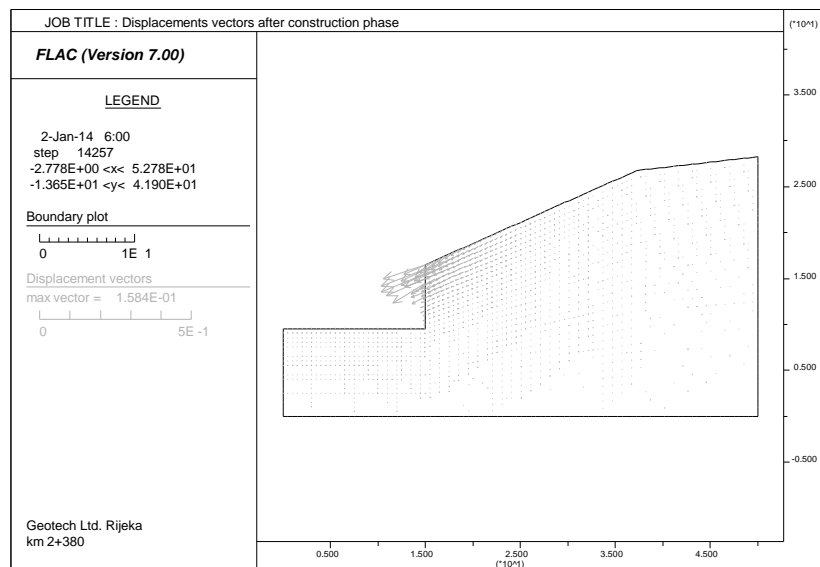


Figure 6.6 Cross section at km 2+380 – displacement vectors after construction phase

Most parts of the horizontal displacements (Figure 6.7) were realized in the upper part of the cut in region up to 10.0 m distance from the excavation phase. Greater displacements were noted in the zone of residual soil to completely weathered flysch that was represented with geotechnical units with very low strength and deformability parameters.

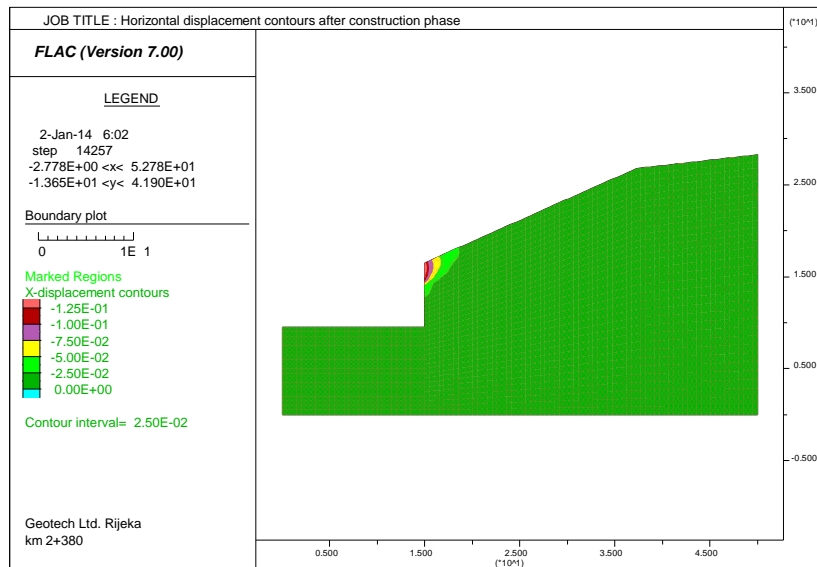


Figure 6.7 Cross section at km 2+380 – horizontal displacement contours after construction phase

6.2. Results of service period analysis – cross section at km 2+380

The service period analyses were carried out using the initial stress and strain states in the model obtained from construction phase modelling. The soil and rock mass layers in the engineered cut was modelled using the Burger-Mohr-Coulomb model for upper layers, denoted as RS, CW, HW, and MW, whereas the lower layers in the cut, denoted as SW and F, was modelled with the elastic model and was not processed as time dependent (Figure 5.22). The model used for numerical back analysis of service period is presented at Figure 5.23. The same parameters of reinforcing system as for back analysis of construction phase are used. Results of numerical back analysis of the service period for a timestep of 901 days that corresponds to the duration of the monitoring period are presented as follows.

Deformability parameters were obtained from numerical back analysis and are presented at Figure 6.2.

Table 6.2 Cross section km 2+380 – deformability and creep parameters of geotechnical units obtained from service period back analysis

Description	Symbol	Unit	GU 1	GU 2	GU 3	GU 4	GU 5	GU 6
Longitudinal wave velocity	v_p	m/s	0-400	400-800	800-1200	1200-2000	2000-3000	>3000
Weathering grade	-	-	RS/CW	CW/HW	HW/MW	MW/SW	SW/F	F
Model	-	-	cvisc	cvisc	cvisc	cvisc	cvisc	elastic
Cohesion	c	kPa	15	25	25	50	75	75
Friction angle	ϕ	°	28	32	32	32	32	32
Mass density	γ	kg/m ³	2000	2000	2000	2000	2000	2150
Poisson coefficient	ν	-	0,38	0,38	0,38	0,38	0,38	0,38
Shear modulus of Maxwell unit	G_M	Pa	5,0E+05	2,0E+06	3,5E+06	1,5E+07	5,0E+07	1,0E+08
Shear modulus of Kelvin unit	G_K	Pa	5,0E+06	2,0E+07	3,5E+07	1,5E+08	5,0E+08	-
Maxwell viscosity	η_K	Pamin	5,0E+13	5,0E+13	7,5E+13	1,0E+14	1,0E+14	-
Kelvin viscosity	η_M	Pamin	5,0E+15	5,0E+15	7,5E+15	1,0E+16	1,0E+16	-

Total vertical stress contours at the end of the service period of 901 days are presented at Figure 6.8 and total horizontal stress contours is presented at Figure 6.9.

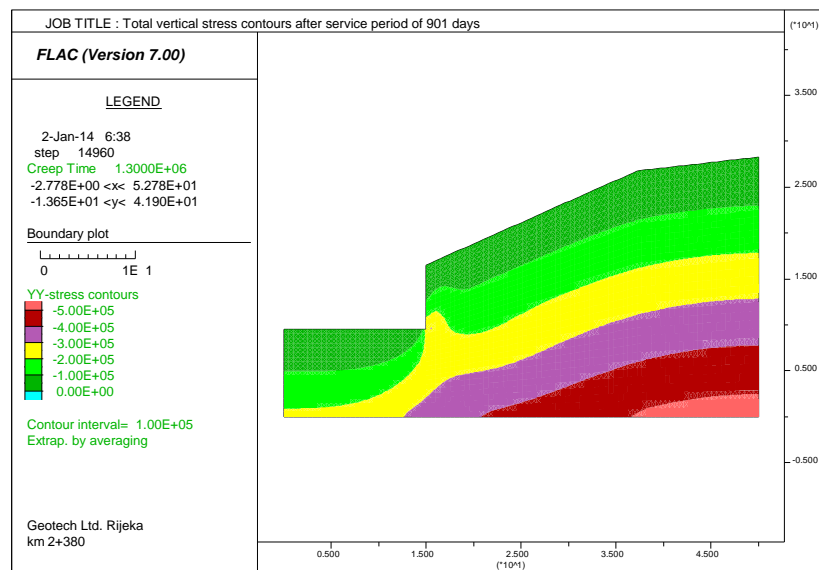


Figure 6.8 Cross section at km 2+380 – total vertical stress contours after service period of 901 days

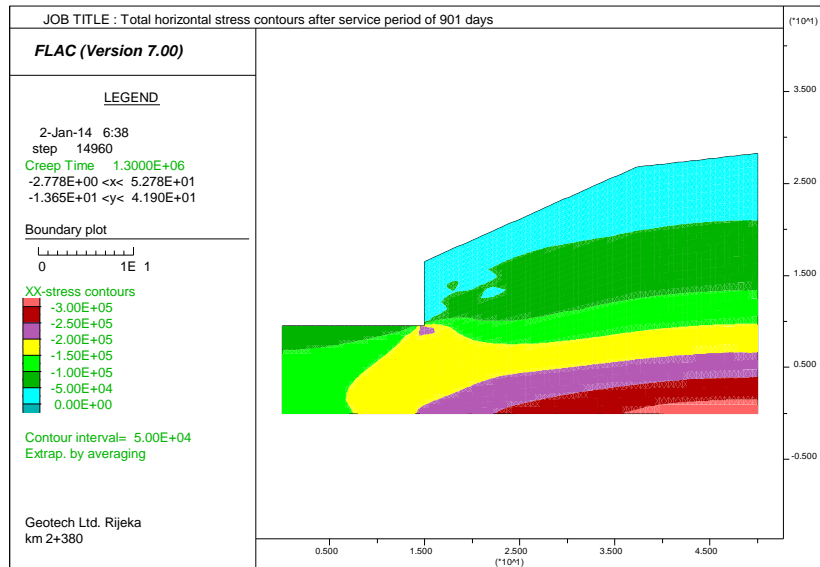


Figure 6.9 Cross section at km 2+380 – total horizontal stress contours after service period of 901 days

Axial forces realized in rockbolt in the construction phase are presented at Figure 6.10. Maximum force (145.2 kN) was realized in upper rockbolt, while in the second and third row the forces were 114.8 kN and 73.6 kN respectively. At the bottom rockbolt the axial force of 14.9 kN was activated because of stress redistribution over time.

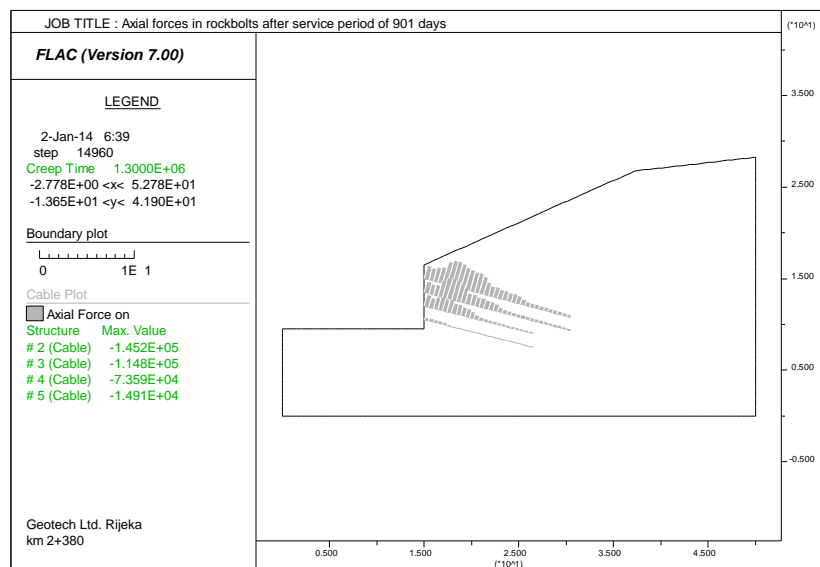


Figure 6.10 Cross section at km 2+380 – axial forces in rockbolts after service period of 901 days

Displacement vectors after the construction phase (Figure 6.11) have shown that displacements are slightly increasing over time and most of them were realized in the upper part of the cut in residual soil or completely weathered flysch.

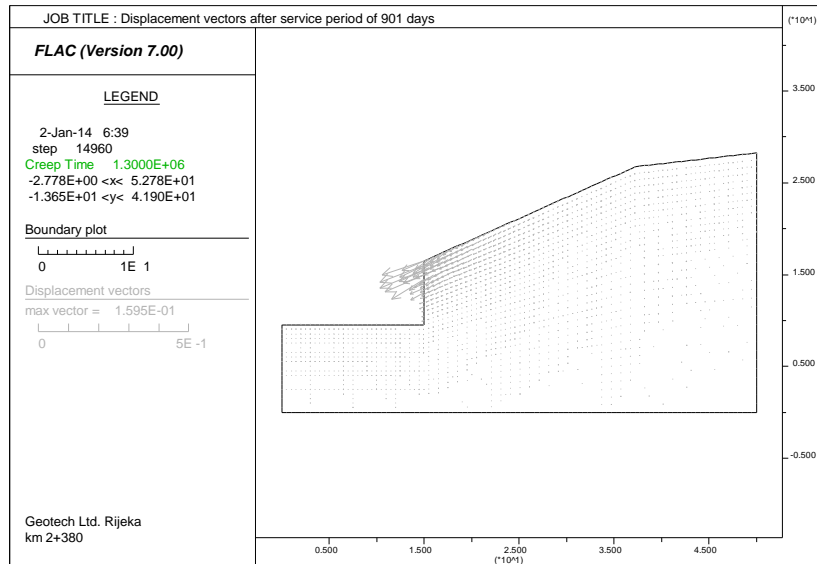


Figure 6.11 Cross section at km 2+380 – displacement vectors after service period of 901 days

Horizontal displacement contours after the service period of 901 days (Figure 6.12) were slightly increasing and are hardly visible. Disposition of horizontal displacements was similar to the construction phase.

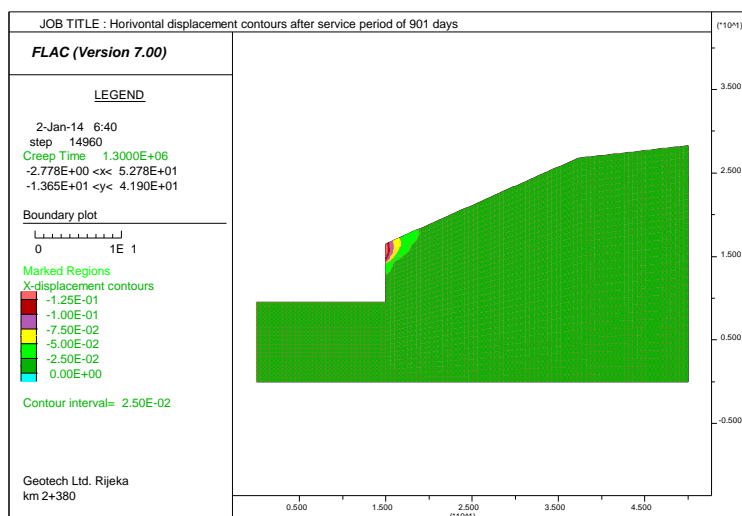


Figure 6.12 Cross section at km 2+380 – horizontal displacement contours after service period of 901 days

6.3. Results of construction phase analysis – cross section at km

2+440

Total vertical stress contours at equilibrium state are presented at Figure 6.13 and total horizontal stress condition is presented at Figure 6.14.

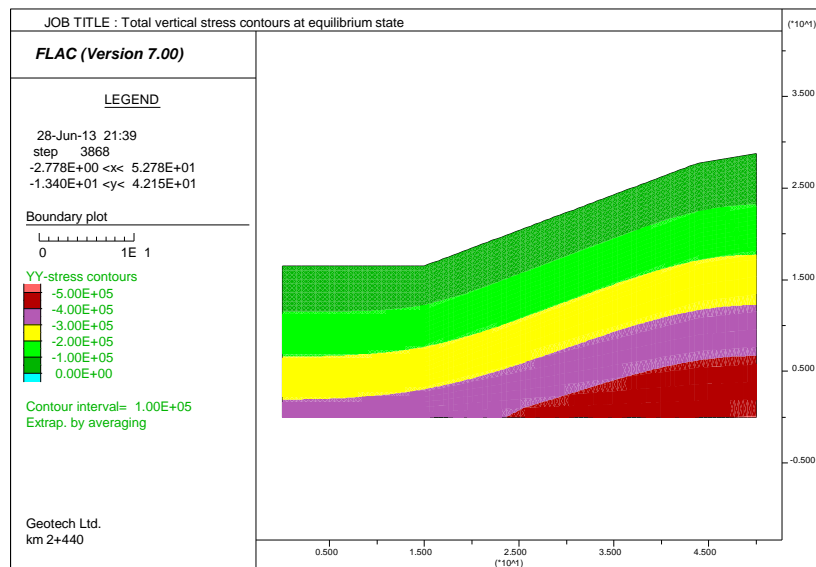


Figure 6.13 Cross section at km 2+440 – total vertical stress contours at equilibrium state

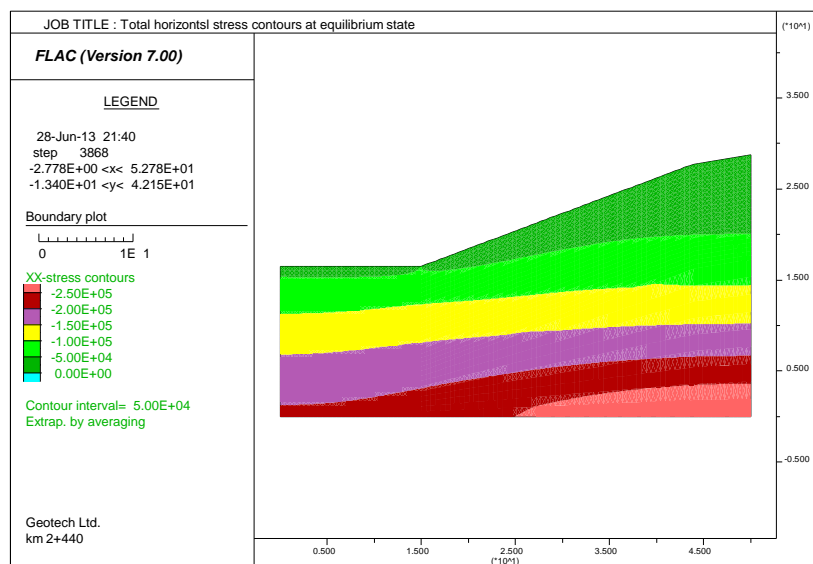


Figure 6.14 Cross section at km 2+440 – total horizontal stress contours at equilibrium state

Numerical back analyses have modelled the stages following the construction of the reinforced cut – excavation and rockbolts and sprayed concrete installation. Reinforcements of the cut were simulated in four excavation stages and after each reinforced system was installed – Figure 5.26. Geotechnical unit thickness, depth and associated longitudinal seismic wave velocities are summarized in Table 5.5 and the model used for numerical analysis with user-define groups of geotechnical units is presented at Figure 5.25. Rockbolts in the model were defined as structural cables, with the stiffness obtained from in-situ pull-out tests, and the shotcrete was modelled as liner beam elements. Properties of the beam elements and cable elements are presented in Table 5.6.

Deformability parameters were obtained from numerical back analysis and are presented in Table 6.3.

Table 6.3 Cross section km 2+440 – deformability parameters of geotechnical units obtained from construction phase back analysis

Description	Symbo l	Unit	GU 1	GU 2	GU 3	GU 4	GU 5	GU 6
Longitudinal wave velocity	v_p	m/s	0-400	400-800	800-1200	1200-2000	2000-3000	>3000
Weathering grade	-	-	RS/CW	CW/HW	HW/MW	MW/SW	SW/F	F
Model	-	-	cvisc	cvisc	cvisc	cvisc	cvisc	elastic
Cohesion	c	kPa	15	25	25	50	75	75
Friction angle	ϕ	°	28	32	32	32	32	32
Mass density	γ	kg/m ³	2000	2000	2000	2000	2000	2150
Poisson coefficient	ν	-	0,38	0,38	0,38	0,38	0,38	0,38
Shear modulus	G	Pa	3.0E+06	1.0E+07	1.0E+07	3.0E+07	1.0E+08	1.5E+08

Total vertical stress contours at the end of the construction phase are presented at Figure 6.15 and total horizontal stress contours are presented at Figure 6.16.

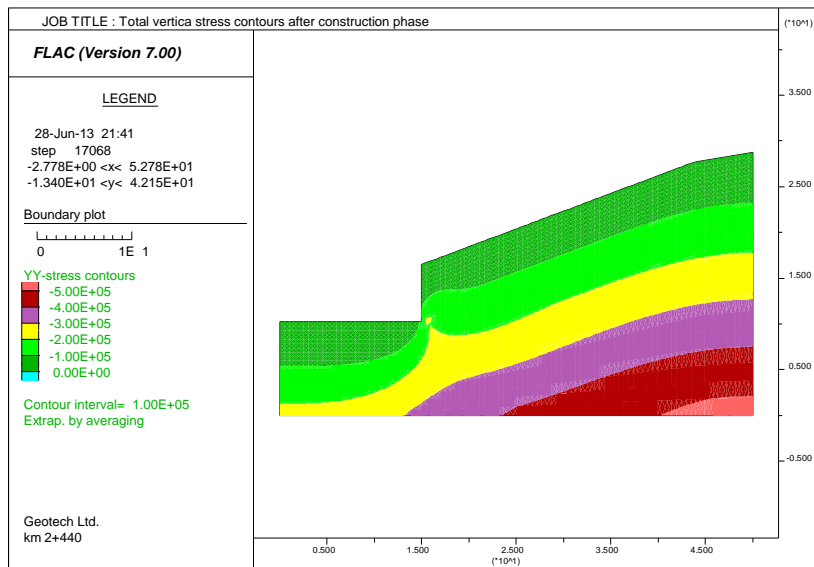


Figure 6.15 Cross section at km 2+440 – total vertical stress contours after construction phase

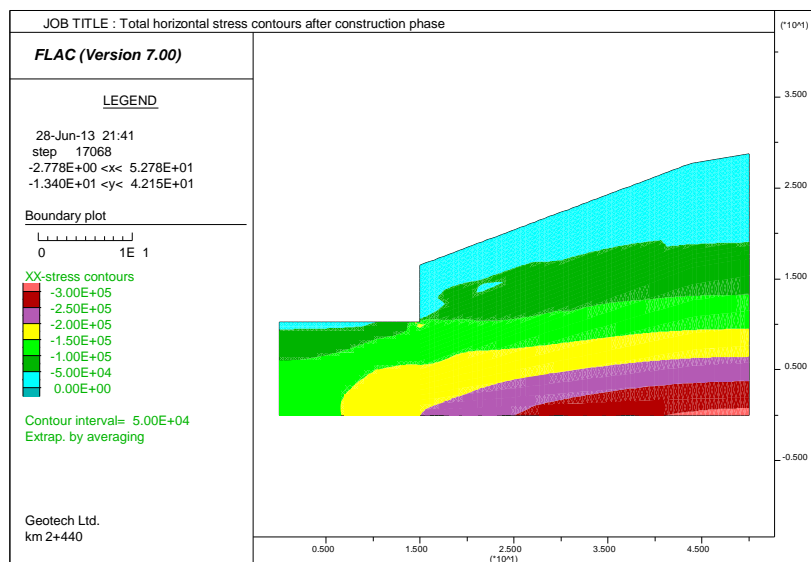


Figure 6.16 Cross section at km 2+440 – total horizontal stress contours after construction phase

Axial forces realized in rockbolt in the construction phase are presented at Figure 6.17. Maximum force (101.2 kN) was realized in upper rockbolt while in the second and third row the forces are 70.3 kN and 57.3 kN respectively. At the bottom rockbolt null force was activated because it was installed after the final excavation of the model. Most part of the forces was activated into the first half of the rockbolt length while in the other parts the forces are minimalized.

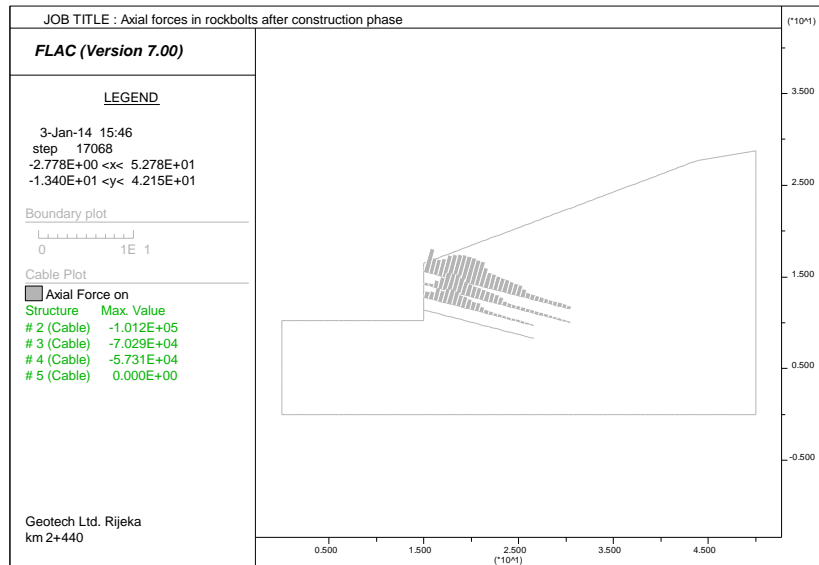


Figure 6.17 Cross section at km 2+440 – axial forces in rockbolts after construction phase

Displacement vectors after the construction phase (Figure 6.18) have shown that maximum displacements were realized in the upper part of the cut in residual soil or completely weathered flysch. Local plasticity was noticed in this part of the model, which can be the cause of this behaviour.

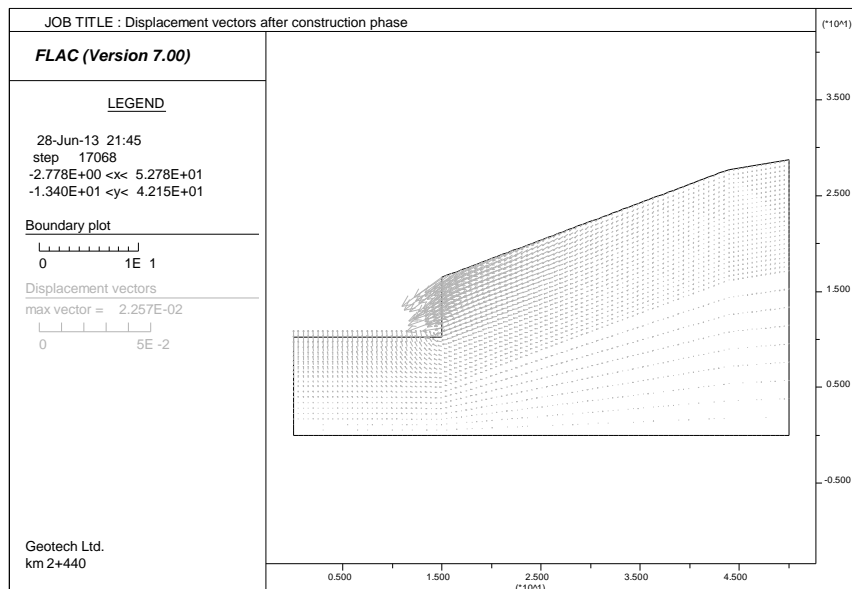


Figure 6.18 Cross section at km 2+440 – displacement vectors after construction phase

Most part of the horizontal displacements (Figure 6.19) were realized in the upper part of the cut in region up to 10.0 m distance from the excavation phase. Greater displacements were noted in the zone of residual soil to completely weathered flysch which are represented with geotechnical units with very low strength and deformability parameters.

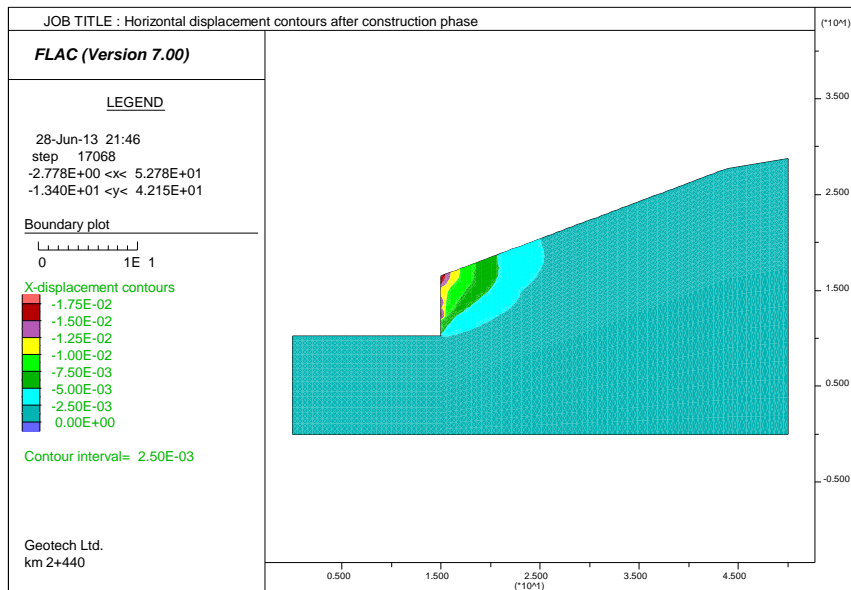


Figure 6.19 Cross section at km 2+440 – displacement vectors after construction phase

6.4. Results of service period analysis – cross section at km 2+440

The service period analyses were carried out using the initial stress and strain states in the model obtained from construction phase modelling. The soil and rock mass layers in the engineered cut were modelled using the Burger-Mohr-Coulomb model for upper layers, denoted as RS, CW, HW, and MW, whereas the lower layers in the cut, denoted as SW and F, were modelled using the elastic model and were not processed as time dependent. Model used for numerical back analysis of service period is presented at Figure 5.28. The same parameters of reinforcing system are used as for back analysis of the construction phase. Results of numerical back analysis of the

service period for timestep of 901 days that corresponds to the duration of the monitoring period are presented as follows.

Deformability parameters were obtained from numerical back analysis and are presented in Table 6.4 Cross section km 2+440 – deformability and creep parameters of geotechnical units obtained from service period back analysis.

Table 6.4 Cross section km 2+440 – deformability and creep parameters of geotechnical units obtained from service period back analysis

Description	Symbo l	Unit	GU 1	GU 2	GU 3	GU 4	GU 5	GU 6
Longitudinal wave velocity	v_p	m/s	0-400	400-800	800-1200	1200-2000	2000-3000	>3000
Weathering grade	-	-	RS/CW	CW/HW	HW/MW	MW/SW	SW/F	F
Model	-	-	cvisc	cvisc	cvisc	cvisc	cvisc	elastic
Cohesion	c	kPa	15	25	25	50	75	75
Friction angle	ϕ	°	28	32	32	32	32	32
Mass density	γ	kg/m ³	2000	2000	2000	2000	2000	2150
Poisson coefficient	ν	-	0,38	0,38	0,38	0,38	0,38	0,38
Shear modulus of Maxwell unit	G_M	Pa	3.0E+06	1.0E+07	1.0E+07	3.0E+07	1.0E+08	1.5E+08
Shear modulus of Kelvin unit	G_K	Pa	3.0E+07	1.0E+08	1.0E+08	3.0E+08	1.0E+09	-
Maxwell viscosity	η_K	Pamin	5.0E+13	5.0E+13	7.5E+13	1.0E+14	1.0E+14	-
Kelvin viscosity	η_M	Pamin	5.0E+15	5.0E+15	7.5E+15	1.0E+16	1.0E+16	-

Total vertical stress contours at the end of the service period of 901 days are presented at Figure 6.20 and total horizontal stress contours are presented at Figure 6.21.

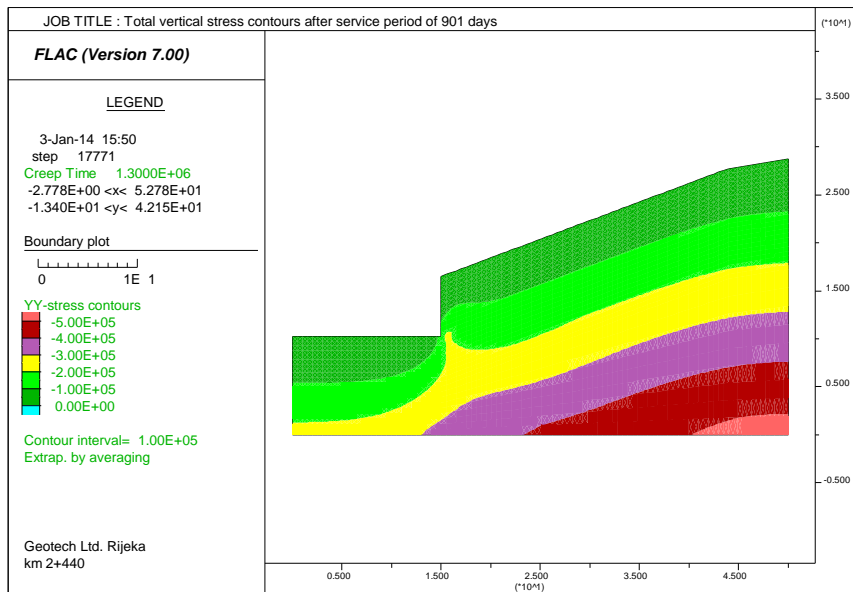


Figure 6.20 Cross section at km 2+440 – total vertical stress contours after service period of 901 days

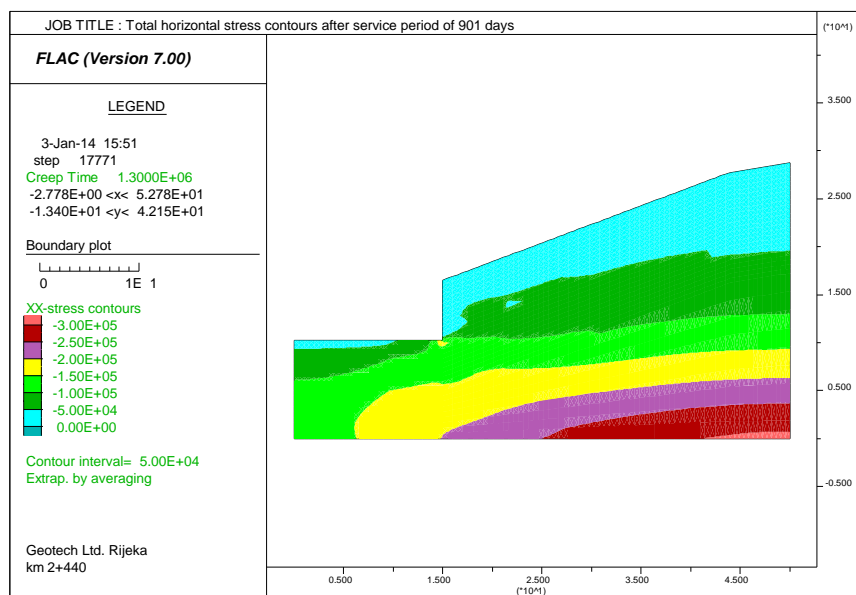


Figure 6.21 Cross section at km 2+440 – total horizontal stress contours after service period of 901 days

Axial forces realized in rockbolt in the construction phase are presented at Figure 6.22. Maximum force (105.4 kN) was realized in upper rockbolt, while in the second and third row the forces were 76.0 kN and 67.7 kN respectively. At the bottom rockbolt the axial force of 17.9 kN was activated because of stress redistribution over time.

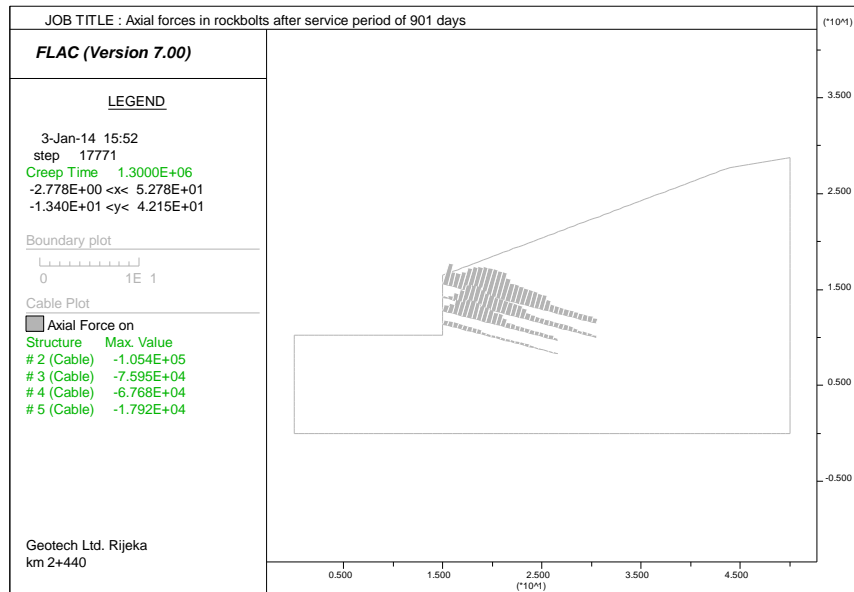


Figure 6.22 Cross section at km 2+440 – axial forces in rockbolts after service period of 901 days

Displacement vectors after the construction phase (Figure 6.23) have shown that displacements were slightly increasing over time and most of them were realized in the upper part of the cut in residual soil or completely weathered flysch.

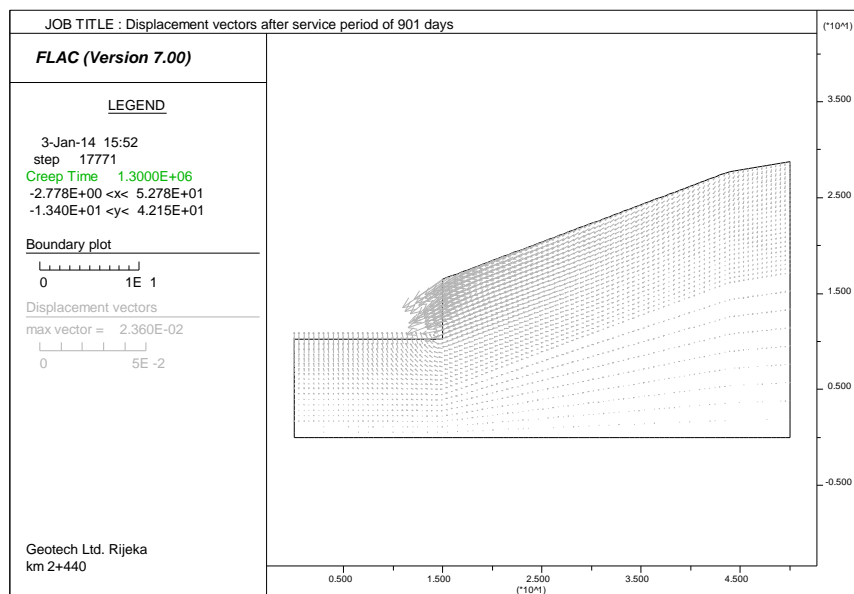


Figure 6.23 Cross section at km 2+440 – displacement vectors after service period of 901 days

Horizontal displacement contours after service period of 901 days (Figure 6.24) were slightly increasing and are hardly visible. Disposition of horizontal displacements was similar to the construction phase.

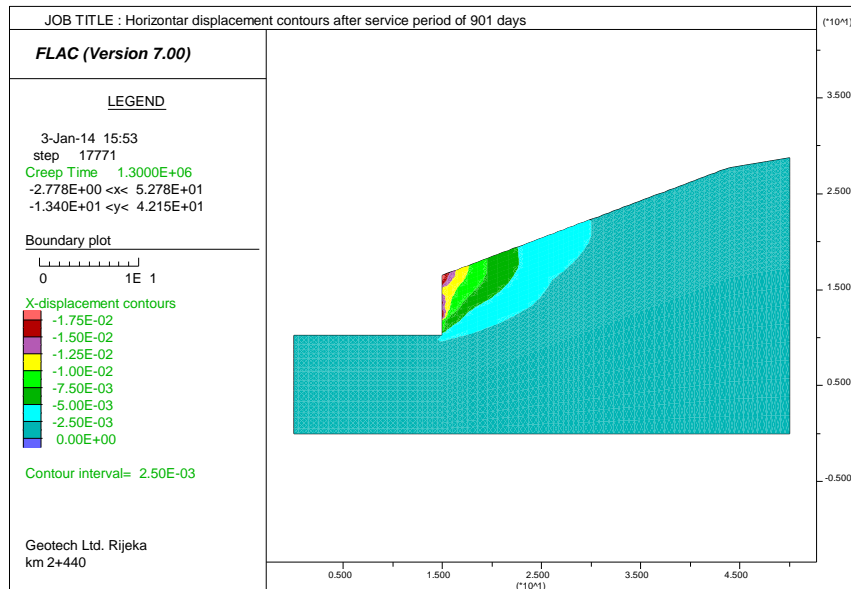


Figure 6.24 Cross section at km 2+440 – horizontal displacement contours after service period of 901 days

6.5. Verification of the numerical model and parameters

Verification of the numerical model and parameters is based on comparison of simulation data (obtained from numerical analysis) and measured data (obtained from measurement results). Comparison is focused at horizontal displacements at vertical inclinometer because these are the most significant indicator of displacements of engineered cuts in the construction phase and in the service period. Verification and calibration of numerical modelling is carried out on several points through the upper part of the cut where most of the displacements occurred.

Comparison of simulation results and measured data of horizontal displacements at vertical inclinometer at cross section 2+380 is presented at Figure 6.26. It is evident from the graph, that the curves obtained from numerical analysis closely follow the

measurement data. This is particularly visible in the upper part of the weathered profile (in upper 7.0 m) where the overall displacements are much greater than in the bottom part of the cut.

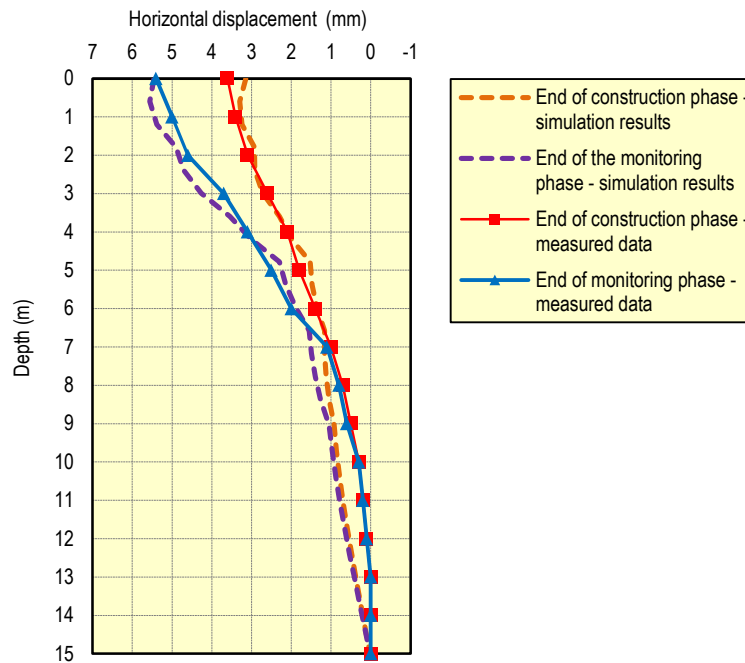


Figure 6.25 Comparison of simulation results and measured data of horizontal displacements at vertical inclinometer at cross section km 2+380

Similar matching of horizontal displacement at vertical inclinometer between the simulation results and measured data for cross section at km 2+440 is presented at Figure 6.26.

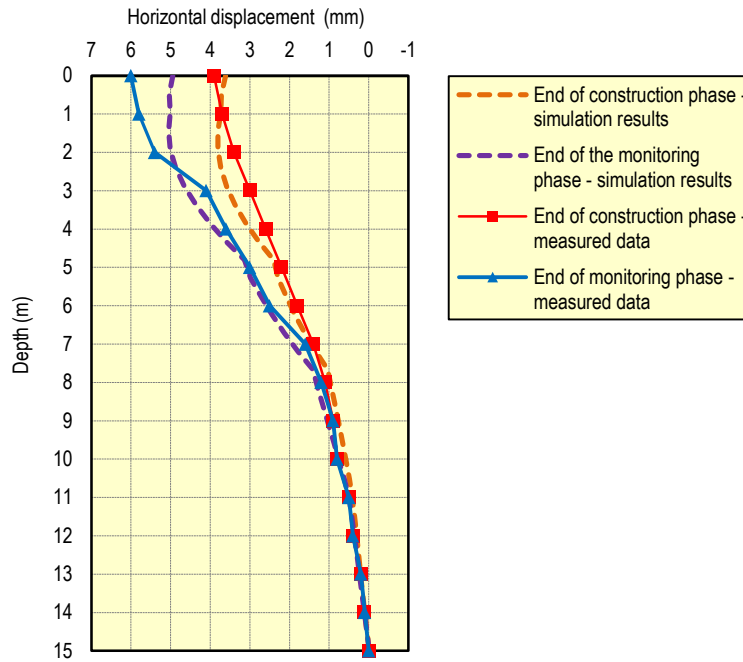


Figure 6.26 Comparison of simulation results and measured data of horizontal displacements at vertical inclinometer at cross section km 2+440

6.6. Influence of time dependent behaviour of slope on the reinforcing system

According to presented results in the previous chapter, it is evident that slopes behave as time dependent and that values of displacements are increasing over time but have the tendency to settle and become a constant. The values of these time dependent or delayed displacements are significant and have influence on the cut reinforced system. It is evident that the stress-strain relation of reinforcement system changes during the time of the service period.

According to the Figure 6.5 and Figure 6.10 for cross section at km 2+380 and to the Figure 6.17 and Figure 6.22 for cross section at km 2+440, the forces at the reinforcement system (axial forces in rockbolts) and the distribution of these forces change during time. Changes in maximal forces and the distribution of forces in the

upper three rows of rockbolts are visible during the service period while at the bottom row of rockbolt the axial forces are activated during time caused by stress redistribution over time.

Figure 6.27 and Figure 6.28 present distribution of forces in rockbolts at the end of construction phase and at the end of monitoring phase (service period of 901 days) at cross section km 2+380 and km 2+440 respectively.

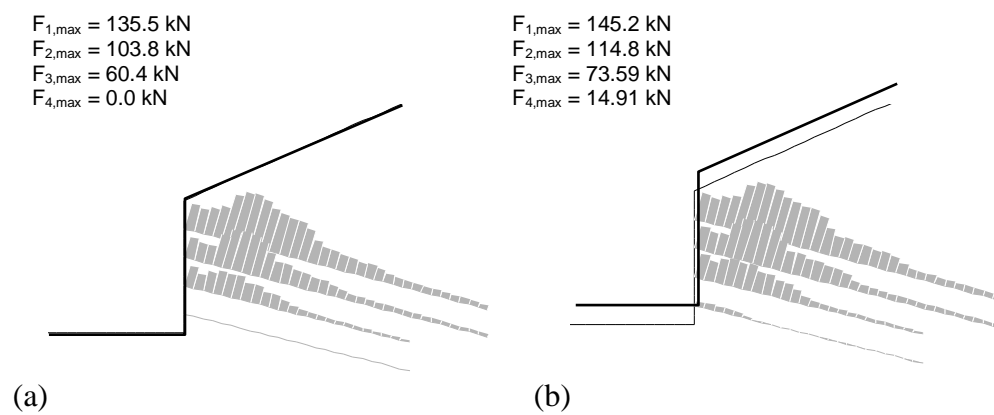


Figure 6.27 Distribution of axial forces activated in rockbolts at cross section km 2+380 with maximum activated forces in each rockbolt row: (a) at the end of construction phase; (b) at the end of monitoring phase (service period of 901 days).

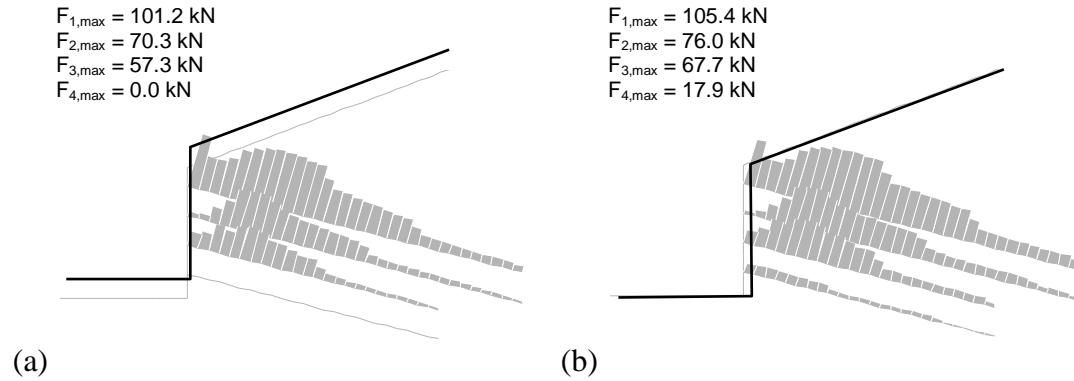


Figure 6.28 Distribution of axial forces activated in rockbolts at cross section km 2+440 with maximum activated forces in each rockbolt row: (a) at the end of construction phase; (b) at the end of monitoring phase (service period of 901 days).

At cross section km 2+380 in the first (upper) row of rockbolts the forces are increasing over time from 135.5 kN at the end of construction phase to 145.2 kN at the end of monitoring phase (service period of 901 days), in the second row the forces are increasing from 103.8 kN to 114.8 kN, and at the third row from 60.4 kN to 73.59 kN. Over time the fourth (bottom) row of rockbolts is activated and forces are increasing from 0.0 kN to 14.91 kN at the end of monitoring phase (service period of 901 days). Similar behaviour is noticed at the cross section in km 2+440 where in the first (upper) row of rockbolts forces are increasing over time from 101.2 kN at the end of construction phase to 105.4 kN at the end of monitoring phase (service period of 901 days), in the second row the forces are increasing from 70.3 kN to 76.0 kN and at the third row from 57.3 kN to 67.7 kN. Over time the fourth (bottom) row of rockbolts is activated and forces are increasing from 0.0 kN to 17.9 kN at the end of monitoring phase (service period of 901 days).

Except the changes of maximal axial forces in rockbolts, changes are noticed in distribution of these forces. Although the service period of time dependent analysis is only 901 days, it is visible that distribution curve of axial forces in third row of

rockbolts slightly changes during time. These changes of distribution of forces would be more clearly visible after a service period of 25 years, which will be presented in the next chapter. Similar to the end of the construction phase, most of the rockbolts are activated in the first half of length while at the other half the axial forces are minimised.

Values of axial forces at rockbolts at cross section at km 2+380 during time period of 901 days are presented at Figure 6.29 and for cross section at km 2+440 at Figure 6.30.

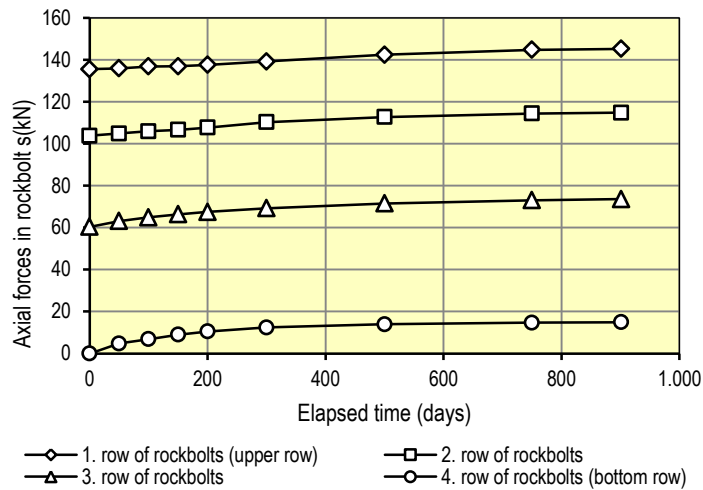


Figure 6.29 Axial forces in rockbolts at cross section at km 2+380 during time period of 901 days

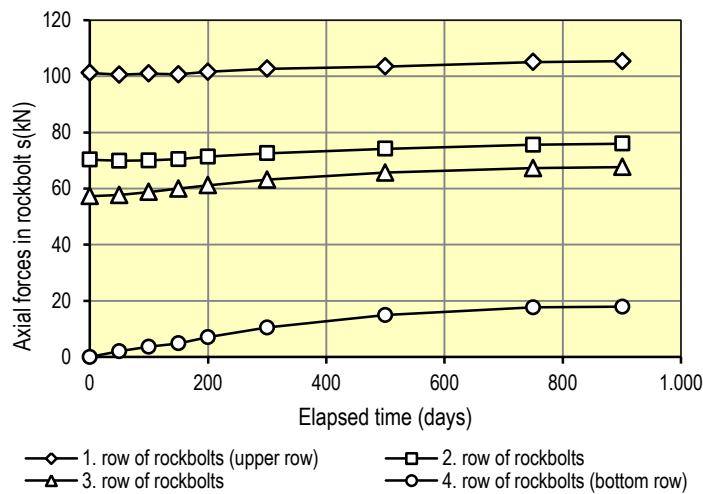


Figure 6.30 Axial forces in rockbolts at cross section at km 2+440 during time period of 901 days

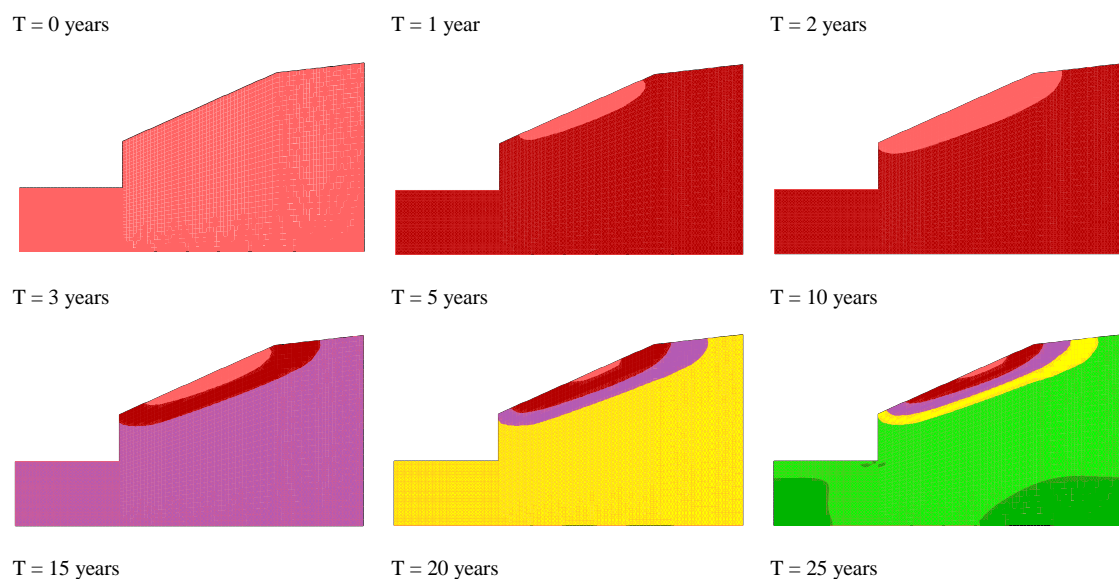
According to presented results, the time dependent behaviour of the slope has a significant impact on the reinforcing system – installed rockbolts in cuts. Over time, due to redistribution of stress in the slope, the axial forces are changing and gradually and slightly increasing, while the bottom rockbolt becomes active. During the time period of 901 days, which was the period of the monitoring phase, changes are visible and are indicating that these forces could be even higher as time goes by. Axial forces in rockbolts should be predicted through a time period of 25 years, which will be presented in the next chapter.

7. PREDICTING THE TIME DEPENDENT BEHAVIOUR OF REINFORCED CUTS

Based on the conducted research it is possible to predict the time dependent behaviour of the reinforced cut for a long time period in weak rock mass such as flysch. Predicting the time dependent behaviour of the reinforced cut for a long time period of 25 years has been carried out using numerical models and parameters established earlier in this research for cross sections at km 2+380 and 2+440.

7.1. Predicting the time dependent behaviour – cross section at km 2+380

Predicting time dependent behaviour of the reinforced cut at km 2+380 is conducted using the numerical model presented at Figure 5.23 and deformability and creep parameters presented in Table 6.2. Distribution of horizontal displacements over a time period of 25 years is presented at Figure 7.1. and distribution of the axial forces in rockbolts is presented at Figure 7.2.



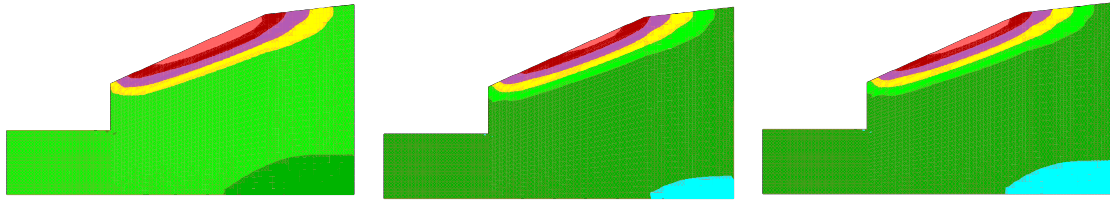


Figure 7.1 Contours of horizontal displacements in slope at km 2+380 with contour interval of 1.0 mm over a time period of 25 years realised after the end of construction phase

It was observed that most of the displacement occurred during the first several years at the beginning of the service period, after construction of the reinforced cut was finished. These displacements could be characterised as delayed deformation and belong to the primary creep period. After 10 years of service period, up to 25 years, the displacements will not be increasing. All displacements are located in the upper and middle part of the cut, while no increasing of displacements will occur in the lower, reinforced part of cut.

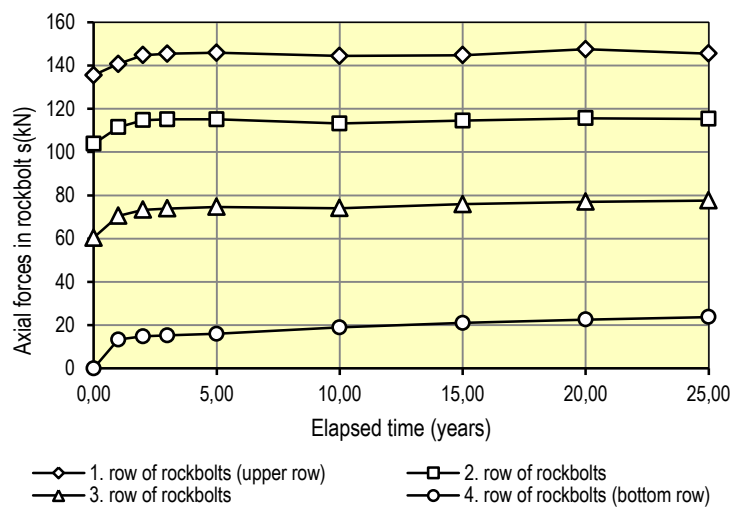


Figure 7.2 Axial forces in rockbolts at cross section at km 2+380 during time period of 25 years

A similar situation could be seen for distribution of axial forces in rockbolts. Axial forces in rockbolts increase during the first 5 years of service period, while the other 20 years stay relatively constant.

7.2. Predicting the time dependent behaviour – cross section at km

2+440

Predicting time dependent behaviour of the reinforced cut at km 2+440 is conducted using the numerical model presented at Figure 5.28 and deformability and creep parameters presented in Table 6.4. Distribution of horizontal displacements over a time period of 25 years is presented at Figure 7.3. and distribution of axial forces in rockbolts is presented at Figure 7.4.

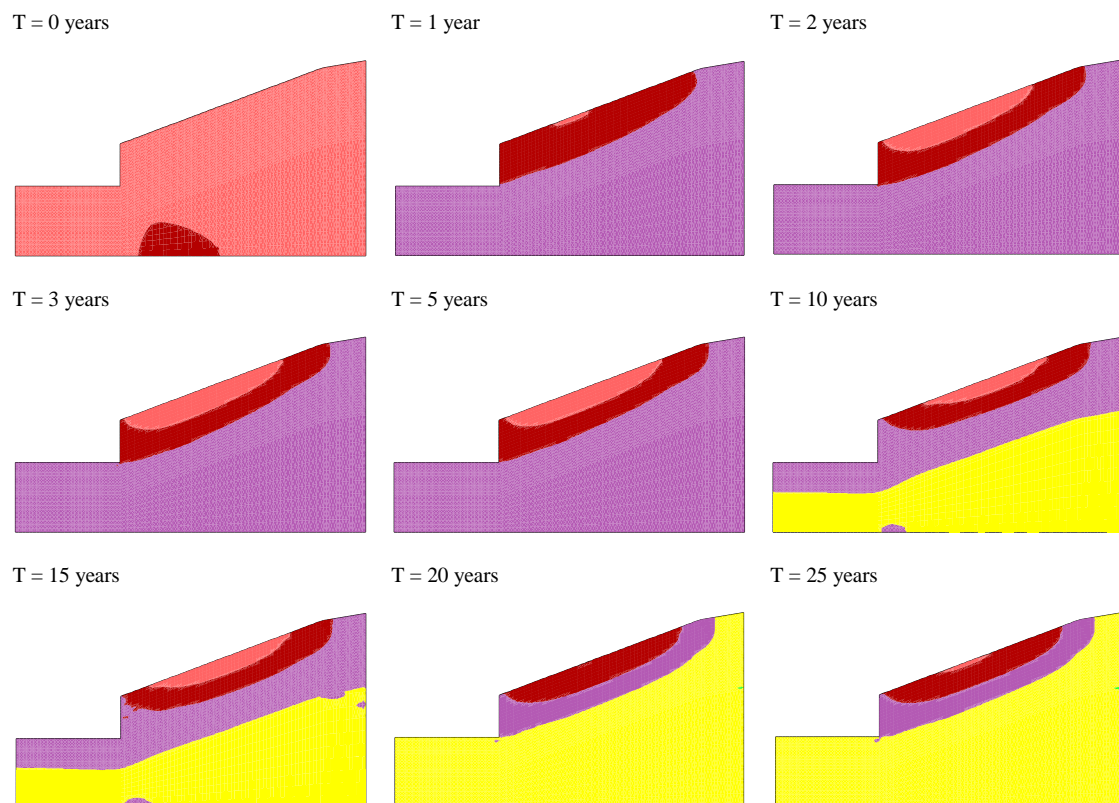


Figure 7.3 Contours of horizontal displacements in slope at km 2+440 with contour interval of 0.5 mm over time period of 25 years realised after the end of construction phase

It was observed that most of the displacement occurred during the first several years at the beginning of the service period, after construction of the reinforced cut was completed. These displacements could be characterised as delayed deformation and belong to the primary creep period. After 5 years of service period, up to 25 year, the

displacements are relatively constant and are slightly increasing. In contrast to the previous model, displacements are situated in the middle part of the slope and also in the position of the reinforced cut.

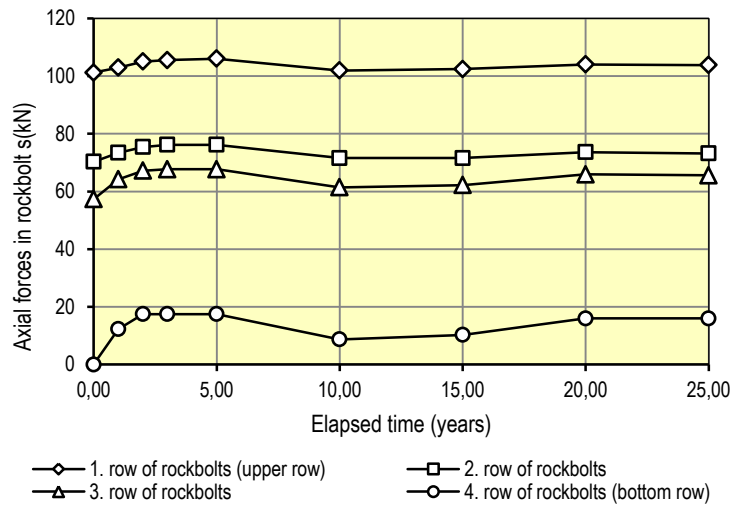


Figure 7.4 Axial forces in rockbolts at cross section at km 2+440 during a time period of 25 years

A similar situation could be seen for distribution of axial forces in rockbolts. Axial forces in rockbolts increase during the first 5 years of service period, while the other 20 years are relatively constant with small relaxation at 10th year.

8. DISCUSSION AND CONCLUSIONS

8.1. Overview of the thesis

The Adriatic Motorway, section Orehovica – Draga Sv. Kuzam of D8 road near the City of Rijeka was built in weathered flysch rock mass. Measured data from installed monitoring equipment during construction phase and in the time period of 3 years of service period at reinforced cuts along the part of Adriatic Motorway near the City of Rijeka were analysed. Analysing the data from installed monitoring equipment at reinforced flysch cuts, it was observed that significant displacements were realized during the service period of construction after the reinforcing works on the cuts were completed.

The scope of this research is directed on selection of a numerical model and obtaining its deformability and creep parameters and to predict the time dependent behaviour of reinforced cuts in flysch rock mass.

It was found possible to detect the thickness of the flysch rock mass weathering profile by performing detailed direct and indirect geotechnical field investigations. According to the seismic refraction method that utilized the refraction of seismic waves on geologic layers and rock/soil units, the numerical model was divided into several geotechnical units with similar geotechnical properties.

To obtain deformability and creep properties of geotechnical units, the direct approach to back analysis was used in numerical modelling. Numerical back analysis were divided into two phases: modelling of construction phase using the linear elastoplastic Mohr-Coulomb model and modelling of service period using the elastoplastic Burger-Mohr-Coulomb model. Verification of the numerical model and

obtained parameters was based on comparison of simulation data and measured data of horizontal displacements at vertical inclinometer.

Comparison of simulation results and measured data of horizontal displacements at vertical inclinometers was carried out at cross sections in km 2+380 and km 2+440. It is evident from obtained results that the curves obtained from numerical back analysis closely follow measured data. Particularly this is visible in the upper part of the weathered profile (in upper several metres of the cuts) where the overall displacements are much greater than in the lower part of the cuts.

Proposed numerical models and resulting deformability and creep flysch rock mass parameters were used to predict time dependent behaviour of reinforced cuts for a long service period within 25 years. This prediction was also done for axial forces in rockbolts. It was found that most of the realized delayed displacement of the slope and most of the changes of the axial forces in the rockbolts occurred in the first several years after the construction was completed.

Based on the conducted research, recommendations for the strength, deformation, and creep properties of the weathering profile of a flysch rock mass and guidelines for future researches are given.

8.2. Conclusions

The results of field investigations have shown that it is not possible to determine the disposition of the different grades of the weathered profile (from residual soil (RS) to fresh rock mass (F)) precisely, but it is possible to determine the depth and the location of the fresh flysch rock mass. Geophysical investigations in correlation with other geotechnical investigations such as engineering geological determination and

classification of core material and laboratory tests or in-situ tests made it possible to determine the borders of the slightly weathered (SW) and the fresh (F) flysch rock mass. These borders also denote the thicknesses of layers in the weathering profile of the flysch rock mass, which is necessary information to carry out numerical analysis.

Based on the geotechnical field investigation results, numerical back analyses were performed in two phases: a construction phase and a service period. Back analysis of the behaviour of reinforced cuts in the flysch rock mass were performed using a trial and error method to obtain the deformability and creep parameters of geotechnical units in the numerical model. Calibration of the numerical model was carried out from the bottom of a cut in the model, where no or very small displacements were measured, towards the surface of a slope, where large displacements were measured.

The service period analyses were carried out using the initial stress and strain states in the model obtained from the construction phase modelling. The soil and rock mass layers in the cut were modelled using the Burger-Mohr-Coulomb model for upper layers, denoted as residual soil (RS), completely weathered (CW), highly weathered (HW), moderately weathered (MW) and slightly weathered (SW) flysch rock mass, whereas the lower layer in the cut, denoted as fresh (F) flysch rock mass, was modelled with the classic elastoplastic Mohr-Coulomb model and was not processed as time dependent.

The determination of the Burger model parameters for each geotechnical unit was the most challenging part of the numerical analysis. The shear modulus of the Kelvin unit, G_K , that controls primary creep, was set to be ten times higher than the shear modulus of the Maxwell unit, G_M ($G_K / G_M = 10$). The creep parameters of the viscosity of the Kelvin unit, η_K , and the Maxwell unit, η_M , were taken as the ratio $R =$

$\eta_M/\eta_K = 100$. Using these relationships in the parameter selection, the number of parameters that should be determined in the creep back analysis was considerably reduced.

Following deformability and creep parameters of a flysch rock mass according to weathering grade were obtained from numerical back analysis:

- The shear modulus of the Maxwell unit, G_M , varied from $5.0\text{E}+05$ Pa (km 2+380) for residual soil (RS) to completely weathered (CW) and $3.0\text{E}+06$ Pa (km+2440) to $5.0\text{E}+07$ Pa (km 2+380) and $1.0\text{E}+08$ Pa (km 2+440) for slightly weathered (SW) to fresh (F) flysch rock mass,
- The shear modulus of the Kelvin unit, G_K , varied from $5.0\text{E}+06$ Pa (km 2+380) and $3.0\text{E}+07$ Pa (km+2440) for residual soil (RS) to completely weathered (CW) to $5.0\text{E}+08$ Pa (km 2+380) and $1.0\text{E}+09$ Pa (km 2+440) for slightly weathered (SW) to fresh (F) flysch rock mass,
- Maxwell viscosity, η_M , varied from $5.0\text{E}+13$ Pamin (km 2+380 and km 2+440) for residual soil (RS) to completely weathered (CW) to $1.0\text{E}+14$ Pamin (km 2+380 and km 2+440) for slightly weathered (SW) to fresh (F) flysch rock mass,
- Kelvin viscosity, η_K , varied from $5.0\text{E}+15$ Pamin (km 2+380 and km 2+440) for residual soil (RS) to completely weathered (CW) to $1.0\text{E}+16$ Pamin (km 2+380 and km 2+440) for slightly weathered (SW) to fresh (F) flysch rock mass.

Verification of numerical model and parameters was based on comparison of simulation data (obtained from numerical analysis) and measured data (obtained from measurement results). Verification and calibration of numerical modelling was carried

out on several points through the upper part of the cut where the most of the displacements occurred. It was shown that curves obtained from numerical analysis closely follow measurement data. This is particularly visible in the upper part of the weathered profile of the cuts where the overall displacements were much higher than in the lower part of the slope.

According to presented results of numerical back analysis it was evident that the slopes behave as time dependent and that values of displacements are increasing over time, but have the tendency to settle and became a constant value after several years of service period. The values of these time dependent or delayed displacements were significant and thus had influence on the reinforced system of the cut. It was evident that during the service period the stress and strain states of reinforcement system were significantly changed. Forces at the reinforcement system (axial forces in rockbolts) and the distribution of these forces were changing during service period. Changes of maximal forces and the distribution of forces along the rockbolt in upper three rows of rockbolts occurred during the service period, while the axial forces in the bottom row of rockbolts were activated over time caused by stress redistribution and time dependent deformation of rock mass.

Time dependent behaviour of reinforced cuts at km 2+380 and km 2+440 was predicted for long time service period of 25 years. Distribution of horizontal displacements in the cuts and distribution of the axial forces along the rockbolts were analysed and calculated. It was observed that most of the displacements occurred in first several years after construction of the reinforced cut was completed, at the beginning of the service period. These displacements could be characterised as delayed deformation and belong to the primary creep period. After 10 years of service

period, up to 25 year, the displacements would not increase. All displacements are located in the upper and middle part of the cuts, while no increasing of the displacements would be in the lower reinforced part of the cut. A similar behaviour could be seen for developing of axial forces distributions along the rockbolts. Axial forces in rockbolts would increase during the first 5 years of service period, while the other 20 years would be constant without any significant changes.

It is important to mention that for other rock mass types with different parameters or cuts with different reinforced systems, the time dependent behaviour would be realised in a longer time period. This could cause gradual increase of forces in rockbolts over time and could lead to reaching the bearing capacity of the reinforced system and finally to the collapse of the construction.

This shows that understanding of time dependent behaviour of weak rock mass, including the flysch rock mass, is important for understanding the overall redistribution of time dependent strains and stresses in cuts and engineering slopes. During the geotechnical design process the reinforced cuts in weak rock masses should be thoroughly analysed not only in construction phase, but also during the long time service period. The monitoring period should be prolonged much more than it is usual in practice nowadays.

8.3. Future researches

More detailed laboratory test of rock and rock mass should be included in further research with an emphasis on investigation of creep of rock and time dependent behaviour of rock mass.

For numerical modelling of time dependent behaviour of weak rock mass and back analysis more complex model should be developed using neural networks for identification of strength, deformability and creep parameters instead of using ratios between them.

It is necessary to define new systems and methodology of monitoring techniques on geotechnical constructions, which will be adjusted to scientific researches of time dependent behaviour, and higher number of measurements will be carried out.

Furthermore, a new database of time dependent behaviour of weak rock mass should be established with information from different locations and different weak rocks (geological and geotechnical conditions of the site, results from numerical analyses and back analyses, reinforcing systems etc.).

That would enable a better understanding of the time dependent behaviour of weak rocks mass and would give a better basis for future designing of reinforced cuts in weak rock mass.

REFERENCES

- Afrouz, A. A. (1992), Practical Handbook of Rock Mass Classification Systems and Modes of Ground Failure: CRC Press, Boca Raton, FL, 195 p.
- Aksoy, C. O. (2008), Review of rock mass rating classification: Historical developments, applications, and restrictions, *Journal of Mining Science*, January 2008, Volume 44, Issue 1, pp 51-63.
- Apuani, T., Masetti, M., Rossi, M. (2007) Stress–strain–time numerical modelling of a deep-seated gravitational slope deformation: Preliminary results, *Quaternary International* 171–172 (2007) 80–89.
- Arbanas, Ž., Benac, Č., Andrić, M., Jardas, B. (1994) Geotechnical Properties of Flysch on the Adriatic Motorway from Orehovica to St. Kuzam, In: *Proceedings of the Symposium of Geotechnical Engineering in Transportation Projects*, Croatian Geotechnical Society 1: 181-190 (*In Croatian*).
- Arbanas, Ž., Benac Č., Jardas B. (1999) Small Landslides on the Flysch of Istria, *Proc. 3th Conf. Slovenian Geotech.*, 1, Portorož, Sloged, Ljubljana, 81-88.
- Arbanas, Ž., Kovačević, M. S., Grošić, M., Jardas, B. (2005) Some Experience During Open Pit Excavation in limestone rock mass, *Proc. EUROCK 2005 – Impact of Human Activity on the Geological Environment*, Brno 2005, Czech Republic, Ed. P. Konečný, A.A. Balkema Publishers, Taylor & Francis Group, London, pp. 31-36.
- Arbanas, Ž., Grošić, M., Dugonjić, S. (2008a) Behaviour of the reinforced cuts in flysch rock mass, *Proc. of 1. Int. Conf. On Transportation Geotechnics*, Nottingham, UK, Ed. E. Ellis, Y. Hai-Sui, G-McDowell, A. Dawson and N. Thom, Taylor and Francis Group, Balkema, London UK: 283-291.
- Arbanas, Ž., Grošić, M., Briški G. (2008b) Behaviour of Engineered Slopes in Flysch Rock Mass, *Proc. 1st Southern Hemisphere Int. Rock Mechanics Symp.* 16.-19. September 2008, Perth, Australia, Ed. Y. Potvin, J. Carter, A. Dyskin and R. Jeffrey, Australian Centre for Geomechanics, Perth, Vol. 1, Mining and Civil; pp. 493-504.
- ASTM (1992) Standard test method for slake durability of shales and similar weak rocks, D 4644-87. American Society for Testing and Materials.
- ASTM (2002) Standard test method for determining in situ creep characteristics of rock, D 4553-02. American Society for Testing and Materials.
- Aydan, O., Akagi, T., Kawamoto, T. (1996) The squeezing potential of rock around tunnels: Theory and prediction with examples taken from Japan. *Rock Mech. Rock Engng.* 29, 125-143.
- Barata, F. E. (1969) Landslides in the tropical region of Rio de Janeiro. *Proceedings of the 7th International Conference on Soil Mechanics and Foundation Engineering*, Mexico, II, 507-516.
- Barla, G., Bonini, M., Debernardi, D. (2008) Time Dependent Deformations in Squeezing Tunnels, *The 12th International Conference of International Association for Computer Methods and Advances in Geomechanics (IACMAG)*, 1-6 October, 2008 Goa, India.
- Barton, N. (2000) *TBM tunneling in jointed and faulted rock*, Rotterdam: Balkema.
- Barton, N. R., Lien, R., Lunde, J. (1974) Engineering classification of rock masses for the design of tunnel support, *Rock Mech.*, 6, 189-239.
- Bérest, P., Bergues, J., Duc, N. M. (1979) Comportement des roches au cours de la rupture: application a l'interprétation d'essais sur des tubes épais. *Rev française Géotech* 9:5–12 (*In French*).
- Bernabe, Y., Fryer, T. D., Shively, R. M. (1994) Experimental observations of the elastic and inelastic behaviour of porous sandstones. *Geophys J Int* 117:403–18.

- Bhandari, A., Inoue, J. (2005) Continuum damage mechanics for hysteresis and fatigue of quasi-brittle materials and structures, *Int. J. Numer. Anal. Meth. Geomech.* 29 (11), 1087–1107.
- Bieniawski, Z. T. (1978) Determining rock mass deformability: Experience from case histories. *Int. J. Rock Mechanics Mineral Science & Geomechanics Abstract*, Vol. 15, pp. 237 – 247.
- Bieniawski, Z. T. (1989) *Engineering rock mass classifications*. John Wiley & Sons, New York, 251 p.
- Bozzano, F., Martino, S., Montagna, A., Prestininzi, A. (2012) Back analysis of a rock landslide to infer rheological parameters, *Engineering Geology* 131–132 (2012) 45–56
- Brace, W. F. , Bombolakis, E. G. (1963) A note on brittle crack growth in compression, *J Geophys Res* 68(12):3709–13.
- Bray, J. W. (1967) A study of jointed and fractured rock, Part I. *Rock Mechanics and Engineering Geology*, 5–6(2–3), 117–136.
- Brown, E. T., Hoek, E. (1978) Trends in relationships between measured rock in situ stresses and depth. *Int. J. Rock Mech. Min. Sci. & Geomech. Abstr.* 15: 211-215.
- Brunčić, A. (2008) Protecting of flysch rock mass slopes in Rijeka area, M. Sc. Thesis, Zagreb: Univeristy of Zagreb: 153p (*In Croatian*).
- Brunčić, A., Arbanas, Ž., Kovačević, M. S. (2009) Design of engineered slopes in flysch rock mass, *Proceedings of the 17th International Conference on Soil Mechanics and Geotechnical Engineering*, Eds. Hamza, M., Shahien, M., El-Mossallamy, Y.
- BSI (1981) *Code of Practice for site investigations*, BS 5930. British Standards Institution, London. 147p.
- Caterpillar (1996) *Handbook of Ripping*, 10th ed.: Caterpillar, Inc., Peoria, IL, p. 9.
- Chandler, R. J. (1969) The effect of weathering on the shear strength properties of Keuper marl. *Géotechnique*, 19, 321-334.
- Cividini, A., Jurina, L., Gioda, G. (1981) Some Aspects of Characterization Problems in Geomechanics. *Int J Rock Mech Min Sci & Geomech Abstr* 18: 487-503
- Cividini, A., Maier, G., Nappi, A. (1983) Parameter estimation of a static geotechnical model using a Bayes' rule approach. *International Journal of Rock Mechanics and Mining Sciences* 20, 215-226.
- Clerici, A. (1992) *Engineering Geological Characterization of Weak Rocks: Classification, Sampling and Testing*, ISRM Symposium Eurock'92, Rock Characterization, J.A. Hudson (ed.), Chester UK, 1992, 179–182.
- Clerici, A. (1993) Indirect determination of the modulus of deformation of rock masses - Case histories, *Proc. Conf. Eurock '93*, pp. 509 - 517.
- Cooling, C. M., Hudson, J. A., Tunbridge, L. W. (1988) In Situ rock stresses and their measurements in the U.K. Part II, Site experiments and stress field interpretation. *Int. J. Rock Mech. Min. Sci. & Geomech. Abstr.* 25, 6: 371-382.
- Cristescu, N., Fota, D., Medves, E. (1987) Tunnel Support Analysis Incorporating Rock Creep, *Int. J. Rock Mech. Min. Sci. & Geomech. Abstr.* Vol. 24, No. 6, pp. 321-330, 1987
- Cristescu, N. D. (1989) *Rock Rheology*, Dordrecht: Kluwer Academic.
- Cristescu, N. D. (1994) Viscoplasticity of geomaterials, In: Cristescu ND, Gioda G, editors. *Viscoplastic behaviour of geomaterials*. New York: Springer. p. 103–207.

- Cristescu, N. D. (2001) Elasticity of porous materials, In: Lemaitre J, editor. Handbook of materials behavior models. New York: Academic Press. p. 71–90.
- Cristescu, N. D., Hunsche, U. (1998) Time Effects in Rock Mechanics, Wiley, 342 pages
- Croatian Geological Survey (1990) Motorway Rijeka – Trst. Section: Orehovica – Draga – Vitoševo, Subsection: Draga – Vitoševo, Report for route main design (chainage km 1+980 – km 5+360), Book 1, engineering geological report, Zagreb (*In Croatian*).
- Dearman, W. H., (1976) Weathering classification in the characterization of rock: a revision, Int. Assoc. Eng. Geol. Bull., 13, p. 123 –128.
- Debernardi, D. (2008) Viscoplastic behaviour and design of tunnels, PhD Thesis, Politecnico di Torino, Department of Structural and Geotechnical Engineering, Italy.
- Deere, D. U., Miller, R. P. (1966) Engineering classification and index properties for intact rock, Tech. Rept. No. AFWL-TR-65-116, Air Force Weapons Lab., Kirtland Air Force Base, New Mexico.
- Deere, D. U., Patton, F. D. (1971) Slope stability in residual soils, Proceedings of the 4th Pan-American Conference on Soil Mechanics and Foundation Engineering, Puerto Rico, 1, 87-170.
- Desai, C. S., Abel, J. F. (1972) Introduction to the finite element method; a numerical method for engineering analysis, Van Nostrand Reinhold Co., 1971 - Technology & Engineering: 477 p
- Desai, C. S., Christian, J. T. (1977) Numerical Methods in Geomechanics, New York: McGraw-Hill
- DIN (1987) Subsoil and ground water. Designation and description of soil and rock. Borehole log for boring without continuous taking of core samples in soil and rock, DIN 4022 Part 1. Deutsches Institut für Normung e.V., Berlin (*In German*).
- DIN (2004) Geotechnical investigation and testing – Identification and classification of rock – Part 1: Identification and description (ISO 14689-1:2003). DIN EN ISO 14689-1. Deutsches Institut für Normung e.V., Berlin (*In German*).
- Dusseault, M. B., Fordham, C. J. (1993) Time-dependent behavior of rocks. In Comprehensive rock engineering, vol. 3. Oxford: Pergamon p. 119–49.
- Eberhardt, E., Thuro, K., Luginbuehl, M. (2005) Slope instability mechanisms in dipping interbedded conglomerates and weathered marls – the 1999 Ruffi landslide, Switzerland, Engineering geology 77 p. 35-56.
- Edelbro, E. (2003) Rock Mass Strength: A Review, Technical Report. Lulea University of Technology. Department of Civil Engineering, Division of Rock Mechanics.
- Eykhoﬀ, P. (1974) System identification - Parameter and state estimation, edn. John Wiley and Sons, Great Britain, 147-151, 519-526.
- Fabre, G., Pellet, F. (2006) Creep and time-dependent damage in argillaceous rocks, International Journal of Rock Mechanics & Mining Sciences 43 (2006) 950–960.
- Fakhimi, A. A., Fairhurst, C. (1994) A model for the time-dependent behavior of rock. Int. J. Rock Mech. Min. Sci. 31, 117-126.
- Farmer, I. W. (1983) Engineering Behaviour of Rock, 2nd edition. Chapman and Hall, London.
- Feng, J., Chuhan, Z., Gang, W., Guanglun, W. (2003) Creep Modeling in Excavation Analysis of a High Rock Slope, , Journal of Geotechnical and Geoenvironmental Engineering, ASCE, Vol. 129, No. 9, September 2003, pp. 849-857.

- Foo, B., Lima, A. A., Vries, B., Ozturk, H. (2011) Practical application of support systems to address weak rock mass in underground mines (update), *Studia Geotechnica et Mechanica*, Vol. XXXIII, No. 3, 2011.
- Fookes, P. G. (1997) Tropical residual soils: a Geological Society Engineering Group Working Party revised report, Geological Society, p184.
- Fookes, P. G., Horswill, P. (1970) Discussion on engineering grade zones. *Proceedings of the In Situ Investigations in Soils and Rocks*, London, 53-57.
- Fuenkajorn, K., Sriapai, T., Samsri, P. (2012) Effects of Loading Rate on Strength and Deformability of Maha Sarakham Salt, *Engineering Geology* (2012), Volumes 135–136, 15 May 2012, Pages 10–23
- Geoarheo (2013) Gephysical investigation report, Draga Location; Zagreb (*In Croatian*).
- Geofizika (1991) Gephysical investigation report, Motorway Rijeka – Trst, Section: Orehovica – Draga – Vitoševo, Geofizika, Department for Engineering Geology, Zagreb (*In Croatian*).
- Geological Society Engineering Group (1995) The description and classification of weathered for engineering purposes, Working Party Report, Quarterly Journal of Engineering Geology, Vol. 28, 207-242.
- Geotechnical Control Office, Hong Kong (1979), Manual for slopes, Government printer, Hong Kong, 1st edition.
- Gioda, G. (1985) Some remarks on back analysis and characterization problems. *Proceedings, 5th International Conference on Numerical Methods in Geomechanics*, Nagoya, Japan, 1-5 April, 1985, pp. 47-61.
- Gioda, G., Maier, G. (1980) Direct Search Solution of an Inverse Problem in Elastoplasticity: Identification of Cohesion, Friction Angle and In-situ Stress by Pressure Tunnel Tests. *Int J Num Meth Engng* 15: 1823-1848
- Gioda, G., Sakurai, S. (1987) Back analysis procedures for the interpretation of field measurements in geomechanics. *International Journal for Numerical and Analytical Methods in Geomechanics* 11, 555-583.
- Gonze, P. (1988) Techniques de calcul utilisees en congelation des terrains. In *La thermome canique des roches*, vol. 16. BRGM. (*In French*).
- Goodman, R. E. (1989) *Introduction to Rock Mechanics*, second ed. In: Wiley, New York
- Grimstad, E., Barton, N. (1993) Updating the Q-system for NMT. *Proc. Int. Symp. on Sprayed Concrete*, Fagernes, Norway 1993, Norwegian Concrete Association, Oslo, 20 p.
- Grošić, M., Arbanas, Ž. (2014) Time-dependent Behaviour of Reinforced Cuts in Flysch Rock Mass, *Acta geotechnica Slovenica*, 2014/1, 5-17.
- Grošić, M., Vidović, D., Arbanas, Ž. (2013) Influence of in-situ stress variation on results of back analysis – an open pit case study, In *proceeding of: Rock Mechanics for Resources, Energy and Environment, EUROCK 2013*, At Wroclaw, Poland, Volume: 1.
- Guan, Z., Jiang, Y., Tanabashi, Y., Huang, H. (2008) A new rheological model and its application in mountain tunnelling, *Tunnelling and Underground Space Technology* 23 (2008) 292–299.
- Guan, Z., Jiang, Y., Tanabashi, Y. (2009) Rheological parameter estimation for the prediction of long-term deformations in conventional tunnelling, *Tunnelling and Underground Space Technology* 24 (2009) 250–259.

- Hencher, S. R., Martin, R. P. (1982) The description and classification of weathered rocks in Hong Kong for engineering purposes, Proceedings of the 7th Southeast Asian Geotechnical Conference, Hong Kong, 1, 125-142.
- Herget, G. (1988) Stresses in rock, Rotterdam: Balkema.
- Hoek, E. (1999) Support for Very Weak Rock Associated with Faults and Shear from Rock Support and Reinforcement Practice in Mining, E. Villaescusa et al. (editors), A.A Balkema, Rotterdam, Brookfield.
- Hoek, E. (2000) Practical rock engineering. URL: <http://www.rockscience.com>, April. 2013.
- Hoek, E., Brown, E. T. (1980) Underground excavations in rock, London: Instn. Min. Metall.
- Hoek, E., Brown, E. T. (1997) Practical estimates of rock mass strength, International Journal of Rock Mechanics and Mining Sciences, 34(8), 1165–1186.
- Hoek, E., Brown, E. T. (1988a) The Hoek-Brown failure criterion – a 1988 update. In Proceedings of the 15th Canadian Rock Mechanics Symposium, Toronto. Edited by J.H. Curran. Department of Civil Engineering, University of Toronto, Toronto, pp. 31–38.
- Hoek, E., Brown, E. T. (1998b) Practical estimates of rock mass strength. Int J Rock Mech Min Sci 34:1165–1186.
- Hyett, A., Hudson J. A. (1989) In situ stress for underground excavation design in a naturally fractured rock mass, Rock Mechanics as a Guide for Efficient Utilization of Natural Resources. In: Proceedings of the 30th US Symposium of Rock Mechanics: 293-300.
- Hoek, E., Wood, D., Shah, S. (1992) A modified Hoek-Brown failure criterion for jointed rock masses. In: Proceedings of the international ISRM Symposium on Rock Characterisation – EUROCK '92, British Geotechnical Society, Chester, September, 1, 209-214.
- Hoek, E., Kaiser, P. K., Bawden, W. F. (1995) Support of underground excavations in hard rock. A.A. Balkema/Rotterdam/Brookfield.
- Hoek, E., Carranza-Torres, C., Corkum, B. (2002) Hoek-Brown failure criterion – 2002 Edition. Proc. 5th North American Rock Mechanics Symposium, Toronto, July 2002, 267-273.
- Hoek, E., Marinos, P., Benissi, M. (1998) Applicability of the Geological Strength Index (GSI) Classification for Very Weak and Sheared Rock Masses. The Case of the Athens Shist Formation. Bull. Eng. Geol. Env., No. 57, pp.151-160.
- Hoek, E., Marinos, P. (2000) Predicting Tunnel Squeezing. Tunnels and Tunneling International. Part 1 – November 2000, Part 2 – December 2000.
- Hunsche, U., Albrecht, H. (1990) Results of true triaxial strength tests on rock salt. Eng Fract Mech 35:867–77.
- Hudson, J., Harrison, J. (1997) Engineering Rock Mechanics. Pergamon, London.
- IAEG (1981) Rock and soil description and classification for engineering geological mapping. Bulletin of International Association of Engineering Geology, 24, 253-274.
- ISRM (1975) Commission on terminology, symbols and graphic representation, International Society for Rock Mechanics (ISRM).
- ISRM (1978) Suggested methods for the quantitative description of discontinuities in rock masses. International Journal of Rock Mechanics Mining Sciences and Geomechanics Abstracts, 15, 319-368.

- ISRM (1981) Rock Characterization, Testing and Monitoring, ISRM Suggested Methods, Brown ET (editor), Pergamon Press, Oxford, p 211.
- Isaacson, E. de St. Q. (1957) Research into the rock burst problem on the Kolar gold field. Mine and Quarry Engineering, December: 520-526.
- Ishizuka, Y., Koyama, H., Komura, S. (1993) Effect of strain rate on strength and frequency dependence of fatigue failure of rocks. In: Pasamehmetoglu AG, Kawamoto T, Waittaker BN, Aydan O (eds) Assessment and Prevention of Failure Phenomena in Rock Engineering. A. A. Balkema, Rotterdam, pp. 321–327.
- Itasca Consulting Group Inc. (2011) FLAC, Fast Lagrange Analysis of Continua, Version 7.0, User Manual. Minneapolis.
- Jaeger, J. C. (1971) Friction of rocks and stability of rock slopes. The 11th Rankine Lecture. Géotechnique 21(2), 97-134.
- Jaeger, J. C., Cook, N. G. W. (1979) Fundamentals of Rock Mechanics. Third Edition, Chapman and Hall, London.
- Jaky, J. (1948) Pressure in silos. International Proceedings of 2nd ICSMFE, Rotterdam, Vol. 1: 103-107.
- Jeng, F. S., Huang, T. H. (1998) Shear dilatational behavior of weak sandstone. In: Proceedings of the regional symposium on sedimentary rock Engineering. Taipei, Taiwan: Public Construction Commission p. 262–7.
- Jing, X. D., Al-Harthy, S., King, M. S. (2002) Petrophysical properties and anisotropy of sandstones under true triaxial stress conditions, Petrophysics, v.43, pp.358-364.
- King, M. S., Chaudhry, N. A., Shakeel, A. (1995) Experimental ultrasonic velocities and permeability for sandstones with aligned cracks, Int. J. Rock Mech. Mining. Sci., v.32, pp.155-163.
- King, M. S. (2002) Elastic wave propagation in and permeability for rocks with multiple parallel fractures. Int. J. Rock Mech. Mining Sci., v. 39, pp.1033-1043.
- Klein, S. (2001) An Approach to the Classification of Weak Rock for Tunnel Project, RETC Proceedings
- Knill, J. L., Jones, K. S. (1965) The recording and interpretation of geological conditions in the foundations of the Roseires, Kariba and Latiyan dams. Géotechnique, 15, 94-124.
- Kodama, J., Nishiyama, E., Kaneko, K. (2009) Measurement and interpretation of long-term deformation of a rock slope at the Ikura limestone quarry, Japan, International Journal of Rock Mechanics & Mining Science 46. P 148-158
- Kohmura, Y., Inada, Y. (2006) The effect of the loading rate on stress-strain characteristics of tuff. Journal of the Society of Materials Science (Japan) 55(3), 323–328.
- Kranz, R. L., Harris, W. J., Carter, N. L. (1982) Static fatigue of granite at 200°C. Geophys. Res. Lett. 9, 1±4.
- Kumar, A. (1968) The effect of stress rate and temperature on the strength of basalt and granite. Geophysics 33(3), 501–510.
- Lama, R. D., Vutukuri, V. S. (1978) Handbook on mechanical properties of rocks. Trans Tech Publications, Clausthal, Germany, 1978, 1650 p.

- Lauffer, H. (1958) Classification for tunnel construction, *Geologie und Bauwesen*, 24(1), 46-51. (*In German*).
- Lee, S. G., De Freitas, M. H. (1989) A revision of the description and classification of weathered granite and its application to granites in Korea: *Quarterly Journal Engineering Geology*, Vol. 22, No. 1, pp. 31–48.
- Lemaitre J., Chaboche J. L. (1996) *Mecanique des materiaux solides*. Dunod, 253-341. (*In French*).
- Li, Y., Xia, C. (2000) Time-dependent tests on intact rocks in uniaxial compression. *Int. J. Rock Mech. Min. Sci.* 37(3), 467–475.
- Likar, J., Vesel, G., Dervarič, E., Jeromel, G. (2006) Time-dependent Processes in Rocks, *RMZ – Materials and Geosnvironment*, Vol. 53, No. 3, pp. 285-301.
- Little, A. L. (1969) The engineering classification of residual tropical soils. *Proceedings of the 7th International Conference on Soil Mechanics and Foundation Engineering, Mexico, Special Session on Engineering Properties of Lateritic Soils, Mexico*, 1-10.
- Malan, D. F. (1999) Simulating the Time-dependent Behaviour of Excavations in Hard Rock, *Rock Mech. Rock Engng.* 32 (2), 123-155.
- Maranini, E., Brignoli, M. (1999) Creep behavior of a weak rock: experimental characterization, *International Journal of Rock Mechanics and Mining Sciences*, 1999, 36 (1): 127–138.
- Marinos, P. (2004) Rock Mass Characterisation in Engineering Practice. *Razprave IV. Posvetovanja Slovenskih geoteknikov, SLOGED, Rogaška Slatina*, pp.339-343.
- Marinos, P, Hoek, E. (2000) GSI – A geologically friendly tool for rock mass strength estimation. *Proc. GeoEng2000 Conference, Melbourne*. 1422-1442.
- Marinos, P., Hoek, E. (2001) Estimating the Geotechnical Properties of Heterogeneous Rock Masses such as Flysch. *Bull. Eng. Geol. Env.*, No. 60, pp. 85-92.
- Martinetti, S., Ribacchi, R. (1980) In situ stress measurements in Italy. *Rock Mechanics* 9: 31-47.
- Melton, M. A. (1965) Debris-covered hillslopes of the southern Arizona desert – consideration of their stability and sediment contribution. *Journal of Geology* 73, 715-729.
- Moye, D. G. (1955) Engineering geology for the Snowy Mountain scheme. *Journal of the Institution of Engineers, Australia*, 27, 287-298.
- Nemat-Nasser, S., Horii, H. (1982) Compression-induced non-planar crack extension with application to splitting, exfoliation and rock-burst, *J Geophys Res*; 87(B8):6805–21.
- Nemat-Nasser S., Obata, M. (1988) A microcrack model of dilatancy in brittle materials. *ASME J Appl Mech*; 55: 24–35.
- Neilson, J. L. (1970) Notes on weathering of the Silurian rocks of the Melbourne district. *Journal of the Institution of Engineers*, 42, 9-12.
- Newbery, J. (1970) Engineering geology in the investigation and construction of the Batang Padang hydro-electric sheme, Malaysia. *Quarterly Journal Engineering Geology*, 3, 151-181.
- Nickmann, M., Spaun, G., Thuro, K. (2006): Engineering geological classification of weak rocks. In: *Proc. 10th International IAEG Congress 2006, Nottingham: Paper number 492, IAEG London*.

- Okada, T., Tani, K., Ootsu, H., Toyooka, Y., Hosono, T., Tsujino, T., Kimura, H., Naya, T., Kaneko, S. (2006) Development of in-situ triaxial test for rock masses, *International Journal of the JCRM*, Japanese Committee for Rock Mechanics, Volume 2, Number 1, October 2006, pp.7-12
- Okubo, S., Fukui, K., Hashiba, K. (2008) Development of a transparent triaxial cell and observation of rock deformation in compression and creep tests, *International Journal of Rock Mechanics & Mining Sciences* 45 351–361
- Okubo, S., Nishimatsu, Y., He, C., Chu, S.Y., (1992) Loading rate dependency of uniaxial compressive strength of rock under water-saturated condition. *Journal of the Society of Materials Science (Japan)* 41(463), 403–409.
- Olsson, W. (1995) Development of anisotropy in the incremental shear moduli for rock undergoing inelastic deformation. *Mech Mater*; 21:231–42.
- Pellet, F., Hajdu, A., Deleruyelle, F., Besnus, F. (2005) A viscoplastic model including anisotropic damage for the time dependent behaviour of rock. *Int. J. Numer. Anal. Meth. Geomech.* 29 (9), 941–970.
- Perzyna, P. (1966) Fundamental problems in viscoplasticity, *Advances in Applied Mechanics*, (9): 243–377.
- Palmström, A. (1995) RMI – A rock mass characterisation system for rock engineering purposes. Ph. D. thesis, University of Oslo, Norway, 400 p.
- Palmström, A., Singh, R. (2001) The Deformation Modulus of Rock Masses – comparisons between in situ tests and indirect estimates, *Tunnelling and Underground Space Technology*, Vol. 16, No. 3, pp. 115 - 131.
- Peck, R. B. (1969) Advantages and limitations of the observational method in applied soil mechanics. *Geotechnique*, 19 (2), 171-187.
- Phillips, D. W. (1931) Further investigation of the physical properties of coal-measure rocks and experimental work on the development of fractures. *Trans. Inst. Min. Engineers*, 82: 432-450
- Piteau, D. R. (1970) Geological factors significant to the stability of slopes cut in rock. *Proc. Symp. on Planning Open Pit Mines*, Johannesburg, South Africa, pp. 33-53.
- Pinho, A., Rodrigues-Carvalho, J., Gomes, C., Duarte, I. (2006) Overview of the evaluation of the state of rock weathering by visual inspection, *IAEG 2006 Engineering Geology for Tomorrow's Cities*, The Geological Society of London, paper 260
- Pomeroy, C. D. (1956) Creep in coal at room-temperature, *Nature*, 178: 279-280
- Powderham, A. J. (1994) An overview of the observational method: development in cut and cover bored tunnelling projects. *Geotechnique*, 44 (4), 619-636.
- Powderham, A. J. (1998) The observational method – application through progressive modification. *Civil Engineering Practice: Journal of the Boston Society of Civil Engineers Section/ASCE*, 13 (2), 87-110.
- Powderham, A. J. (2002) The observational method – learning from projects. *Proceedings of the Institution of Civil Engineers: Geotechnical Engineering*, 155 (1), 59-69.
- Powderham, A. J., Nicholson, D. P. (1996) The way forward. In: *The observational method in geotechnical engineering* (D. P. Nicholson & A. J. Powderham ed.). Thomas Telford, London.
- Ramamurthy, T. (1995) Bearing capacity of rock foundations, In: *Yoshinaka & Kikuchi (Eds.), Rock foundation*, Balkema, Rotterdam.

- Ray, S. K., Sarkar, K., Singh, T. N. (1999) Effect of cyclic loading and strain rate on the mechanical behaviour of sandstone. *Int. J. Rock Mech. Min. Sci.* 36(4), 543–549.
- Read, S. A. L., Richards, L. R., Perrin, N. D. (1999) Applicability of the Hoek-Brown failure criterion to the New Zealand greywacke rocks. *Proceedings 9th International Congress on Rock Mechanics*, Paris, August, G.Vouille and P. Berest Eds., Vol. 2, pp. 655-660.
- Reiner, M. (1964) *Physics Today*, Vol. 17, No 1 p. 62
- Ribacchi, R. (1988) Rock mass deformability: In situ tests, their implementation and typical results in Italy. Sakurai, S. (ed), In: *Proceedings of 2nd International Symposium on Field Measurements in Geomechanics*: 171-192. Rotterdam: Balkema.
- Riedmüller, G., Schubert, W. (1999) Critical comments on quantitative rock mass classifications, *Felsbau*, 17(3).
- Roctest Limited (2008) Instruction manual, Borehole dilatometer (Rock pressuremeter), Model Probex
- Romana, M. (1985) New adjustment ratings for application of Bieniawski classification to slopes. In: *Proceedings of the International Symposium on the Role of Rock Mechanics*, 49- 53.
- Rummel, F. (1986) Stresses and tectonics of upper continental crust – a review, *Proc. Int. Symp. On Rock Stress and Rock Stress Measurements*, pp.177-186.
- Ruxton, B. P., Berry, L. (1957) Weathering of granite and associated erosional features in Hong Kong. *Bulletin of Geological Society of America*, 68, 1263-1292.
- Sakurai, S., Abe, S. (1981) Direct strain evaluation technique in construction of underground opening. *Proceedings, 22nd U.S Symposium on Rock Mechanics: Rock Mechanics from Research to Application*, MIT, Cambridge, Massachusetts, pp. 278- 282.
- Sakurai, S., Takeuchi, K. (1983) Back analysis of measured displacements of tunnels. *Rock Mechanics and Rock Engineering* 16 (3), 173-180.
- Sakurai, S., Shimizu, N., Matsumuro, K. (1985) Evaluation of plastic zone around underground openings by means of displacement measurements. *Proceedings, 5th International Conference on Numerical Methods in Geomechanics*, Nagoya, Japan, 1-5 April, 1985, pp. 111-118.
- Samsri, P., Tepnarong, P., Fuenkajorn, K. (2011) Determination of salt creep properties using modified point load technique, *Rock Mechanics, Fuenkajorn & Phien-wej (eds)*.
- Sancio, R. T., Brown, I. (1980) A classification of weathered foliated rocks for use in slope stability problems. *Proceedings of the 3rd Australia – New Zealand Conference on Geomechanics*, Wellington, 2, 2.81-2.86.
- Santarelli, F. J., Brown, E. T. (1989) Failure of three sedimentary rocks in triaxial and hollow cylinder compression test. *Int. J. Rock Mech. Min. Sci. Geomech. Abstr*; 26(5):401-13.
- Santi, P. M. (1995) *Classification and Testing of Weak and Weathered Rock Materials: A Model Based on Colorado Shales*: Unpublished PhD dissertation, Colorado School of Mines, Golden, CO, 286 p.
- Santi, P. M. (2006) *Field Methods for Characterizing Weak Rock for Engineering, Environmental & Engineering Geoscience*, Vol. XII, No. 1, February 2006, pp. 1-11.
- Santi, P. M., Doyle, B. C. (1997) The locations and engineering characteristics of weak rock in the U.S. In Santi, P. M. and Shakoor, A. (Editors), *Characterization of Weak and Weathered Rock Masses*, Association of Engineering Geologists Special Publication #9: Association of Engineering Geologists, Denver, CO, pp. 1–22.

- Saunders, M. K., Fookes, P. G. (1970) A review of the relationship of rock weathering and climate and its significance to foundation engineering. *Engineering Geology*, 4, 289-325.
- Serafim, J. L., Pereira, J. P. (1983) Consideration of the geomechanics classification of Bieniawski. *Proc. Int. Symp. on Engineering Geology and Underground Constructions*, pp. 1133 - 1144.
- Shao, J., Chau, K., Feng, X. (2006) Modeling of anisotropic damage and creep deformation in brittle rocks. *Int. J. Rock Mech. Min. Sci.* 43 (4), 582–592.
- Sharma, V. M., Singh, R. B. (1989) Deformability of rock mass. *Proc. Conf. Application of rock mechanics in river valley projects*, Roorkee, pp. II-7 – II-12.
- Sheory, P. R. (1994) A theory for in situ stresses in isotropic and transversely isotropic rock, *Int. J. Rock Mech. Min. Sci. & Geomech. Abstr.* 31(1): 23-34.
- Sheorey, P. R., Biswas, A. K., Choubey, V. D. (1989) An empirical failure criterion for rocks and jointed rock masses. *Eng. Geol.* 26, 141-159.
- Singh, B., Goel, R. K. (2011) *Engineering Rock Mass Classification, Tunneling, Foundations, and Landslides*. Elsevier.
- Sowers, G. F. (1973) Settlement of waste disposal fills. In *Proceedings of the 8th International Conference on Soil Mechanics and Foundation Engineering*, Moscow, ID, pp. 207–210.
- Szavits-Nossan, A. (2006) Observations on the observational Methods, *Proceeding of XIII Danube-European Conference on Geotechnical Engineering, Active Geotechnical Design in Infrastructure Development*, J. Logar, A. Gaberc and B. Majes (eds), Slovenian Geotechnical Society, Ljubljana, May 29-31, Vol. 1, pp.171-178
- Talobre, J. A. (1967) *La Mecanique des Roches*, 2nd edn, Paris: Dunod. In French
- Tani, K. (1999) Proposal of new in-situ test methods to investigate strength and deformation characteristics of rock masses, *Proc. 2nd Int. Symp. on Pre-failure Deformation Characteristics of Geomaterials*, 1, 357-364.
- Tani, K., Nozaki, T., Kaneko, S., Toyooka, Y., Tachikawa, H. (2003) Down-hole triaxial test to measure average stress-strain relationship of rock mass, *Soils and Foundations*, Vol. 43, No. 5, 53-62.
- Terzaghi, K. (1946) Introduction to tunnel geology. In R. V. Proctor & T. L. White (Eds.), *Rock tunnelling with steel supports* (p. 271). Youngstown, OH: Commercial Shearing & Stamping Co.
- Terzaghi, K. (1962) Measurements of stresses in rock, *Geotechnique*, Vol. XII, No. 2, June 1962.: 105-124.
- Terzaghi, K., Peck, R. B. (1967) *Soil mechanics in Engineering Practice*. John Wiley, New York.
- Terzaghi, K., Richart, F. E. (1952) Stresses in rock about cavities. *Géotechnique*, Vol.3: 57-90.
- Tomanović, Z. (2006) Rheological model of soft rock based on test on marl. *Mechanics of Time-dependent Materials*, 10, 2, 135-154
- Tomanovic, Z. (2009) Influence of K_0 on creep properties of marl. *Int. J. Acta Geotechnica Slovenica*, pp. 14-29.
- Tomanović, Z. (2012) The stress and time dependent behaviour of soft rocks, *Građevinar* 64, 12, pp. 993-1007

- Tsai, L. S., Hsieh, Y. M., Weng, M. C., Huang, T. H., Jeng, F. S. (2008) Time-dependent deformation behaviors of weak sandstones, *International Journal of Rock Mechanics & Mining Sciences* 45 (2008) 144–154
- Underwood, L. B. (1967) Classification and identification of shales: *Journal Soil Mechanics Foundations Division, ASCE*, Vol. 93, No. SM-6, pp. 97–116.
- Vardakos, S. (2007) Back-analysis Methods for Optimal Tunnel Design, Ph. D. Thesis, Faculty of the Virginia Polytechnic Institute and State University, 168p.
- Vargas, M. (1953) Some engineering properties of residual clay soils occurring in southern Brazil. *Proceedings of the 3rd International Conference on Soil Mechanics and Foundation Engineering, Zurich*, 1, pp. 259-268.
- Wakeling, T. R. M. (1970) A comparison of the results of standard site investigation methods against the results of a detailed geotechnical investigation in Middle Chalk at Mundford, Norfolk. In *situ investigations in soils and rocks*. British Geotechnical Society, London, pp. 17-22.
- Ward, W. H., Burland, V. B., Gallois, R. W. (1968) Geotechnical assessment of a site at Mundford, Norfolk for a large proton accelerator. *Géotechnique*, 18, 399-431.
- Welsh, R. A., Vallejo, L. E., Lovell, L. W., Robinson, M. K. (1991) The U.S. Office of Surface Mining (OSM) proposed strength-durability classification system: In Kane, W. F. and Amadei, B. (Editors), *Detection of and Construction at the Soil/ Rock Interface*, ASCE Geotechnical Special Publication No. 28: ASCE, New York, pp. 125–140.
- Weng, M. C., Jeng, F. S., Huang, T. H., Lin, M. L. (2005) Characterizing the deformation behavior of tertiary sandstones. *Int J Rock Mech Min Sci*, 42:388–401.
- White, R. M., Richardson, T. L. (1987) Predicting the difficulty and cost of excavation in the Piedmont. In Smith, R. E. (Editor), *Foundations and Excavations in Decomposed Rock of the Piedmont Province*: ASCE Geotechnical Special Publication No. 9: ASCE, New York, pp. 15–36.
- Wong, T. F. (1982) Micromechanics of faulting in Westerly granite. *Int J Rock Mech Min Sci*;19: 46–9.
- Yahya, O. M. L., Aubertin, M., Julien, M. R. (2000) A unified representation of the plasticity, creep and relaxation behavior of rock salt, *International Journal of Rock Mechanics and Mining Sciences*, 37 (5): 787-800.
- Yang, S., Jiang, Y. (2010) Triaxial mechanical creep behavior of sandstone, *Mining Science and Technology* 20 (2010) 0339–0349.
- Yu, C. W. (1998) Creep characteristics of soft rock and modelling of creep in tunnel. PhD Thesis, Department of Civil and Environmental Engineering University of Bradford, U.K.
- Yu, C. W., Chern, J. C. (1994) Creep Modelling of an Endangered Slope Adjacent to Wusheh Dam, Taiwan, *Proc. 7th Int. Congr. Int. Asso. of Engineering Geology (IAEG)*, Lisbon.
- Yudhbir, Lemanza, W., Prinzl, F. (1983) An empirical failure criterion for rock masses. In: *Proceedings of the 5th International Congress on Rock Mechanics*, Melbourne, Balkema, Rotterdam, 1, B1-B8.
- Zhang, S., Nakano, H., Xiong, Y., Nishimura, T., Zhang, F. (2010) Temperature-controlled triaxial compression/creep test device for thermodynamic properties of soft sedimentary rock and corresponding theoretical prediction, *Journal of Rock Mechanics and Geotechnical Engineering*. 2010, 2 (3): 255–261

Zhang, Z. L., Xu, W. Y., Wang, W., Wang, R. B. (2012) Triaxial creep tests of rock from the compressive zone of dam foundation in Xiangjiaba Hydropower Station, *International Journal of Rock Mechanics & Mining Sciences* 50 (2012) 133–139

Zoback, M. L. (1992) First and second-order patterns of stress in the lithosphere: the World Stress Map Project. *J. Geophys. Res.* 97(B8): 11761-11782.

LIST OF FIGURES

Figure 2.1 Position of weak rock between cohesive soils and hard rocks (Nickmann et al., 2006)	7
Figure 2.2 Schematic diagram of the weathering profile mapped in the Ruffi slide area (Eberhardt et al., 2005).....	14
Figure 2.3 Typical stress vs. deformation curve recorded in a deformability test of a rock mass (Palmström and Singh, 2001)	28
Figure 2.4 Typical short-term stress-strain curves of sandstone under different confining pressure (Yang and Jiang, 2010).....	30
Figure 3.1 Time-strain curve and creep phases for specimen under constant load (Lama and Vutukuri, 1978).....	34
Figure 3.2 Dilatancy boundary and creep phases (Cristescu and Hunsche, 1998)	42
Figure 3.3 Uniaxial creep test with increasing the temperature (Cristescu and Hunsche, 1998).....	43
Figure 3.4 The limit curve and its links with creep path (AB) or relaxation path (AC) (Fabre and Pellet, 2006).....	44
Figure 3.5 The definition of Stress Strength Ratio (SSR) (Yu, 1998)	46
Figure 3.6 Deviatoric pressure vs. axial steady creep rate and vs. lateral steady creep rate (Zhang, 2012)	47
Figure 3.7 Characteristic strain-time creep curve (Yang and Jiang, 2010).....	47
Figure 3.8 Devices for uniaxial creep tests (Tomanović, 2009)	48
Figure 3.9 Uniaxial creep test results under different stresses (left) and comparative creep diagram after unloading in axial direction (right) (Tomanović, 2009)	49
Figure 3.10 Diagram of creep uniaxial test of prismatic and plate specimens (Tomanović, 2009).....	50
Figure 3.11 Diagram of creep biaxial test of plate specimens; (a) with vertical stress 2.0 MPa, where $K_0 = 1.0$; (b) with vertical stress 2.0 MPa, where $K_0 = 0.0$; (c) with vertical stress 2.0 MPa, where $K_0 = 0.3$ (Tomanović, 2009)	51
Figure 3.12 Diagram of creep triaxial test (Tomanović, 2009)	52
Figure 3.13 Typical borehole dilatometer test equipment (Roctest, 2008).....	54
Figure 3.14 Radial deformation vs. time in the borehole dilatometer test (Goodman, 1989).....	55
Figure 3.15 Typical rigid plate bearing test setup schematic (ASTM, 2002)	56
Figure 3.16 Test procedure of an in-situ triaxial test for rock masses (Tani et al., 2003).....	58
Figure 3.17 Comparison of simulation and measured data for convergence of Ureshino Tunnel Line 1, Nagasaki (Guan et al., 2008)	62
Figure 3.18 Comparison of simulation and measured data for convergence of Saint Martin La Porte access adit (Lyon-Turin Base Tunnel) (Barla et al., 2008).....	64
Figure 3.19 Comparison of measured and calculated displacements of roof measuring point for Trojane tunnel at four cross sections (Likar et al., 2006).....	65

Figure 3.20 Relative displacement at Ikura limestone quarry measured by extensometers ID-2 (a) and ID-1 (b) for a period of more than 7 years (Kodama et al., 2009)	66
Figure 3.21 Comparison of measured and calculated relative displacements for extensometer ID-2 at Ikura quarry (Kodama et al., 2009)	67
Figure 3.22 Joint discretization for cross section for the south slope of Three Gorges (Feng et al., 2003)	68
Figure 3.23 Comparison of displacements between numerical results and field measurements for the south slope (Feng et al., 2003).....	69
Figure 4.1 Basic explicit calculation cycle in FLAC (Itasca, 2011)	74
Figure 4.2 General solution procedure in FLAC (Itasca, 2011)	76
Figure 4.3 Mohr-Coulomb failure criterion in FLAC (Itasca, 2011)	80
Figure 4.4 Domains used in the definition of the flow rule in Mohr-Coulomb model (Itasca, 2011)	82
Figure 4.5 Sketch of Burger viscoplastic Mohr-Coulomb model: (a) volumetric behaviour, and (b) deviatoric behaviour	82
Figure 4.6 Cable material behaviour for cable elements (Itasca, 2011).....	85
Figure 4.7 Conceptual mechanical representation of fully bonded reinforcement which accounts for shear behaviour of the grout annulus (Itasca, 2011)	86
Figure 5.1 Location of the Adriatic Motorway near the City of Rijeka, Republic of Croatia	94
Figure 5.2 Reinforced cut in flysch rock mass at km 2+440; (a) during construction phase and (b) after finished secondary lining	96
Figure 5.3 (a) Schematic engineering-geological map of the Draga Valley; (b) Schematic engineering-geological cross-section of the Draga Valley (Arbanas et al., 1994).....	98
Figure 5.4 Process and grades of weathering in flysch rock mass (Grošić and Arbanas, 2013).....	99
Figure 5.5 Situation plan of Adriatic Motorway (from km 2+300 to 2+500) with position of geotechnical investigation works: geotechnical core drilling (green) and geophysical investigations (magenta).....	100
Figure 5.6 Results of geophysical investigation – seismic refraction; (a) profile RF-1 at km 2+380; (b) profile RF-2 at km 2+440 (Georheo, 2013)	107
Figure 5.7 Results of geophysical investigation – MASW; (a) profile MASW 1-2 at km 2+380; (b) profile MASW 2-3 at km 2+380 (Georheo, 2013).....	108
Figure 5.8 Results of geophysical investigation – MASW; (a) profile MASW 3-2 at km 2+440; (b) profile MASW 4-1 at km 2+440 (Georheo, 2013).....	108
Figure 5.9 Geotechnical cross sections used for numerical analysis; (a) cross section at chainage km 2+380; (b) cross section at chainage km 2+440	109
Figure 5.10 Cross sections with monitoring equipment; (a) cross section at chainage km 2+380; (b) cross section at chainage km 2+440	110
Figure 5.11 Horizontal displacement vs. depth measured at vertical inclinometer at km 2+380	112
Figure 5.12 Horizontal displacement vs. time measured at vertical inclinometer at km 2+380	113

Figure 5.13 Horizontal displacement vs. distance measured at horizontal deformer at km 2+380.....	113
Figure 5.14 Horizontal displacement vs. time measured at horizontal deformer at km 2+380.....	114
Figure 5.15 Horizontal displacement vs. depth measured at vertical inclinometer at km 2+440	115
Figure 5.16 Horizontal displacement vs. time measured at vertical inclinometer at km 2+440	115
Figure 5.17 Horizontal displacement vs. distance measured at horizontal deformer at km 2+440.....	116
Figure 5.18 Horizontal displacement vs. time measured at horizontal deformer at km 2+440.....	116
Figure 5.19 Cross section km 2+380 –finite difference grid used for numerical analysis.....	117
Figure 5.20 Cross section km 2+380 – user-defined groups used for construction phase back analysis.....	119
Figure 5.21 Cross section km 2+380 – construction phases used in back analysis	120
Figure 5.22 Cross section km 2+380 – Grid zone models used for numerical back analysis for service period.....	122
Figure 5.23 Cross section km 2+380 – user-defined groups used for numerical back analysis for service period.....	123
Figure 5.24 Cross section km 2+4400 –finite difference grid used for numerical analysis.....	124
Figure 5.25 Cross section km 2+440 – user-defined groups used for construction phase back analysis.....	126
Figure 5.26 Cross section km 2+4400 – construction phases used for back analysis.....	127
Figure 5.27 Cross section km 2+440 – Grid zone models used for numerical back analysis for service period.....	129
Figure 5.28 Cross section km 2+440 – user-defined groups used for numerical back analysis for service period.....	129
Figure 6.1 Cross section at km 2+380 – total vertical stress contours at equilibrium state	131
Figure 6.2 Cross section at km 2+380 – total horizontal stress contours at equilibrium state	132
Figure 6.3 Cross section at km 2+380 – total vertical stress contours after construction phase	133
Figure 6.4 Cross section at km 2+380 – total horizontal stress contours after construction phase.....	134
Figure 6.5 Cross section at km 2+380 – axial forces in rockbolts after construction phase	134
Figure 6.6 Cross section at km 2+380 – displacement vectors after construction phase	135
Figure 6.7 Cross section at km 2+380 – horizontal displacement contours after construction phase.....	136
Figure 6.8 Cross section at km 2+380 – total vertical stress contours after service period of 901 days.....	137
Figure 6.9 Cross section at km 2+380 – total horizontal stress contours after service period of 901 days	138
Figure 6.10 Cross section at km 2+380 – axial forces in rockbolts after service period of 901 days	138
Figure 6.11 Cross section at km 2+380 – displacement vectors after service period of 901 days.....	139

Figure 6.12 Cross section at km 2+380 – horizontal displacement contours after service period of 901 days.....	139
Figure 6.13 Cross section at km 2+440 – total vertical stress contours at equilibrium state	140
Figure 6.14 Cross section at km 2+440 – total horizontal stress contours at equilibrium state	140
Figure 6.15 Cross section at km 2+440 – total vertical stress contours after construction phase	142
Figure 6.16 Cross section at km 2+440 – total horizontal stress contours after construction phase	142
Figure 6.17 Cross section at km 2+440 – axial forces in rockbolts after construction phase	143
Figure 6.18 Cross section at km 2+440 – displacement vectors after construction phase	143
Figure 6.19 Cross section at km 2+440 – displacement vectors after construction phase	144
Figure 6.20 Cross section at km 2+440 – total vertical stress contours after service period of 901 days.....	146
Figure 6.21 Cross section at km 2+440 – total horizontal stress contours after service period of 901 days.....	146
Figure 6.22 Cross section at km 2+440 – axial forces in rockbolts after service period of 901 days	147
Figure 6.23 Cross section at km 2+440 – displacement vectors after service period of 901 days.....	147
Figure 6.24 Cross section at km 2+440 – horizontal displacement contours after service period of 901 days.....	148
Figure 6.25 Comparison of simulation results and measured data of horizontal displacements at vertical inclinometer at cross section km 2+380	149
Figure 6.26 Comparison of simulation results and measured data of horizontal displacements at vertical inclinometer at cross section km 2+440	150
Figure 6.27 Distribution of axial forces activated in rockbolts at cross section km 2+380 with maximum activated forces in each rockbolt row: (a) at the end of construction phase; (b) at the end of monitoring phase (service period of 901 days).	151
Figure 6.28 Distribution of axial forces activated in rockbolts at cross section km 2+440 with maximum activated forces in each rockbolt row: (a) at the end of construction phase; (b) at the end of monitoring phase (service period of 901 days).	152
Figure 6.29 Axial forces in rockbolts at cross section at km 2+380 during time period of 901 days	153
Figure 6.30 Axial forces in rockbolts at cross section at km 2+440 during time period of 901 days	153
Figure 7.1 Contours of horizontal displacements in slope at km 2+380 with contour interval of 1.0 mm over a time period of 25 years realised after the end of construction phase	156
Figure 7.2 Axial forces in rockbolts at cross section at km 2+380 during time period of 25 years.....	156
Figure 7.3 Contours of horizontal displacements in slope at km 2+440 with with contour interval of 0.5 mm over time period of 25 years realised after the end of construction phase	157
Figure 7.4 Axial forces in rockbolts at cross section at km 2+440 during a time period of 25 years	158

LIST OF TABLES

Table 2.1 Summary of engineering properties of weak rock from the literature (Santi, 2006)	9
Table 2.2 Scale of weathering grades of rock mass (Dearman, 1976.).....	12
Table 2.3 GSI estimate for heterogeneous rock masses such as flysch (Marinos and Hoek, 2001)	18
Table 2.4 Field estimates of uniaxial compressive strength of intact rock (Hoek and Marinos, 2001)	20
Table 2.5 Values of the constant m_i (Hoek and Marinos, 2001)	21
Table 2.6 Classification of weak rocks based on the behaviour in the 3-cyclic wetting-drying-test and the crystallization test (Nickmann et al., 2006)	22
Table 2.7 Short-term mechanical parameters of sandstone under different confining pressure (Yang and Jiang, 2010)	30
Table 3.1 Table of laboratory tests on rocks suitable for the determination of creep properties of intact rock (Cristescu and Hunshe, 1998).....	38
Table 5.1 Photodocumentation of open cuts with GSI estimation (Brunčić, 2008).....	104
Table 5.2 GSI estimate for flysch rock mass at Adriatic Motorway (modified form Marinos and Hoek, 2001 and Brunčić, 2008)	106
Table 5.3 Cross section km 2+380 – longitudinal wave velocities, thickness and weathering grade of geotechnical units	119
Table 5.4 Cross section km 2+380 – Properties of rockbolts and shotcrete	121
Table 5.5 Cross section km 2+440 – longitudinal wave velocities, thickness and weathering grade of geotechnical units	125
Table 5.6 Cross section km 2+440 – Properties of rockbolts and shotcrete	128
Table 6.1 Cross section km 2+380 – deformability parameters of geotechnical units obtained from construction phase back analysis	133
Table 6.2 Cross section km 2+380 – deformability and creep parameters of geotechnical units obtained from service period back analysis.....	137
Table 6.3 Cross section km 2+440 – deformability parameters of geotechnical units obtained from construction phase back analysis	141
Table 6.4 Cross section km 2+440 – deformability and creep parameters of geotechnical units obtained from service period back analysis.....	145

APPENDIX 1 – NUMERICAL CODE KM 2+380

```

config creep

grid 100,33

model mohr i=1,100 j=1,33

group 'User:model_insitu' notnull

model elastic notnull group 'User:model_insitu'

prop density=2000.0 bulk=3.83e9 shear=1e9 notnull group 'User:model_insitu'

gen (0.0,0.0) (0.0,9.5) (15,9.5) (15,0.0) i 1 31 j 1 20

gen (15,0) (15,9.5) (37.25, 16.75) (37.25, 0) i 31 75 j 1 20

gen (37.25, 0) (37.25, 16.75) (50, 18.25) (50, 0) i 75 101 j 1 20

gen (0, 9.5) (0, 16.5) (15, 16.5) (15, 9.5) i 1 31 j 20 34

gen (15, 9.5) (15, 16.5) (37.25, 26.75) (37.25, 16.75) i 31 75 j 20 34

gen (37.25, 16.75) (37.25, 26.75) (50, 28.25) (50, 18.25) i 75 101 j 20 34

fix x i 101 j 2 34

fix x i 1 j 2 34

fix x y j 1

set gravity=10.0

history 999 unbalanced

solve

initial xdisp 0 ydisp 0

initial xvel 0 yvel 0

group '0-400' j 31 33

model cvisc group '0-400'

prop density=2000.0 bulk_mod=1.92e6 shear_mod=5e5 cohesion=15000.0 friction=28.0 k_shear=5e6
k_viscosity=5E13 viscosity=5E15 group '0-400'

group '400-800' j 28 30

model cvisc group '400-800'

prop density=2000.0 bulk_mod=7.67e6 shear_mod=2e6 cohesion=25000.0 friction=32.0 k_shear=2e7
k_viscosity=5E13 viscosity=5E15 group '400-800'

group '800-1200' j 26 27

model cvisc group '800-1200'

```

```

prop density=2000.0 bulk_mod=1.34E7 shear_mod=3.5E6 cohesion=25000.0 friction=32.0
k_shear=3.5e7 k_viscosity=7.5E13 viscosity=7.5E15 group '800-1200'

group '1200-2000' j 23 25

model cvisc group '1200-2000'

prop density=2000.0 bulk_mod=5.75E7 shear_mod=1.5E7 cohesion=50000.0 friction=32.0
k_shear=1.5E8 k_viscosity=1E14 viscosity=1E16 group '1200-2000'

group '2000-3000' j 19 22

model cvisc group '2000-3000'

prop density=2000.0 bulk_mod=1.92E8 shear_mod=5E7 cohesion=75000.0 friction=32.0 k_shear=5E8
k_viscosity=1E14 viscosity=1E16 group '2000-3000'

group '>3000' j 1 18

model elastic group '>3000'

prop density=2150.0 bulk=3.83E8 shear=1E8 group '>3000'

model null i 1 30 j 29 33

model null i 1 30 j 29 33

solve

struct prop 1001 e=30e9 i=0.00028125 a=0.15

struct prop 2001 e=200e9 kbond=7.285e9 sbond=100000 yield=400000 a=0.000879 spac 1.8

struct node 1 grid 31,34

struct node 2 grid 31,33

struct node 3 grid 31,32

struct node 4 grid 31,31

struct node 5 grid 31,30

struct node 6 grid 31,29

struct beam begin node 1 end node 2 seg 1 prop 1001

struct beam begin node 2 end node 3 seg 1 prop 1001

struct beam begin node 3 end node 4 seg 1 prop 1001

struct beam begin node 4 end node 5 seg 1 prop 1001

struct beam begin node 5 end node 6 seg 1 prop 1001

struct node 7 15.0,15.0 slave x y 4

struct node 8 30.5,10.75

```

```

struct cable begin node 7 end node 8 seg 32 prop 2001

model null i 1 30 j 26 28

solve

struct node 40 grid 31,28

struct node 41 grid 31,27

struct node 42 grid 31,26

struct beam begin node 6 end node 40 seg 1 prop 1001

struct beam begin node 40 end node 41 seg 1 prop 1001

struct beam begin node 41 end node 42 seg 1 prop 1001

struct node 43 15.0,13.5 slave x y 40

struct node 44 30.5,9.3

struct cable begin node 43 end node 44 seg 32 prop 2001

model null i 1 30 j 23 25

solve

struct node 76 grid 31,25

struct node 77 grid 31,24

struct node 78 grid 31,23

struct beam begin node 42 end node 76 seg 1 prop 1001

struct beam begin node 76 end node 77 seg 1 prop 1001

struct beam begin node 77 end node 78 seg 1 prop 1001

struct node 79 15.0,12.0 slave x y 76

struct node 80 26.5,9.0

struct cable begin node 79 end node 80 seg 24 prop 2001

model null i 1 30 j 20 22

solve

struct node 104 grid 31,22

struct node 105 grid 31,21

struct node 106 grid 31,20

struct beam begin node 78 end node 104 seg 1 prop 1001

struct beam begin node 104 end node 105 seg 1 prop 1001

```

```
struct beam begin node 105 end node 106 seg 1 prop 1001  
struct node 107 15.0,10.5 slave x y 104  
struct node 108 26.5,7.5  
struct cable begin node 107 end node 108 seg 24 prop 2001  
set crdt auto  
solve age ...
```


APPENDIX 2 – NUMERICAL CODE KM 2+440

```

config creep

grid 100,33

model mohr i=1,100 j=1,33

group 'User:model_insitu' notnull

model elastic notnull group 'User:model_insitu'

prop density=2000.0 bulk=3.83e9 shear=1e9 notnull group 'User:model_insitu'

gen (0.0,0.0) (0.0,5) (15,5) (15,0.0) i 1 31 j 1 10

gen (15,0) (15,5) (44, 16.25) (44, 0) i 31 88 j 1 10

gen (44, 0) (44, 16.25) (50, 17.25) (50, 0) i 88 101 j 1 10

gen (0, 5) (0, 16.5) (15, 16.5) (15, 5) i 1 31 j 10 34

gen (15, 5) (15, 16.5) (44, 27.75) (44, 16.25) i 31 88 j 10 34

gen (44, 16.25) (44, 27.75) (50, 28.75) (50, 17.25) i 88 101 j 10 34

fix x i 101 j 2 34

fix x i 1 j 2 34

fix x y j 1

set gravity=10.0

solve

initial xdisp 0 ydisp 0

initial xvel 0 yvel 0

group '0-400' j 33

model cvisc group '0-400'

prop density=2000.0 bulk_mod=1.15e7 shear_mod=3e6 cohesion=15000.0 friction=28.0 k_shear=3e7
k_viscosity=5E12 viscosity=5E14 group '0-400'

group '400-800' j 29 32

model cvisc group '400-800'

prop density=2000.0 bulk_mod=2.87E7 shear_mod=7.5e6 cohesion=25000.0 friction=32.0
k_shear=7.5e7 k_viscosity=5E12 viscosity=5E14 group '400-800'

group '800-1200' j 25 28

model cvisc group '800-1200'

```

```

prop density=2000.0 bulk_mod=2.88E7 shear_mod=7.5E6 cohesion=25000.0 friction=32.0
k_shear=7.5e7 k_viscosity=7.5E12 viscosity=7.5E14 group '800-1200'

group '1200-2000' j 20 24

model cvisc group '1200-2000'

prop density=2000.0 bulk_mod=1.15E8 shear_mod=3E7 cohesion=50000.0 friction=32.0 k_shear=3E8
k_viscosity=1E13 viscosity=1E15 group '1200-2000'

group '2000-3000' j 16 19

model cvisc group '2000-3000'

prop density=2000.0 bulk_mod=1.192E8 shear_mod=5e7 cohesion=75000.0 friction=32.0
k_shear=5E8 k_viscosity=1E13 viscosity=1E15 group '2000-3000'

group '>3000' j 1 15

model elastic group '>3000'

prop density=2150.0 bulk=5.75E8 shear=1.5E8 group '>3000'

model null i 1 30 j 31 33

solve

struct prop 1001 e=30e9 i=0.00028125 a=0.15

struct prop 2001 e=200e9 kbond=7.285e9 sbond=100000 yield=400000 a=0.000879 spac 1.8

struct node 1 grid 31,34

struct node 2 grid 31,33

struct node 3 grid 31,32

struct node 4 grid 31,31

struct node 5 grid 31,30

struct beam begin node 1 end node 2 seg 1 prop 1001

struct beam begin node 2 end node 3 seg 1 prop 1001

struct beam begin node 3 end node 4 seg 1 prop 1001

struct beam begin node 4 end node 5 seg 1 prop 1001

struct node 6 15,15.6 slave x y 4

struct node 7 30.5,11.5

struct cable begin node 6 end node 7 seg 32 prop 2001

model null i 1 30 j 27 30

solve

```

```

struct node 39 grid 31,29

struct node 40 grid 31,28

struct node 41 grid 31,27

struct beam begin node 5 end node 39 seg 1 prop 1001

struct beam begin node 39 end node 40 seg 1 prop 1001

struct beam begin node 40 end node 41 seg 1 prop 1001

struct node 42 15,14.2 slave x y 4

struct node 43 30.5,10

struct cable begin node 42 end node 43 seg 32 prop 2001

model null i 1 30 j 24 26

solve

struct node 75 grid 31,26

struct node 76 grid 31,25

struct node 77 grid 31,24

struct beam begin node 41 end node 75 seg 1 prop 1001

struct beam begin node 75 end node 76 seg 1 prop 1001

struct beam begin node 76 end node 77 seg 1 prop 1001

struct node 78 15,12.8 slave x y 4

struct node 79 26.6,9.7

struct cable begin node 78 end node 79 seg 24 prop 2001

model null i 1 30 j 21 25

solve

struct node 103 grid 31,23

struct node 104 grid 31,22

struct node 105 grid 31,21

struct beam begin node 77 end node 103 seg 1 prop 1001

struct beam begin node 103 end node 104 seg 1 prop 1001

struct beam begin node 104 end node 105 seg 1 prop 1001

struct node 106 15,11.4 slave x y 4

struct node 107 26.6,8.3

```

struct cable begin node 106 end node 107 seg 24 prop 2001

set crdt auto

solve age ...

BIOGRAPHY

Mirko Grošić was born on January 25, 1980 in Rijeka. He finished grammar school in Opatija in 1998, and went on to graduate from the Faculty of Civil engineering, University of Rijeka in 2003, majoring in construction with his work “Protection of Open Pit Stari Grad, City of Rijeka”. Upon graduating he started working at the Civil Engineering Institute of Croatia d.d. Zagreb, Branch office Rijeka, as a manager of geotechnical field investigations and geotechnical design of motorways, and later as a designer in geotechnics. In 2008 he started his own company, Geotech d.o.o. Rijeka for geotechnical designing and consulting, where he has been working since as a designer and general manager. He started his doctoral studies in 2006 at the Faculty of Civil engineering, University of Rijeka.

As a part of his job, Mirko Grošić has been continuously developing and perfecting his knowledge of geotechnical field investigations and geotechnical design on infrastructure projects such as motorways, roads and railways, slope protection and rockfall protection, open pit protection, landslides and retaining walls. As a designer he has individually signed about 100 preliminary, main and detail designs in the field of geotechnics, most of which have been built, and 150 geotechnical reports (about 20 designs of open pit protection, 60 designs of slope and rockfall protection, 10 designs of landslides mitigations, 30 foundation designs, 20 designs of retaining walls and over 150 geotechnical reports). He is a frequent attendee of national and international conferences and professional courses in the area of geotechnics, and often actively partakes as a lecturer or participant.

Alongside his work experience, he collaborated with the Faculty of Civil engineering, University of Rijeka as an assistant in the field of geotechnics: Soil mechanics, Geotechnical engineering and Foundation engineering.

Mirko Grošić has published 2 scientific papers in magazines, 13 papers in internationally reviewed conference proceedings, 2 papers in reviewed conference proceedings, 2 papers in non-reviewed conference proceedings, and 1 book chapter. He participated in 6 international conferences (XIII Danube - European Conference on Geotechnical Engineering, 2006, Ljubljana, Slovenia; 11. Congress of International Society for Rock Mechanics, 2007, Lisbon, Portugal; International Symposium on Rock Slope Stability in Open Pit Mining and Civil Engineering, 2007, Perth, Australia; 5th Conference of Slovenian geotechnics, 2008, Nova Gorica, Slovenia; 10th International Symposium on Landslides and Engineered Slopes, 2008, Xian, China; Regional symposium of the International Society for Rock Mechanics, Eurock 2009, Cavtat, Republic of Croatia) and national conferences (Priopćenja 4. Savjetovanja Hrvatskog geotehničkog društva, 2006, Opatija; 4. Hrvatski kongres o cestama, 2007, Cavtat; Dani podzemne gradnje, 2011, Zagreb; Dani inženjera 2010, 2011, 2013, Opatija; Hrvatski graditeljski forum, 2013, Zagreb; 6. Savjetovanja Hrvatskog geotehničkog društva, 2013, Zadar).